Examining the Pathogenesis of Enterovirus 71 Using Human Cellular Models

Thesis submitted in accordance with the requirements of the University of Liverpool for the degree of Doctor in Philosophy by

Jonathan Andrew Cox

UNIVERSITY OF LIVERPOOL

April 2018

Examining the Pathogenesis of Enterovirus 71

Using Human Cellular Models

Jonathan Andrew Cox

Enterovirus 71 (EV71) is a global infectious disease that affects millions of people. The virus is the main etiological agent for hand, foot and mouth disease with outbreaks and epidemics being reported globally. Infection can cause severe neurological, cardiac and respiratory problems in children under the age of 5. Despite on-going efforts, little is known about the pathogenesis of EV71, how the host immune system responds to the virus and the molecular mechanisms behind these responses.

The aims of my project are:

To establish an *in vitro* infection system to study EV71 viral kinetics to elucidate if there any difference between virus isolates that cause mild and neurotropic disease?

To study the difference in infectivity and immune response in an *ex vivo* human blood infection system to see immune involvement plays a role in this neurotropism

To assess the ability of the different isolates to infect and cross the blood brain barrier to see if neurovirulence increases the ability to infect or cross the blood brain barrier

To study the inflammatory pathways involved in EV71 immunopathogenesis to see if the different severities of disease induce different pathways.

What I found:

Virus isolates from patients with severe outcomes have higher levels of infectivity

Only the isolates from the most severe patients can replicate in an *ex vivo* PBMC system

CD4+ T Cells are the main instigators of EV71 replication in PBMCs

Severe EV71 isolates show an increased ability to disrupt the BBB

IL-36γ could be a involved in a novel pathway related to infection severity

Acknowledgements

I would like to thank my supervisors Prof. Lisa Ng, Prof. Julian Hiscox, Dr Michael J. Griffiths and Prof. Tom Solomon for their support and for pushing me the whole way, I would not have made it this far without you. I would also like to thank all the LN Group members and the Brain Infection Group members for their constant support, help and hard work throughout this thesis.

I would also like to thank several special people who, without them, I wouldn't be here.

My mum and dad. You have always supported me and pushed me to be the best I can, I wouldn't have gotten this far without your help and support, and definitely your hospitality.

Rachael, Matt, Frankie and Abby. You have always been there, whether as family, as a friend or just as someone to annoy. I couldn't ask for better people to grow up with.

Stavros. You have helped me so much throughout this PhD, but you were more than just a mentor, you were a friend, and then became family. I can never thank you enough.

Cheryl. I don't think I could have survived Singapore without you. You were always there, whether I needed to talk science, or anything else. Thanks so much twin.

Hannah. I am so happy to have met you, you make every day feel better. Your constant encouragement and love have helped push me through this. I hope to return the favour soon.

Table of Contents

Chapter 1

Introduction

1.1.0 Background

Hand, foot and mouth disease (HFMD) is a common infection caused by a number of viruses, commonly from the *Picornaviridae* family, and notably enterovirus 71 (EV71), coxsackie A6 (CA6) and coxsackie A16 (CA16) (1, 2). HFMD predominantly affects young children, however older children and adults can also be affected (3, 4). The main symptoms of the disease are fever, and blisters on the hands, feet and mouth. Other usual clinical signs of HFMD include, nausea, vomiting, sore throat, fatigue, malaise, loss of appetite and irritability. About 3 to 5 days after exposure to the virus, flat, red or discoloured bumps appear, almost rash-like, on the skin around the hands, feet mouth and buttocks of the patient. These can often blister and become vesicular sores (5). This rash is rarely itchy for infants, but it can be extremely itchy for an adult with the disease. The disease, whilst quite infectious, is normally self-limiting and symptoms usually disappear 7 to 10 days after disease onset (Fig 1) (5-10). Although HFMD is typically a mild illness, severe complications can sometimes occur. These include encephalitis, meningitis, acute flaccid paralysis, cardiorespiratory failure and can be fatal (Fig 1)(11).

The coverage of HFMD, with the exception of Polar regions, is global in distribution (12-21). The disease is most prevalent in the Asian-Pacific region where it has been endemic since the 1990's; and has subsequently caused large-scale epidemics every few years (21-30). Unfortunately, there are no specific anti-viral treatments for any of the viruses that cause HFMD.

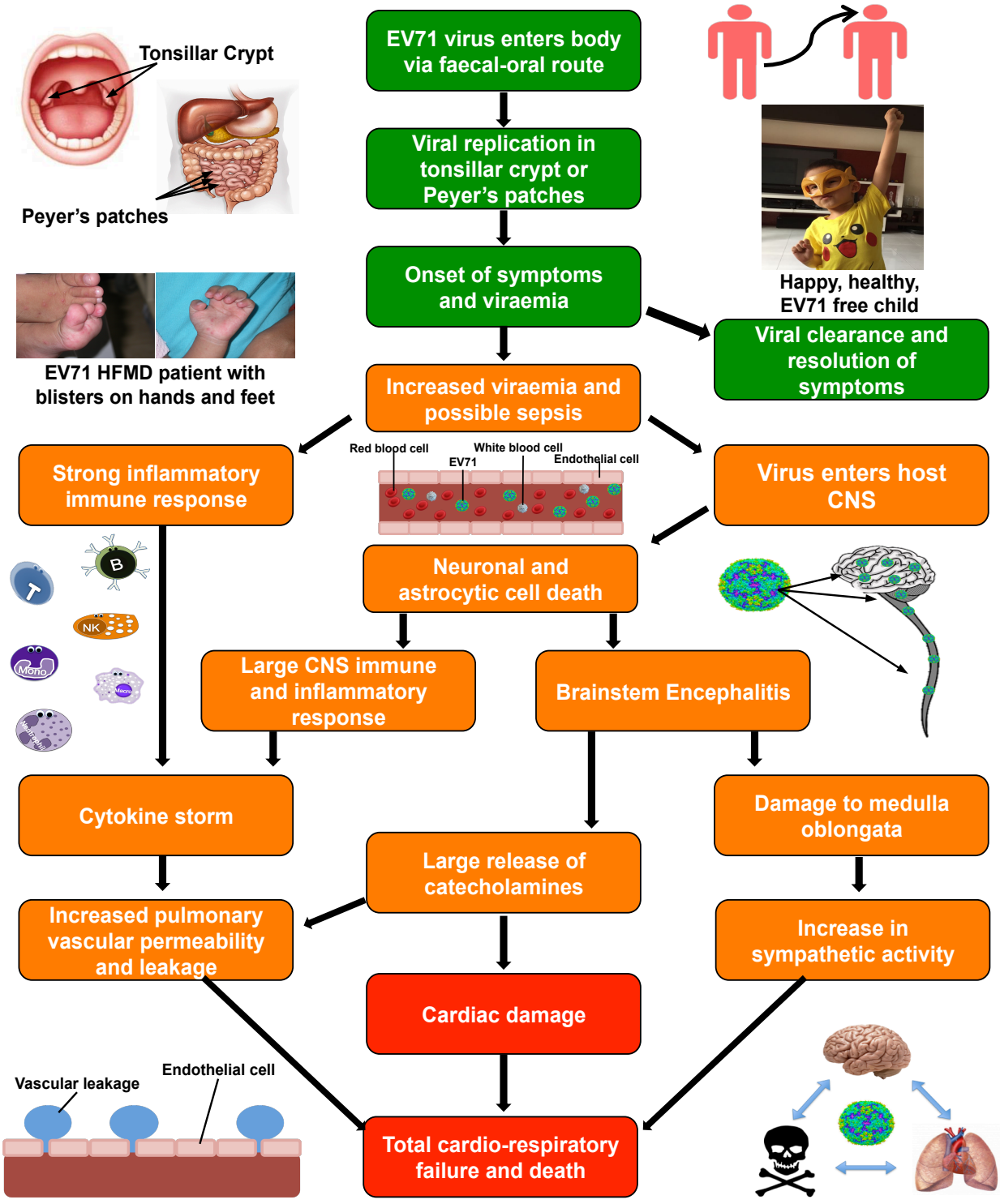

<u>Figure 1.</u> The immunopathophysiology of EV71 and the symptoms it leads to. Flow diagram representing the pathogenesis and immune response to an EV71 infection. **Green** represents outcomes with mild symptoms that are usually resolved in 7-10 days, including photos of patient with hand, foot and mouth disease symptoms (left) and a healthy child (right). **Orange** shows pathophysiology and host responses which lead to moderate to severe outcomes and **red** symbolises severe to fatal outcomes. The photographs in this figure were published with consent from the parent /legal guardians of the children.

Therefore, the treatment strategies for mild HFMD consist of palliative care including rehydration, analgesics for painful blisters and anti-inflammatories to reduce swelling (31-33). There is also no specific treatment of more severe HFMD that can be complicated by cardiorespiratory collapse. Key treatments are mechanical ventilation and inotropic support. Empirical treatments such as IVIG and continuous renal replacement therapy have been used in recent Asian outbreaks, but there are largely anecdotal (32, 33).

1.2.0 Epidemiology and Spread

HFMD usually affects children between the ages of 6 months to 5 years old; as this is the time when they no longer receive the benefits of passively transferred maternal antibodies. These antibodies can aid in protecting them from the etiological agents i.e. EV71 that cause the disease, when their own immune system is not fully developed to fight the virus on its own (34). After the first encounter with the virus the child should start producing antibodies against the viral agent. These antibodies may offer a cross protective effect the next time the child encounters a HFMD causing virus (35-37).

The main etiological agents of HFMD are the coxsackievirus A16 (CA16) and enterovirus 71 (EV71), both of which are from the *Enterovirus A* species of the Enterovirus genus of the *Picornaviridae* family (38-40).

Other viruses such as coxsackie A5, A6, A9, A10, B2, and B5 have also been reported to cause the disease (17, 41-46). Of the two main, etiological agents that cause HFMD, only EV71 leads to neurological complications. (Fig 1) (7, 24, 33). Since the almost total eradication of poliovirus, EV71 has become the most important neurotropic *Enterovirus* in the world. However, there is still much that is unknown about the interactions of this virus and more studies are required in this area to fully unravel the complete mechanism of EV71 (47, 48).

EV71 has been found all over the world with different symptoms and clinical manifestations seen during different outbreaks. The virus was first isolated in California, USA in 1969 from patients suffering from central nervous system (CNS) infections with cutaneous signs (49). EV71 was next seen in Europe, in Bulgaria and Hungary where patients suffered from CNS infections with cardiorespiratory failure and acute flaccid paralysis (50, 51). EV71 was also starting to be seen in Asia at this time, with Japan reporting outbreaks of HFMD and CNS infections caused by EV71 (52, 53).

In 1997 an outbreak of EV71 presenting with HFMD, cutaneous infections, CNS infections, cardiorespiratory collapse and sudden death was reported in Malaysia (8, 54). Since then, outbreaks and epidemics of EV71 with these clinical manifestations have become endemic to the Asian-Pacific region (21-30).

This protracted epidemic has drawn specific scientific interest. These outbreaks, with their larger variety of symptoms have drawn more questions that need answering about EV71 and its pathophysiology.

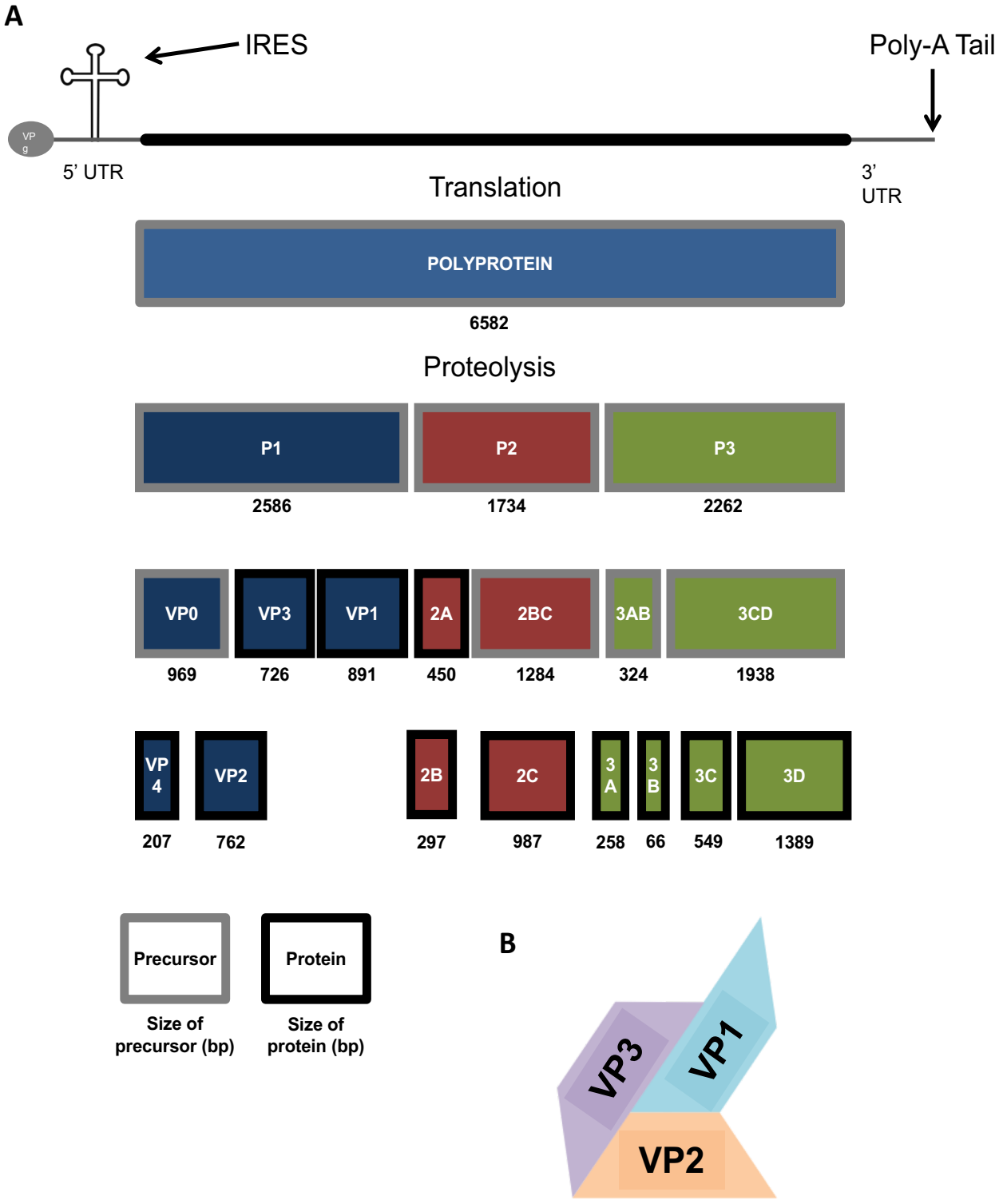

Figure 2. The genomic and molecular make up of the EV71 genome.
(A) Diagram showing the EV71 genome, polyprotein and protein products produced during EV71 replication, size in base pairs (bp) also show. **(B)** Picture representation of the T=3 structure of the VP1-3 structural genes of the EV71 capsid.

1.3.0 Biology of EV71

1.3.1 Genome Organisation

EV71 is a positive sense RNA virus, with a genome approximately 7.4kb long with one open reading frame coding for the 4 structural (VP1-4) and 7 non-structural proteins (2A-C and 3A-D) (55). The genome is initially translated as a single polyprotein, which is then cleaved into the three cleavage intermediates P1, P2 and P3 (Fig 2). P1 is cleaved into VP3, VP1 and VP0 (which is then in turn cleaved to form VP4 and VP2). The VP1, VP2 and VP3 proteins form a surface pentameric subunit together with the VP4 protein, attached to the inner surface (Fig 2). The capsid is formed by a quasi-T = 3 symmetry of 60 copies of this subunit to form an icosahedral capsid (56).

P2 is cleaved to form the viral protease 2A, and the 2BC polyprotein, which is then further cleaved in to the two non-structural proteins 2B and 2C. The protein 2B is thought to be a viroporin (57), which is important for the replication of the viral genome. It is thought to create a pore in the ER of the host cell and consequently releases Ca_2+ ions in the cell's cytoplasm, which may trigger membrane trafficking and viral protein transport (57). 2C is one of the most complex proteins in the EV71 genome, however its full function has not been discovered yet. 2C has been shown to play a role in encapsidation (58), cellular membrane rearrangement (59), immune evasion (60), RNA replication (60) and uncoating (61).

P3 is initially cleaved into 3AB and 3CD, and then further proteolysed to form the 3A, 3B, 3C and 3D proteins (Fig 2) (62). 3A localises the replication complex of the virus to the surface vesicle membranes, it also inhibits ER-to-Golgi apparatus transport in host cells and causes the Golgi complex to disassemble. This results in the depletion of IFN receptors and MHC (63). The 3B protein is also known as VPg (viral protein genome-linked), which acts as an initiator for EV71 replication by covalently linking the genomic RNA (64). 3C is EV71's other protease, which is responsible for most of the cleavage of the junction sites within the EV71 polyprotein (65). It also acts as part of the replication complex by binding to the 5'UTR of the viral RNA (66). Another function of the 3C protein is the cleavage of host immune factors such as TRIF (67) and RIG-I (68), to aid viral immune evasion. EV71's 3D protein acts as a RNA-directed RNA polymerase, which replicates the viral genomic RNA (69).

EV71 has been divided in to 6 genogroups, A, B, C, D, E and F. The genogroups B and C can be further divided into the sub-genogroups B0-B5 and C1-C5. These genotypes were identified through genetic analysis of the VP1 gene (40). All of the genogroups of EV71 have an amino acid (aa) sequence similarity of over 90% to the virus genogroup A prototype BrCr strain; with B > 92.2%; C > 91.9%; D = 95.2%; E > 93.6% and F > 93.6% (70). They also have a high amino acid sequence similarity within the subgenogroups individually, with A > 94.9%; B > 95.9%; C > 94.2%; E = 96.9% and F = 96.9% (information on D not available) (70). While the B and C subgroups have a global distribution, D, and E and F are restricted

to India and Africa respectively (70). Further phylogenetic analysis and Bayesian relaxed molecular clock method experiments suggests than EV71 originally emerged from CA16 around 1941 (40).

1.3.2 Virus life cycle

As humans are the only known hosts of EV71, all transmission is assumed to be human-to-human. The virus can survive on external surfaces for up to 3 days, so direct human-to-human contact is not always necessary as the virus can be picked up from these contaminated areas (71). The main route of transmission is through the faecal-oral route (71), however it can also be spread through contact with virally contaminated vesicular fluid, surfaces, fomites and oral secretions as well as respiratory droplets (Fig 1) (72). EV71 has been also found in faecal samples of symptomatic patients up to 75 days after infection, and up to 14 days in the throat (73).

Evidence suggests that the initial phase of replication occurs in lymphoid tissues of the tonsillar crypt (74) and in the Peyer's patches of the small intestine (Fig 1) (71). The virus undergoes further replication in the adjacent lymph nodes (cervical and mesenteric lymph nodes respectively) and this often leads to a mild viraemia (75). In the majority of patients, viral infection is controlled at this point and the patients remain asymptomatic (76). However, if the viral infection is not controlled, the virus will then reach high titres, and disseminate to the skin and mucous membranes to cause HFMD. In a small proportion of patients, EV71 can also enter the central nervous system and cause severe complications (Fig 1) (72). It has been

noted that children who had detectable viraemia after 3 days had significantly more severe complications (Fig 1) (75).

Retrograde axonal transport has been proposed as the method of entry to the brain and CNS for EV71, as when mice were inoculated at the hind limbs with EV71 the virus appeared to be spread from the lower to the upper spine (77). However, with many receptors for EV71, including one on lymphocytes (78) retrograde axonal transport may not be the only mode of entry. After gaining entry to the brain and CNS, EV71 causes neuronal and astrocytic cell death (Fig 1) (79, 80), which in turn leads to the CNS immune and inflammatory response and brainstem encephalitis (Fig 1) (79). This leads to the mass release of certain cytokines, known as a cytokine storm (81). There have been many cytokines implicated in EV71 brainstem encephalitis which have been discovered to be significantly increased in patients that suffer from pulmonary oedema. These include IL-1β, IL-1RA, G-CSF (82), IL-6, IL-10, TNF-α and IFN-γ (Fig 1) (81, 83, 84). The destruction of the brainstem during EV71 infection, including the vasomotor and respiratory centres leads to a surge of catecholamines and autonomic dysfunction (85, 86), which may be the cause of cardiorespiratory problems (Fig 1).

It is currently unknown what is the exact cause of cardiac failure and pulmonary oedema but is thought to be a combination of these elements, cytokine storm and brainstem destruction.

1.3.3 Host Receptors

At least five molecules have been identified as possible cell surface receptors for EV71. Scavenger receptor B2 (SCARB2) (87), P-selectin glycoprotein ligand-1 (PSGL-1) (78) sialylated glycan (88), heparan sulphate (89) and annexin II (Anx2) (90) have been reported to act, individually, as receptors for EV71. The most characterised of these five are scavenger receptor class B member 2 (SCARB2) and P-selectin glycoprotein 1 (PSGL-1) (78, 91). SCARB2 (also known as LIMP-2) is a highly abundant protein found in the lysosomal membrane, which participates in the reorganisation and membrane transport of the endosomal/lysosomal compartment. SCARB2 can acts as a receptor for all strains of EV71 and is considered the critical receptor for infection (92). PSGL-1, which is primarily expressed on the surface of leukocytes, is involved in leukocyte rolling/interacting with the vascular endothelium in the early stages of inflammation (93). A post translational modification, namely the tyrosine sulphation at the N-terminus of PSGL-1 was identified as being crucial for the binding of PSGL-1 to EV71 and for viral replication in lymphocytes (94). Some EV71 subgroups do not utilise PSGL-1 as a receptor to enter immune cells, as they cannot bind to the receptor. Only viruses with a G or Q amino acid at residue 145 of the structural protein VP1 can bind to PSGL-1 (95).

Mouse L929 cells that normally do not support EV71 infections, became highly infected with EV71 after being transfected and overexpressed with

either SCARB2 or PSGL-1 (92). Although the L-SCARB2 cells were shown to be more susceptible to EV71 infection than L-PSGL-1 cells, they bound with a lower amount of EV71 when compared with the L-PSGL-1 cells. This indicates that the binding ability of the receptor does not determine the infection efficiency of said receptor (92).

1.4.0 Infection and Immunity

As there is currently no effective treatment available for EV71, understanding virus/host interactions in greater detail will provide an increased knowledge base for the successful development of medical countermeasures (4).

The innate immune response is one of the body's earliest ways of fighting off pathogens (96). This immune response uses specific receptors that can recognise diverse foreign moieties and then launch an immune response to try and limit the infection (96). The innate immune response is much less specific than the adaptive immune response, but much more rapid and reacts instantaneously upon the discovery of pathogens. The first line of defence contributes by effectively limiting the infectivity of a pathogen, as well as activating the adaptive immune response to help destroy and clear the pathogenic organism (96).

Host cells, both immune and non-immune contain innate receptors called pattern-recognition receptors (PRRs), which can recognise materials/molecules of pathogens, and components of cell damage/death. These PRRs recognise the pathogens via the detection of PAMPS (pathogen associated molecular patterns) (97). PRRs can also recognise molecules from stressed/dying cells, named danger associated molecular patterns (DAMPs) and launch a response (98). The main receptors of viral PAMPs are toll-like receptors (TLRs), nucleotide oligomerisation domain

(NOD) like receptors (NLRs) and retinoic acid inducible gene I (RIG-I) like receptors (RLRs) (99).

1.4.1 Innate Immunity against EV71

EV71 is mainly detected via the RLRs; RIG-I, melanoma differentiation-associated protein 5 (MDA5), and TLR3 (100). The binding of EV71 to the RLRs sets off a signalling cascade activating mitochondrial antiviral-signalling protein (MAVS). MAVS associates with tumour necrosis factor (TNF) receptor associated factor 3 (TRAF3), recruiting TANK-binding kinase 1 (TBK1) and IκB kinase, leading to the phosphorylation of interferon regulatory factors 3 and 7 (IRF-3 and IRF-7) (101) (Fig 3). This phosphorylation causes these two IRF molecules to dimerise, causing the formation of hetero- and homodimers, which translocate to the nucleus and bind to interferon stimulate response elements (ISREs). This leads to the expression of type I interferon genes (101). MAVS activates NF-κB through a caspase 8/10 dependent pathway (102) (Fig 3). TLR3 also activates NF-κB by inducing TIR-domain-containing-adapter-inducting Interferon- β (TRIF), which associates with receptor-interacting protein 1 (RIP1), activating NF-κB (Fig 3). This coordinated network activates many pro-inflammatory cytokines, chemokines, enzymes and adhesion molecules to fight the pathogen (103).

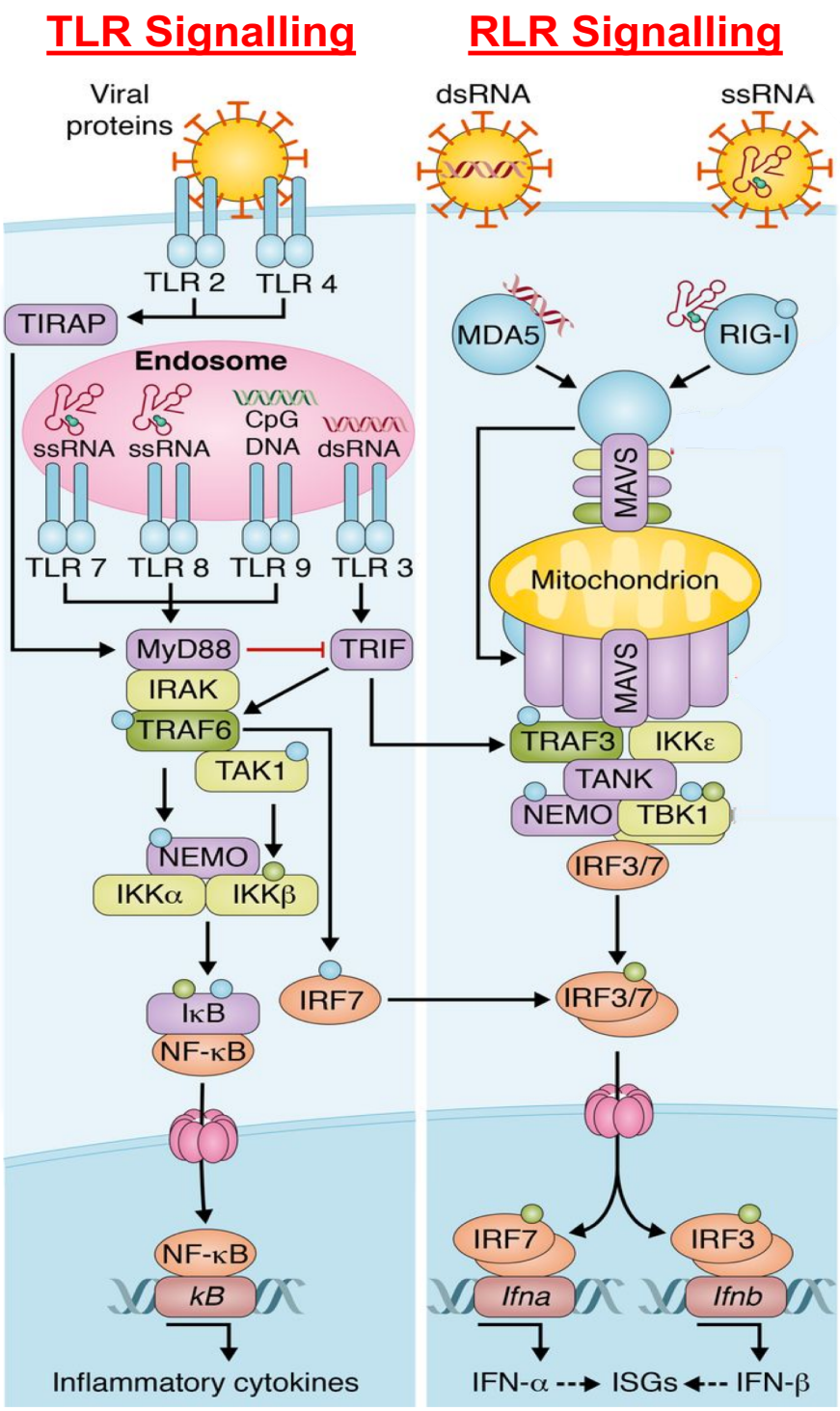

Figure 3. Signalling cascade of TLR's and RLR's during viral infection. PRRs scan both the intra and extracellular environment for pathogenic complexes. If found, ligand-activated receptors bind adaptor proteins and recruit protein kinases and ubiquitin-protein ligases. This causes the regulation of immune signal transduction to transcription factors through post transcriptional modification of signalling cascade proteins. Activated transcription factors then translocate into the nucleus and bind to promoters, stimulating appropriate antiviral gene transcription. Blue and green circles represent ubiquitination and phosphorylation, respectively. Black arrows = activation; red lines = deactivation. Adapted from Heaton *et al;* JEM 2015

Interferons (IFN's) are molecules that are vital to the body's immune response in order to help control virus replication and spread (104). Based on the interaction they have with their receptors, they have been categorised into three groups; type I, type II and type III. Both type I and type III IFNs have been suggested to play vital roles in the defence against viral infections (105). Specific interferon-α (IFN-α; a type I IFN molecule produced by leukocytes) subtypes have been shown to be inhibitors of EV71 infection (IFN-α4, 6, 14 and 16) (106). Unfortunately, IFNs have only been shown to be effective as pre-treatments as *in vivo* and patient studies suggest that IFN's offer little help as a treatment after contraction of the virus (107).

Viral proteases are vital for the processing of most viral polyproteins. EV71 relies on its two proteases, 2A and 3C, to cleave viral protein precursors into their functional forms (Fig 2) (108). These proteases not only cleave viral proteins, they can also cleave host proteins to aid in immune evasion (109). Viral protease 2A has been shown to cleave MDA5, the main cellular receptor for detecting EV71 infection (Fig 3). This cleavage diminishes the production and activation of IRF-3 and IFN type I (110). The EV71 protease 2A can also cleave MAVS at several sites which again leads to the disruption of IRF-3 phosphorylation and a decrease in type I IFN production, leading to increased EV71 propagation, compared to if the response was active (102). Data has been presented that suggests 2A interferes with IFNAR I by reducing its expression (111). The reduction in IFNAR I expression has been postulated as why exogenous IFN has had

limited effect as a treatment (112). However, this hypothesis is still contested by some (113), and more evidence will be needed to address this hypothesis.

Inhibition of the host interferon response has also been shown by the 3C protease (68). 3C interacts with the N-terminal domain of RIG-I preventing the interaction with MAVS and leading to a decrease in nuclear translocation and expression of IRF-3 and IFN (Fig 3) (68). Similarly, EV71 3C has been shown to bind and degrade IRF-9 (114) and to cleave IRF-7 (115) impairing the ability of these two cellular proteins to stimulate the production of ISGs and IFN.

1.4.2 EV71 and host replication factors

The genome of EV71 is uncapped and therefore initiation of translation by ribosomes is facilitated by the presence of a type I internal ribosome entry site (IRES) (116). This tertiary RNA structure is a common feature at the 5' end of picornaviruses. Initiation of translation at an IRES requires specific cellular proteins and their absence can lead to inefficient IRES-dependent translation. During EV71 and general *Picornavirus* infection, host cell factors, known as IRES transacting factors (ITAFs), involved in the initiation of cap-dependent translation on host mRNAs are degraded by viral proteases (109). Thus inhibiting cap-dependent host cell translation and facilitating the translation of viral genomes (which act as an mRNA) (117). During viral infection, EV71 expresses viral protease 2A that cleaves eIF4G, part of the eukaryotic initiation factor 4F complex (eIF4F) needed

for cap dependent translation. Although this results in a significant decrease in the hosts capped mRNA translation, it increases the translation efficiency of the EV71 IRES (118).

Some novel ITAFs for EV71 have also been discovered. Far upstream element binding protein 1 and 2 (FBP1 and 2) have both been identified as novel ITAFs for EV71 (119, 120). FBP1 enhances the replication activity of the virus and IRES-dependent translation. FBP2 however has been shown to be a negative regulator of IRES activity, by out competing the positive ITAF hnRNP1 (116). However, EV71 infection triggers proteasomal, autophagic and caspase activity mechanisms of the host cell, which cleave FBP2, and these cleavage fragments transform FBP2's function from a negative regulator to a positive promoter. (119, 120)

EV71's ability to interrupt, intercept and disrupt the host immune response is critical to the survival and propagation of the virus, and whilst this has a negative effect for the patients, it gives an insight into possible areas that could be targeted to disrupt virus biology.

1.4.3 Adaptive Immunity and EV71

Even though there is still a lack of understanding around the viral infection process. Especially concerning the viral migration from the primary sites of infection e.g. tonsils, Peyer's patches and respiratory mucosa to the brain and CNS via the circulatory and nervous systems. Previous studies have identified possible mechanisms of pathogenesis during EV71 infection (77,

121, 122). Several of the EV71 specific receptors can be found on certain human white blood cells. DC-SIGN has been reported on the surface of immature dendritic cells (123), annexin II, SCARB2 and PSGL-1 have been shown to be expressed on the surface of dendritic cells, monocytes and epithelial cells (78, 90, 124). With PSGL-1 also being found on B cells, T cells and neutrophils (125, 126). EV71 has been found to have the ability to infect immature dendritic cells *in vitro*, offering the possibility that it can migrate from here into the associated tissues and organs e.g. the brainstem and CNS (123). Furthermore, high levels of EV71 have been found in the lymphocytes of infected animal models (127) and human patients (50). This suggests that there is an interaction between these leukocytes and the virus during severe EV71 infection.

1.5.0 Deciphering pathophysiology using *in vitro* and *in vivo* models

1.5.1 In vitro cellular models

In vitro models whilst being the initial “go to” model for viral experiments, can come in many different forms and serve many different purposes. The most basic of these are isolation and viral kinetics, for which rhabdomyosarcoma (RD) cells are the most utilised for EV71 (128). One major advantage of *in vitro* cellular models is that they can be adapted and modified very easily. This aids the discovery of important proteins and cellular functions that would otherwise be extremely difficult. The EV71 cellular receptor, SCARB2 was identified utilising *in vitro* techniques. Mouse L929 cells, not known to be targeted by EV71 were first transfected with RD cell genomic DNA and then infected with EV71. Transcriptomics analysis on highly infected cells identified SCARB2 as the receptor responsible for this new ability to become infected (87). PSGL-1 was discovered using Jurkat cells, an immortalised T cell cell line (78). A retroviral cDNA library from EV71 susceptible Jurkat cells was generated and then used for expression cloning. Transduction of P3U1 produced four colonies that bound to EV71 coated dishes, which all encoded PSGL-1 (78). Without this in vitro model, this discovery may not have occurred as *ex vivo* primary T cells do not easily proliferate (especially without stimulation), and therefore this type of experiment would not have been feasible.

Another advantage of using cell lines is they can provide lines that are not always readily available as primary cells. Primary human monocytes and T cells often not easily accessible due to availability or ethics, however with *in vitro* cell lines such as THP-1 (monocytes) or Jurkat (T cells) these issues can be easily overcome. THP-1 cells have been used to show the role of NLRP3 inflammasome activation and IL-1β maturation during interaction with the EV71 protein 3D (129).

1.5.3 *Ex vivo* models

Whilst they are not always readily accessible, primary *ex vivo* models can be of huge benefit to investigations as they bridge the gap between immortalised *in vitro* cell lines and *in vivo* animal models. They provide insights into how the body might react to an infection without any chance of harm to the host. Understanding EV71's ability to infect immune cells and their possible role in EV71 severity and fatalities was not always clear. However, using *ex vivo* models allowed studies to investigate the direct effect EV71 has on these immune cells and any indirect downstream effects (130). EV71 was shown to directly infect monocytes and lymphocytes from freshly isolated blood mononuclear cells (PBMCs) and induce the production of pro-inflammatory cytokines such as TNF-α and MIF during the course of an infection (130). *Ex vivo* models have been used to show how the activation of JNK1/2 and p38 MAPK pathways can promote EV71 infection in dendritic cells (DCs) (131).

Cell Line	Uses	Benefits	Drawbacks
Rhabdomyosarcoma (RD) - Human Muscle	General viral propagation, general cell assays, detection assays, proliferation assays, viral titre determination	Very easy to grow and proliferate. Easily infectable with all strains of EV71. Can be used for a wide variety of different assays and experiments.	Immortalised cell line, so they have limited characteristics compared to primary cells. RD cells are originally from muscle cells which is not a main target of EV71 so not fully representative.
Vero - African Green Monkey Kidney	Same as RD cells	Very easy to grow and proliferate. If infectable, can be used for a wide variety of assays and experiments. Grow in a monolayer so can be used for plaque assays.	Not as effective as RD cells. Not all virus genotypes/subgenotypes will infect and/or replicate in vero's, hence why RD cells are the main go to cell.
Jurkat - Human T Cell	To study the effect and role of EV71 infection in T cells	Have a close phenotype to primary T cells, but are much easier to grow and cultivate. Do not require any external stimulation to proliferate (e.g. IL-2).	They are an immortalised cell line so their characteristics may deviate from primary T cells which may result in altered or unrealistic phenomenoms.
THP-1 - Human Monocyte	To study the effect and role of EV71 infection in Monocytes	Have a close phenotype to primary monocytes, but are much easier to grow and cultivate. Will only differentiate if stimulated with PMA, unlike primary monocytes which will differentiate with time.	They are an immortalised cell line so their characteristics may deviate from primary monocytes which may result in altered or unrealistic phenomenoms.
SK-N-SH - Human Brain	To study the effect and role of EV71 infection in the brain and neurons	Have a close phenotype to primary neurons, but are much easier to grow and cultivate. Will proliferate spontaneously, compared to primary neurons which only differentiate and do not proliferate.	Immortalised cell line. Do not grow uniformly, tend to grow in clumps. Can become differentiated which will alter the effect of the virus on the cells and produce different response.
L929 - Mouse Connective Tissue	To study the function of EV71 receptors and their ability to facilitate infection	Useful for the study of receptors, any infection seen is due to receptor's interaction with EV71, false positives are rare as wild type cell line cannot be infected.	Cannot be infected by EV71 unless transfected with the appropriate receptors. Can only be used in the study of EV71 receptors and functionality.
PBMCs – Human Peripheral Blood Mononuclear Cells	To study EV71 in primary blood cells and study the effect of EV71 on the immune system and host defence pathways	Closest cells to replicate host response, without doing an in vivo experiment. As no serum or plasma present then it is unlikely there will be any interference from donor antibodies.	Show low level infection with EV71. Not always readily available in the necessary numbers. Ethical approval needed. Cannot easily proliferate, so long term studies difficult.

Table 1. Table showing the commonly used cell lines in EV71 experiments, their uses, benefits and drawbacks.

1.5.4 *In vivo* animal models

Interestingly, *in vivo* mouse models of EV71 have demonstrated an age-dependent susceptibility to the virus (132-135). Non-transgenic, immunocompetent mice are resistant to EV71 infection once they are past the weaning stage, regardless of the route of infection (132-135). In an effort to develop an EV71 mouse model more similar to the onset of human disease, mouse-adapted EV71 strains have been generated that are capable of infecting mice via the oral route, and can cause neuropathology in the brainstem and spinal cord as well as paralysis of the rear limbs (136-138). However, these models still have an age limitation and do not cause the onset of disease after the mice reach 14 days old (136-138). Whilst these models are not ideal due to their age-limiting factor, they have still proven to be useful tools in the examination of EV71 pathogenesis. This model was used in the discovery of type I interferon being an essential innate defence mechanism in the controlling or EV71 infection and that EV71 tries to avoid this mechanism by inhibiting type I interferon through its 3C protease (107, 139).

To get around this age limitation, immunocompromised models such as NOD/SCID (133) and AG129 (135) mice have been used which cause similar features and symptoms seen in the immunocompetent mouse models but in older mice (133), (135). Whilst this is an advantage, it also has its drawbacks, namely immunocompromised mice stray further from

the human model they are trying to replicate and thus give us a less reliable report on what may be causing these symptoms in humans (140).

Transgenic mice containing the human EV71 receptors SCARB2 and PSGL-1 have been generated and been shown to be infected with EV71 to varying degrees (132, 141). Mice expressing the PSGL-1 gene are only susceptible to mouse-adapted strains of EV71, and whilst this model exhibited symptoms that were similar to those seen in wild-type mice, these mice suggest that PSGL-1 cannot provoke EV71 infectivity in mice on its own (141). Transgenic mice that express the human SCARB2 in their CNS neurons, lung pneumocytes, hepatocytes and intestinal epithelium (i.e. similar profile to humans) have been shown to be susceptible to infection by EV71 after they are 6 weeks of age. These mice display symptoms of neurotropism, neuropathology, ataxia, paralysis and death, which are similar to symptoms seen in humans (132).

Non-human primates have been shown to be susceptible to EV71 infection and have since been used in various studies (122, 142). Cynomolgus monkeys show very similar neurological manifestations of symptoms when infected intraspinally or intravenously, including acute flaccid paralysis, ataxia and encephalitis. The animals also presented with a broad viral circulation including spinal cord, cerebrum, brainstem and CNS (122) (142). However, they do not suffer from blisters or lesions on the skin, nor do they suffer from pulmonary oedema (122, 142). A Rhesus monkey model has also been used to assess EV71 infection. These monkeys also

develop CNS infections after intracranial, intravenous, intratrachial or orally given virus. Tissue damage and cellular infiltrates in the lungs were noted in these monkeys, they were not observed in the spleen or pancreas, which also show high viral load. Although these monkeys did not show vesicular lesions on the skin or typical neurological symptoms, half of them did suffer from pulmonary oedema when infected intracranially (143). This is the first model to show this symptom outside of humans, however it is not known if the pulmonary oedema is due to CNS damage and inflammation or if it is a consequence of viral cytolysis in the lungs (143).

Whilst these animal models are not perfect representations of the disease or the route in takes in humans, they still provide us with lots of crucial information on the role of the virus and of the host immune response.

1.6.0 Potential therapeutics for EV71

1.6.1 Antivirals

Many drugs that have been already developed and used to fight other *Picornaviruses*, such as polioviruses and rhinoviruses, were tested for their abilities to limit EV71 infection. These drugs, ribavirin (144, 145), pleconaril (144, 146) and rupintrivir (147) have all shown some sort of protective antiviral effect in mouse models. However, it remains to be seen how this would be translated to human infections. Also as the EV71 genome is synthesised through the virus's 3D polymerase (148), which lacks a proofreading activity, mutations frequently arise and could quickly lead to the generation of antiviral resistant viruses (149).

The recent discovery of the crystal structure of EV71 (56) has shed some insights into possible drug targets for future antivirals against EV71. The resolution of this structure by x-ray crystallography showed the presence of a hydrophobic pocket factor located underneath a depression known as the canyon. It has been postulated that the binding of molecules to this pocket region could stabilise the capsid and therefore inhibit the uncoating process induced by the EV71 receptor (56). Several compounds have been created which bind to this pocket region and showed effective *in vitro* inhibition of EV71 (150-155). However, just a single point mutation was enough to confer resistance against this type of compound (156).

Type I IFN, has been shown as an effective antiviral to treat viral infections such as HCV (157), so experiments were done to investigate IFNs ability as an EV71 therapeutic. Studies have shown in both *in vivo* (107) and *in vitro* (106) systems that IFN could increase the survival rate and reduce EV71 replication (106, 107). However, the viral proteases 2A and 3C have the ability to degrade IFN and the IFN antiviral pathway and may lead to the reduction in expression of interferon-α/β receptor (IFNAR) (68, 102, 110, 112, 115). There have been reports of synergistic effects when 3C inhibitors and IFN are combined (114), but this would have to be combined with a 2A inhibitor to further inhibit the interruption and degradation of IFN.

1.6.3 Monoclonal antibodies

As there is no current antiviral treatment, and vaccine development, whilst currently underway, is not fully approved outside of China, human IVIG has been used on a presumptive basis as a last resort (158). This treatment has perceived positive benefits, possibly through modulatory properties or viral neutralisation, but is not wholly effective and has not been tested via a randomised controlled trial. IVIG also poses a potential risk of infection via other pathogens. Humanised mouse monoclonal antibodies eliminate this risk whilst increasing the specificity against the virus. Humanised mouse monoclonal antibodies against other viruses such as RSV have already been approved by the FDA (159, 160).

There have been several studies that suggest that monoclonal antibodies could be an effective treatment against EV71 infection, and multiple sites

on the virus have been found as possible targets. Plevka et al. raised two antibodies against an empty immature EV71 particle in mice. The structure of this particle, which is similar to the “A” particle seen when EV71 recognises a host cell before genome release, differs from that of a mature virus. These antibodies were shown to neutralise EV71 *in vitro* by instigating a conformational change after incubation with the mature virus, transforming the infectious virus into an “A” particle and instigating genome release (161).

Another antibody, produced against the EV71 virus like particle (VLP) showed potent neutralising capabilities *in vitro* (162) It was later discovered that the antibody bivalently bound across the 2-fold axis of the EV71 virion, potentially preventing the conformational changes in viral capsid proteins required for viral genome release (163).

Antibodies raised in mice against a conserved VP3 knob region have shown protective neutralising effect across the different subgroups of EV71 (164). Whilst both antivirals and monoclonal antibodies remain important tools to fight EV71 infection, a vaccine still serves as our best chance at eradicating this virus, as shown with the almost total eradication of polio after the introduction of the Salk and Sabin vaccines (165).

1.6.4 Vaccines

After the success of the polio vaccines, it was envisioned that EV71, closely related to polio, would also be an easy target for near eradication via a

vaccine. Studies in mice demonstrated that the transfer of antiserum provided protection against EV71, further indicating the attainability of a vaccine (166). EV71 vaccine candidates have been suggested in many different forms; from attenuated strains (167), inactivated whole virus (168), and virus like particles (VLP) (169) to recombinant proteins (170) and peptide vaccines (171).

Live attenuated vaccines have been tested in cynomolgus monkeys and these induced the production of high levels of neutralising antibodies that provided cross protection across the sub groups (172). However, as with all live attenuated vaccines, there is the possibility for the virus to mutate and cause disease. One study showed a vaccine candidate producing mild neurological symptoms and being neurotropic when injected intravenously (167).

DNA vaccines have been attempted for EV71. However, DNA constructs containing EV71 VP1 gene that elicited specific VP1 immunoglobulin G's (IgG's) and neutralising antibodies conferred low levels of antigenicity (173).

Inactivated whole virus vaccines have been shown in mouse models of EV71 to produce very high levels of virus specific antibodies that are cross neutralising (174, 175). These successful pre-clinical studies lead the way for phase I (176) and phase II (177) clinical trials, and since then three vaccines have moved on to phase III clinical trials, all from China and

based on the C4 strain (168, 178, 179). These trials involved over 30,000 children and resulted in the prevention of 90% of HFMD and 80% of other EV71 related symptoms, and the Chinese FDA has approved two of these vaccines. Although these vaccines have only been approved in China, this is a very exciting prospect in the eradication of EV71. However, there is still work to be done on antiviral treatment and therapies for the treatment of patients and to help unravel the mechanisms behind this disease.

1.7.0 The Blood-Brain Barrier

The blood-brain barrier (BBB) is a highly selective, diffusion barrier, formed by the endothelial cells that make up the cerebral microvessels and capillaries, and by astrocytes and pericytes on the brain side (180, 181). Whilst all three cell types are important for the function, structure and integrity of the BBB, the cerebral endothelial cells are particularly crucial. Especially as they form the tight junction seal (182), that is the mainstay of the barrier, and that physically prevents the entry of many dangerous molecules and components into the brain (183). These tight junctions stop these possibly neurotoxic substances from entering the brain via the paracellular route and instead force them towards the transcellular route (184).

Endothelial cells of the BBB are uniquely distinctive from other endothelial cells as their barrier function is majorly enhanced. Cerebral endothelial cells possess a higher density of tight junction complexes compared to other endothelial cells, they also lack fenestrations and have a much more limited level of pinocytic vesicular transport. This combination of attributes allows them to tightly control the blood-brain barrier (183). However, sometimes during acute distress e.g. severe viral infections, BBB function can become impaired and many neurotoxic components could pass through to the brain side of the barrier and wreak havoc (185).

EV71 infections have been shown to induce a type I interferon (IFN) response (186). The dsRNA intermediate synthesised during viral

replication can be recognised by crucial PRRs, notably RIG-I (187), MDA-5 (188) and TLR-3 (189), that coordinate to control the innate immune response including IFN production. MDA5 receptor has been suggested to be more important than the other PRRs in EV71 infection, although TLR-3 and RIG-I do play roles in initiating the production of downstream effectors (187, 190). The signal transduction pathways involving these pattern recognition receptors have been proven to elicit a strong type I IFN response (191, 192). In which IFN serves as an antiviral agent, which aims to inhibit or slow down viral replication or upregulate proinflammatory cytokines for viral clearance (193-195).

However, during EV71 infection, IFN levels have been shown to be reduced, indicating that the active suppression of type I IFN response could be an immune evasion strategy of EV71 (111, 139). Type I IFNs have been proposed to be protective against BBB permeability during neurotropic viral invasion (196). Type I IFNs could directly preserve the structural integrity of the BBB by preferentially activating Rac1 (196, 197). Rac1 is a cytoskeletal regulatory GTPase that stabilises tight and adherens junctions to prevent BBB leakiness (197). The activation of Rac1, in turn, limits and blocks the activation of the antagonist effect of RhoA. RhoA can stimulate a cascade of inflammatory events, including the formation of stress fibres that destabilise TJs and promote BBB permeability (198). Furthermore, type I IFNs can also down-regulate the expression of inflammatory mediators that could compromise endothelial cell function, such as TNF-α and IL-1β (199).

1.8.0 Conclusion

There have been major breakthroughs in EV71 research in the last couple of decades: from the identification of host receptors, to the discovery of molecular mechanisms of virus-host interactions, to the phase III trials for vaccines. Although there is an understanding of EV71 pathogenesis, many areas of uncertainty remain with many mechanisms still not well understood and many pathways that have yet to be proven functionally. There is still a need for an animal model that better mimics the human disease. The development of such models will enable us to gain a much better understanding of the path of EV71 infection, and may give us an insight in to new molecular mechanism that I can target to interrupt the virus and stop the infection.

Chapter 2

Project Aims

2.1.0 To establish an *in vitro* infection system to study EV71 viral kinetics

- Is there any difference between viral isolates that cause mild disease and viral isolates that cause neurotropic disease?

2.2.0 To study the difference in infectivity and immune response in an *ex vivo* human blood infection system

- Does immune involvement play a role in this neurotropism?

2.3.0 To assess the ability of the different isolates to infect and cross the blood brain barrier

- Does neurovirulence increase the ability of EV71 isolates to infect or cross the blood brain barrier?

2.4.0 To study the inflammatory pathways involved in EV71 immunopathogenesis

- How do these pathways compare to those found in the patient samples during outbreaks?
- Do the different severities of disease induce different pathways?

Chapter 3

Materials and Methods

3.1.0 Cell Culture

3.1.1 Cells used

Cell Type	Media Used	Incubator Temperature	CO_2 Conditions	Additional Comments
Rhabdomyosarcoma (RD) Cells	Dulbecco's Modified Eagle's Medium (DMEM) + 10% Foetal Bovine Serum (FBS)	37°C	5%	
VeroE6 Cells	Dulbecco's Modified Eagle's Medium (DMEM) + 10% Foetal Bovine Serum (FBS)	37°C	5%	
Human Cerebral Microvascular Endothelial Cells/D3 (HCMECs)	Dulbecco's Modified Eagle's Medium (DMEM) + 10% Foetal Bovine Serum (FBS) + 500ng/ml Hydrocortisone + 5ng/ml EGF	37°C	5%	Grown on fibronectin coated flask
Primary Human Peripheral Blood Mononuclear Cells (PBMCs)	Iscove's Modified Dulbecco's Medium (IMDM) + 10% Human Serum (HS)	37°C	5%	
Primary Human CD14+ Monocytes	Iscove's Modified Dulbecco's Medium (IMDM) + 10% Human Serum (HS)	37°C	5%	
Primary Human CD4+ T Cells	Iscove's Modified Dulbecco's Medium (IMDM) + 10% Human Serum (HS)	37°C	5%	
Primary Human CD8+ T Cells	Iscove's Modified Dulbecco's Medium (IMDM) + 10% Human Serum (HS)	37°C	5%	

Table 2. Table showing the cell lines used in the following experiments, including information on the media, temperature and CO_2 conditions used.

DMEM, FBS – HyClone; **Hydrocortisone, Epidermal Growth Factor (EGF), Fibronectin, Claycomb Media, Norepinephrine, L-glutamine** – Sigma-Aldrich; **IMDM** – Gibco; **HS** – Innovative Research, Inc.

3.1.2 Cell passaging, propagation and maintenance

RD Cells – RD cells were grown to 90% confluence in DMEM +10% FBS at 37°C in 5% CO_2 in a T150 cell culture flask (Falcon). Once cells reached 90% confluence, they were washed with 1x Dulbecco's phosphate buffered saline (DPBS; Gibco) and trypsinised using 0.125% trypsin-EDTA (Gibco) at 37°C. Cells were dislodged from the flask then resuspended in fresh DMEM + 10% FBS and centrifuged at 1500rpm for 5 minutes. The supernatant was then removed and the cells resuspended in fresh DMEM + 10% FBS, this cell suspension was then added to a new T150 flask with fresh DMEM + 10% FBS and then placed in to an incubator at 37°C with 5% CO_2.

VeroE6 Cells – VeroE6 cells were grown to 90% confluence in DMEM +10% FBS at 37°C in 5% CO_2 in a T150 cell culture flask. Once cells reached 90% confluence, they were washed with 1x Dulbecco's phosphate buffered saline and trypsinised using 0.125% trypsin-EDTA at 37°C. Cells were dislodged from the flask then resuspended in fresh DMEM + 10% FBS and centrifuged at 1500rpm for 5 minutes. The supernatant was then removed and the cells resuspended in fresh DMEM + 10% FBS, this cell suspension was then added to a new T150 flask with fresh DMEM + 10% FBS and then placed in to an incubator at 37°C with 5% CO_2.

HCMEC/D3s – HCMEC/D3s were grown to 90% confluence in HCMEC media (DMEM + 10% FBS + 500ng/ml Hydrocortisone + 5ng/ml Epidermal Growth Factor) at 37°C with 5% CO_2 in T150 flasks coated with fibronectin at 500ng/cm^2. Once cells reached

90% confluence, they were washed with 1x DPBS and trypsinised using 0.125% trypsin-EDTA at 37°C. Cells were dislodged from the flask then resuspended in fresh HCMEC media and centrifuged at 1500rpm for 5 minutes. The supernatant was then removed and the cells resuspended in fresh HCMEC media, this cell suspension was then added to a new fibronectin coated T150 flask with fresh HCMEC media and then placed in to an incubator at 37°C with 5% CO_2.

HL-1 Cardiomyocytes – HL-1 cardiomyocytes were grown to 100% confluence in Claycomb media supplemented with 10% FBS + 100μM Norepinephrine + 2mM L-glutamine at 37°C with 5% CO_2 in T75 flasks coated with 0.02% gelatin/0.2ng/cm^2 fibronectin. Once cells reached 100% confluence and contracting, they were washed with 1x DPBS and trypsinised using 0.05% trypsin-EDTA at 37°C for one minute. Trypsin was then removed and fresh 0.05% trypsin-EDTA was added then incubated for an additional 2 minutes. An equal amount of soybean trypsin inhibitor (Sigma-Aldrich) was then added to inactivate the trypsin. Fresh Claycomb media was added and this suspension was centrifuged at 1500rpm for 5 minutes. The supernatant was then removed and the cells resuspended in supplemented Claycomb Medium. 1/3 of the cell suspension was then into a new gelatin/fibronectin-coated T75 flask, and then placed in to an incubator at 37°C with 5% CO_2.

3.1.3 Cell seeding

The same protocol as cell passaging, propagation and maintenance was followed until the resuspension after centrifugation. After resuspension in their respective media 10µl of the cell suspension was removed and added to 20µl of 0.4%TrypanBlue (Sigma-Aldrich) and mixed via pipette. 10µl of this mixture was then added to a haemocytometer and 4 corner squares of the 3x3 square.

Number of cells/ml =

$(X / D) * Y$ Where X= Number of live cells counted

D= Dilution Factor

Y= 1ml/volume of 1 haemocytometer corner square

e.g. (240 live cells / 4 squares) * 10^4

$=6*10^5$ cells/ml

Calculation for cell seeding

$(A / B) * N = Tc$ Where A= Number of cells needed

B= Number of counted/ml

N= Number of wells/flasks to be seeded

$Tv – Tc = Tm$ Tc= Total volume of cell suspension

Tv= Total final volume of all wells/flasks

Tm= Total respective media required

Tc was then resuspended in Tm and the volume required was added to each well/flask. The cells were then incubated at 37°C with 5% CO_2 overnight.

3.1.4 Cell freezing

The same protocol as cell passaging propagation and maintenance was followed to the point of centrifugation. After centrifugation cells were resuspended in freezing media (10% Dimethyl Sulphoxide (DMSO; Sigma-Aldrich) and 90% FBS), which had been passed through a 0.45µm hydrophilic filter (Sartoris). This was then aliquoted in 1ml aliquots into screw cap cryovials and placed into an isopropanol filled Mr Frosty (Thermo Fischer) and placed into a -80°C freezer to cool the cells at -1°C per minute. Once the cells reach -80°C they were placed into a cryobox and stored in a -80°C freezer or vapour phase liquid nitrogen tank for short term and long-term storage respectively.

3.2.0 Virus Production and Titring

3.2.1 Virus isolates

6 EV71 virus isolates were received from Dr Mong How Ooi and Dr David Perera, from the paediatrics unit of Sarawak general hospital. They were isolated from patients from the 2006 EV71 outbreak in Sarawak, Malaysia. They were isolated from 6 separate patients suffering from a varying degree of symptoms (Table 1).

3.2.2 Viral propagation from clinical isolates

Each of the 6 EV71 virus isolates was received in approximately 60ml of media. 5ml of each isolate was added to a separate t150 flask of 80% confluent RD cells and incubated at 37°C with 5% CO_2 for 1.5 hours. After the incubation, fresh DMEM + 10%FBS was added to the flask and incubated at 37°C with 5% CO_2 for 72 hours or until 90% cytopathic effect (CPE) was seen. The flask was then freeze thawed 3 times at -80°C. the virus was then pre-cleared via centrifugation at 1500rpm for 5 minutes before being aliquoted in to cryovials and stored at -80°C.

3.2.3 Viral propagation

Each EV71 virus isolate was diluted to 5ml at a ratio of 1:20 with DMEM serum free (SF) then added to a t150 flask of 80% confluent RD cells and incubated at 37°C with 5% CO_2 for 1.5 hours. After this incubation, the virus was removed and the flask was replenished with fresh DMEM + 10% FBS and left to incubate at 37°C with 5% CO_2 for 48 hours or until 90% CPE was seen. The virus was then pre-cleared via centrifugation at 1500rpm for 5 minutes before being aliquoted in to cryovials and stored at -80°C.

3.2.4 Viral titration

The viral titre was determined using a tissue culture infective dose 50 (TCID50) assay with RD cells. RD cells were seeded on a 96 well plate at 1.5E4 cells per well. The EV71 isolates were serially diluted in 10-fold dilutions until 10^{-11} in SF DMEM. The dilutions and one row of non-infected control were added to the wells at a volume of 80µl and incubated for 1.5 hours at 37°C with 5% CO_2 for 1.5 hours, being rocked every 20 minutes. After the 1.5 hours, the wells were refreshed with 100µl of fresh DMEM + 10% FBS and incubated for 96 hours at 37°C with 5%CO_2. After 96 hours, the media was removed and the cells were fixed with a 10% formalin solution (Sigma-Aldrich) for 1.5 hours. The formalin was then removed and the cells were stained with 0.5% crystal violet solution for 30 minutes. The crystal violet solution was then washed off and the results were calculated using the Reed-Muench method.

Log_{10} 50% end point dilution =

log_{10} of dilution showing mortality next above 50% -

(difference of logarithms × logarithm of dilution factor).

Difference of logarithms =

[(mortality at dilution next above 50%)-50%] /

[(mortality next above 50%)-(mortality next below 50%)]

3.2.5 Ultracentrifugation

Viral supernatant was filtered through a 0.45 μm hydrophobic filter to remove cell debris. 32ml of this filtered supernatant was then transferred to a centrifuge tube (Beckman Coulter). 4ml of a 20% sucrose solution made up in 1x TNE buffer (50mM Tris-HCl; Sigma-Aldrich, 100mM NaCl; Sigma-Aldrich, 0.5mM EDTA; Promega) was added to form a cushion. Each tube was placed into a centrifuge bucket and the mass of bucket and tube was measured, virus was added or removed to make sure all samples were within 0.1g of each other. The virus was then ultracentrifuged in an Optima L-110k ultracentrifuge (Beckman Coulter) at 28000rpm using a SW32Ti rotor for 4 hours at 4°C. After ultracentrifugation, the medium was removed and the tubes were inverted on to C-fold paper towels until the tubes were dry. 100μl of TE buffer (10mM Tris-HCl, 1mM EDTA) was added to the tubes and resuspended. The tubes were then covered with parafilm and left on ice for 30 minutes. After this time, the virus and TE buffer was resuspended and transferred to pre-chilled cryovials and then stored at -80°C.

3.3.0 Cell Viability Assays

3.3.1 CC50

RD cells were seeded in a 96 well plate at $3x10^4$ per well in 200µl of DMEM +10% FBS, according to the protocol mentioned above, and left to incubate at 37°C with 5% CO_2 for 18 hours. Then 100µl of the medium from each well was removed and 100µl of the drug/treatment in DMEM + 10% FBS was added at the respective concentration to each well. The plate was then returned to the incubator and left for 24 hours. The plate was then equilibrated to room temperature for 30 minutes in the dark. CellTiter-Glo Buffer (Promega) was added to CellTiter-Glo Substrate (Promega). 100µl of media was then removed from each well and 100µl of CellTiter-Glo assay reagents were added. The contents were then mixed for 2 minutes on an orbital shaker at 125rpm to induce cell lysis. The plate was then wrapped in tin foil and incubated in the dark at room temperature for 1 hour to stabilise the luminescent signal. The luminescence was then read using the GloMax-Multi Detection System (Promega) at an integration time of 1.0 second per well.

3.4.0 qRT-PCR Set Up

3.4.1 Primer and probe design

The VP1 region was chosen as the area to design the primers and probe around adapted from Tan et al (200). The nucleotide sequences from the six isolates received were aligned and analysed using MegAlign software (Lasergene, DNA Star). Conserved regions amongst the six isolates were identified and chosen to be used as the forward and reverse primers and the probe. These primers (forward – GAGAGCTCTATAGGAGACAGT) (reverse – GAGAGCTCTATAGGAGACAGT) and the Fam-labelled molecular beacon probe (ACCCACAGGTCAAAACACACA) were synthesised by Integrated DNA Technologies. These primers were verified against all six isolates using a superscript on-step reverse transcription polymerase chain reaction (RT-PCR) with a PlatinumTaq DNA polymerase (Qiagen).

The reactions were made up in the following ratio.

The following RT-PCR cycle and conditions were used.

Reagents	**Vol (µL)**
2x reaction mix	25
Viral RNA	5
F+R	1
Enzyme/RT mix	2
Water	17
Total volume	**50**

Stage	**Temperature and Time**			
cDNA synthesis	50°C, 20 minutes			
Denaturation	94°C, 2 minutes			
PCR	94°C, 15 seconds	55°C, 30 seconds	68°C, 1 minute	40 cycles
Final Extension	68°C, 5 minutes			

3.4.2 RNA standard production

The PCR product was then transformed into plasmid vectors using TOPO cloning. The reagents were mixed into the ratio.

Reagents	**Vol (µL)**
PCR product	2
Salt Solution	1
TOPO vector	1
Water	2
Total Volume	**6**

Then incubated at room temperature for 5 minutes and then placed on ice. 2µl of this reaction mixture was then added to a tube of TOP10 cells and gently mixed, then incubated on ice for 30 minutes. The cell mixture was then heat shocked for 30 seconds at 42°C and then immediately transferred to ice. 250µl of Super Optimal broth with Catabolite repression (SOC) media was then added to the tube which was then capped and shaken at 200rpm for 1 hour at 37°C. 10-50µl of each transformation was spread on separate 2YT plates containing 100µg/ml ampicillin and incubated overnight at 37°C. A representative colony was then selected from each plate and placed into 50µl of nuclease free water then heated at 95°C for 5 minutes.

These samples were then PCR extended using the following reagents and method.

Reagents	**Vol (µL)**
Template	1
PCR buffer	12.5
M13 F+R	1
Water	10.5
Total Volume	**25**

Stage	**Temperature and Time**			
Denaturation	95°C, 15 minutes			
PCR	95°C, 1 minute;	55°C, 30 seconds	72°C, 1 minute	30 cycles
Extension	72°C, 10 minutes			

After the PCR run, the PCR products were then ran on a 2% agarose (Lonza) gel. After confirmation that the colonies contained the correct plasmid another colony was picked and grown in 5ml of 2YT/ ampicillin medium overnight at 37°C. The bacterial cells were then pelleted via centrifugation in a table-top centrifuge at 8000rpm for 3 minutes and the supernatant was removed. The plasmid DNA was then purified from the cells using a QIAprep Spin Miniprep Kit (Qiagen), following the manufactures instructions. The plasmids were then sent to AITbiotech for sequencing.

After confirmation of the sequences the plasmid DNA was linearised using HindIII restriction enzyme in the following ratio for one hour at 37°C.

Reagents	**Vol (µL)**
Plasmid (1ug)	X
Cutsmart buffer	5
Water	44 – X
HindIII	1
Total Volume	**50**

The linear DNA was then cleaned using a MinElute Reaction Clean-up Kit (Qiagen) following the manufacturer's instructions. After this clean up the DNA underwent *in vitro* transcription (IVT) using Megascript IVT (Life Technologies) in the following reagent ratio.

Reagents	**Vol (µL)**
ATP	2
CTP	2
GTP	2
UTP	2
10x reaction mix	2
0.1-1ug linear DNA	X
Enzyme	2
Water	Make total volume up to 20µl
Total Volume	**20**

Once these reagents were mixed they were incubated at 37°C for 4 hours. The reaction was then cleaned up using RNEasy MinElute Clean-up Kit (Qiagen) following the manufacturer's instructions. The viral RNA concentration was calculated via a Ribogreen assay (Life Technologies) following manufacturer's instructions and the fluorescence intensity was measured using Infinite M200 microplate reader (Tecan) at excitation 480nm and emission 520nm. After the extrapolation of the concentration in ng/ml, the RNA copy number was calculated using http://molbiol.edu.ru/eng/scripts/01_07.html. The RNA transcripts were

then diluted to $1x10^{11}$ RNA copies/µl, and then serially diluted to create standards from $1x10^{9}$ to $1x10^{1}$ RNA copies/µl.

3.4.3 Machine set up and program

VP1-targeted qRT-PCR was adapted from Tan et al; 2008(200) with forward and reverse primers (GAGAGCTCTATAGGAGACAGT and GAGAGCTCTATAGGAGACAGT respectively), and an additional novel lab-designed FAM-labeled molecular beacon probe (ACCCACAGGTCAAAACACACA) taken from consensus sequence of the 6 isolates. To assemble the qRT-PCR reaction, 1µl of RNA template was mixed with the following reagents: 4.375µl of nuclease-free H_2O, 6.25µl of 2x premix, 0.5µl of forward and reverse primers (final concentration 400nM) and 0.25µl of each Taqman probe (final concentration 200nM), and 0.125µl RT mix to a final reaction volume of 12.5µl. The thermal cycling conditions were a 30-minute reverse transcription step at 50°C, followed by the initial activation at 95°C for 15 minutes. This was then followed by the 2-step cycle of 1 cycle at 94°C for 15 seconds followed by 45 1 minute cycles at 55°C. Assay exclusivity of EV71-VP1 was confirmed by testing viral RNA extracted from the following viruses, and no cross-reactions were identified: Dengue viruses (DENV serotype 1-4), Chikungunya virus (CHIKV) and O'nyong-nyong virus (ONNV). Analytical sensitivity was also determined using quantitated EV71 RNA transcripts and the lower limit of detection was estimated as 10 copies for the VP1 gene target. RNA transcripts ranging from 10^9 to 10 copies were performed in pentaplicates

to construct standard curve for the qRT-PCR assay to estimate the copy number of EV71 in samples. All qRT-PCR assays were performed on Applied Biosystems (ABI) 7900HT Fast Real-Time PCR System using the Quantitect Probe RT-PCR Kit (Qiagen).

3.5.0 Viral Kinetics

3.5.1 Infection protocol

Individual EV71 isolate *in vitro* infections were performed in RD cells at multiplicity of infection (MOI) 10. Each infectious mix consisted of virus suspension prepared in SF DMEM. RD cells were incubated with the infectious mix in 60mm dishes at 37°C for 1.5h with intermittent rocking before virus inoculum was removed and replaced with DMEM + 10% FBS. Cells were incubated at 37^{o}C and harvested at 0, 3, 6, 12 or 24 hours post infection (hpi). Controls were performed with cells undergoing the same infection condition in the absence of infectious EV71 virus. These controls are referred to as mock-infected samples.

3.5.2 Cell harvesting

At each time point 140µl of media was removed from its respective dish and stored in an eppendorf tube at -80°C to be used for viral RNA extraction. 1ml of the media was also removed and stored in a separate eppendorf at -80°C for cytokine analysis. The cells were then harvested with the remaining media via cell scraping. Half of the cells and media were placed into a 5ml polystyrene tube (Falcon) to be used for flow cytometry and the other half was stored in eppendorf tubes to be used for total RNA extraction.

3.5.3 Staining procedure

After the cells were harvested, the 5ml tube was centrifuged at 1500rpm for 5 minutes. The supernatant was removed and the cells were resuspended in 100µl of LIVE/DEAD fixable aqua dead cell stain (Invitrogen; diluted at 1:400 in DPBS) and incubated at room temperature in the dark for 20 minutes. Cells were then washed with 2ml FACS buffer (DPBS, 2mM EDTA, 5% FBS, 5%HS, 0.1% sodium azide; Sigma-Aldrich) and centrifuged at 1500rpm for 5 minutes. After centrifugation, the supernatant was removed and the pellet was resuspended in 500µl of 1x BD FACS lysing solution to fix the cells. The cells were fixed for 10 minutes at room temperature in the dark. They were then washed in 2ml of FACS buffer and centrifuged at 1500rpm for 5 minutes. The supernatant was again removed and the cells were resuspended in 500µl of BD FACS permeabilising solution 2 and incubated at room temperature for 10 minutes in the dark. The cells were then washed with 2ml of FACS buffer and centrifuged at 1500rpm for 5 minutes, and then the supernatant was removed. After perming, the cells were incubated with an anti-EV71 monoclonal antibody raised in mice, which binds to the VP1 region of the virus (10F0; Thermo Fischer). The cells were incubated with this antibody for 20 minutes in the dark at room temperature. The cells were then washed again with 2ml FACS buffer and centrifuged at 1500rpm for 5minutes. The supernatant was removed and the cells were incubated with a goat anti-mouse antibody conjugated with an allophycocyanin fluorophore (APC; Life Technologies), which binds to any mouse antibodies in the cell suspension. This secondary antibody was incubated for 20 minutes at room temperature in the dark. After the 20 minutes the

cells were washed with 2ml of FACS buffer and centrifuged at 1500rpm for 5 minutes. The supernatant was removed and the cells were resuspended in 200µl of FACS buffer.

3.5.4 vRNA extraction for viral load

Viral RNA (vRNA) was extracted from the 140µl viral supernatant using QIAamp® Viral RNA Mini Kit (QIAGEN) according to manufacturer's instructions. The extracted vRNA was stored in eppendorf tubes at -80°C.

3.6.0 PBMC Infection Model

3.6.1 Isolating PBMCs

Apheresis cones were received from the Health Sciences Authority blood bank Singapore. The blood was expelled from the cone into a 50 Falcon tube using a needle without a bevel (BD) and syringe (BD). The cone was then washed with 25ml of PBSE (DPBS + 2mM EDTA) into the 50ml tube. Ficoll-Paque solution (GE Healthcare) was added to fresh 50ml tube at a ratio of 1:2 Ficoll-Paque:diluted blood. The diluted blood was then slowly layered on top of the Ficoll-Paque. The tube was then centrifuged at 3000rpm for 20 minutes with the lowest break and acceleration setting to separate the cells via gradient centrifugation. After centrifugation, the top plasma layer was removed via aspiration leaving the white disk of PBMCs undisturbed. The PBMCs were transferred to a fresh 50ml tube and washed with 40ml of PBSE and centrifuged at 1500rpm for 5 minutes and then supernatant was removed. 8ml of red blood cell (RBC) lysis buffer (155mM NH_4Cl, 10mM $KHCO_3$, 0.1mM EDTA; Sigma-Aldrich) was added to the cell pellet and the cells were resuspended, and then incubated on ice for 5 minutes. The cells were then washed with 40ml of PBSE and centrifuged at 1500rpm for 5 minutes. The supernatant was removed and the cells were resuspended in 15ml of PBSE. The cells were then counted as previously described after a 2-step 50x dilution in trypan blue using 10µl of cells.

3.6.2 Infection protocol

$2x10^6$ PBMC were seeded in 500µl of IMDM + 10% HS in a 60mm dish. EV71 isolates 1, 3 and 5, plus heat inactivated EV71 and non-infected control (mock) were diluted individually to MOI 5 in SF IMDM to make a total volume of 500µl. The infection mix was then added to the PBMC and incubated at 37°C with 5% CO_2 for 2 hours, rocking every 15 minutes. The virus was then removed and 3ml of fresh IMDM +10% HS was added and the dishes were returned to the incubator for 0, 6, 12 or 24 hours.

3.6.3 Cell harvesting and staining

At each time point, the cells and media were harvested via scraping and transferred, half to 5ml tubes and half to 1.7ml eppendorf tubes. The eppendorf tubes were centrifuged in a table-top centrifuge for 5 minutes at 8000rpm. The supernatant was removed and the cell pellet was resuspended in 500µl of TRIzol reagent (Ambion by Life Technologies) and stored at -80°C. The 5ml tubes were centrifuges at 1500rpm for 5 minutes, 140µl and 1000µl of the supernatant were transferred to eppendorf tubes and stored at -80°C for vRNA extraction and cytokine analysis respectively. The rest of the supernatant was removed and the cells were resuspended in 200µl of 1:400 diluted LIVE/DEAD and incubated at room temperature for 20 minutes in the dark. The cells were then washed with 2ml of FACS buffer and centrifuged at 1500rpm for 5 minutes and then the supernatant was removed. The cells were then resuspended in 200µl of BD Cytofix/Cytoperm for 10 minutes at room temperature. After fixation, the

cells were washed with 2ml of FACS buffer and centrifuged at 1500rpm for 5 minutes. The supernatant was removed and the cells were then permed with 500µl of 0.5% Triton X-100 (BDH VWR) in PBS for 10 minutes at room temperature. After permeabilisation the cells were washed with 2ml of FACS buffer and centrifuged at 1500rpm for 5 minutes, then the supernatant was removed. The cells were then incubated with 100µl of 10F0 anti-EV71 antibody at 4°C. after this incubation the cells were washed with 2ml of FACS buffer and centrifuged at 1500rpm for 5 minutes. The supernatant was removed and the cells were resuspended in 100µl of goat anti-mouse APC antibody at room temperature for 20 minutes. After secondary antibody staining the cells were washed with 2ml of FACS buffer and centrifuged at 1500rpm for 5 minutes and the supernatant was removed. The cells were then stained with a cocktail of surface marker antibodies made up to 100µl in FACS buffer, which consisted of:

Antibody	**Colour**	**Manufacturer**	**Volume (µl)/reaction**
CD45	PE-Cy7	eBioscience	2.5
CD14	PerCP Cy5.5	BD	2.5
CD3	FITC	Biolegend	2.5
CD19	eVolve 605	eBioscience	2.5
CD16	APC Cy7	Biolegend	2.5
CD11c	VioBlue	Miltenyi	2.5
HLA-DR	PE	BD	2.5
CD56	AF700	BD	2.5

They were stained for 20 minutes at room temperature in the dark. After staining the cells were washed with 2ml of FACS buffer and centrifuged at 1500rpm for 5 minutes. The supernatant was removed and the cells were resuspended in 200µl of FACS buffer and then acquired via flow cytometry on a BD Fortessa analyser using BD FACS Diva software.

3.6.4 Flow cytometry analysis

All flow cytometry data acquired was analysed using FlowJo v.10 software and GraphPad prism x7.

3.7.0 Cell Subset Infection

3.7.1 Isolating subsets

Apheresis cones were received from HSA blood bank Singapore. PBMC were isolated from these cones as previously described. Monocytes were isolated from the PBMC using a negative selection EasySep Human Monocyte Enrichment Kit Without CD16 (Stem Cell) following manufacturer's instructions. CD4+ T cells were separately isolated form PBMC using a negative selection EasySep Human CD4+ T Cell Isolation Kit (Stem Cell) following the manufacturer's instructions. CD8+ T cells were isolated form PBMC using a negative selection EasySep Human CD8+ T Cell Isolation Kit (Stem Cell) following the manufacturer's instructions.

3.7.2 Monocyte infection protocol

$2x10^6$ monocytes were seeded in 500µl of IMDM + 10% HS in a 60mm dish. EV71 isolates 1, 3 and 5, plus heat inactivated EV71 and non-infected control (mock) were diluted individually to MOI 5 in SF IMDM to make a total volume of 500µl. The infection mix was then added to the monocytes and incubated at 37°C with 5% CO_2 for 2 hours, rocking every 15 minutes. The virus was then removed and 3ml of fresh IMDM +10% HS was added and the dishes were returned to the incubator for 0, 6, 12 or 24 hours.

3.7.3 CD4+ T cell and CD8+ T cell infection protocol

$2x10^6$ CD4+ or CD8+ T cells were seeded in 500µl of IMDM + 10% HS in a 60mm dish. EV71 isolates 1, 3 and 5, plus heat inactivated EV71 and non-infected control (mock) were diluted individually to MOI 5 in SF IMDM to make a total volume of 500µl. The infection mix was then added to the T cells and incubated at 37°C with 5% CO_2 for 2 hours, rocking every 15 minutes. The virus was then removed and 3ml of fresh IMDM +10% HS was added and the dishes were returned to the incubator for 0, 6, 12 or 24 hours.

3.7.4 Cell harvesting and staining

At each time point, the cells and media were harvested via scraping and transferred, half to 5ml tubes and half to 1.7ml eppendorf tubes. The eppendorf tubes were centrifuged in a table-top centrifuge for 5 minutes at 8000rpm. The supernatant was removed and the cell pellet was resuspended in 500µl of TRIzol reagent (Ambion by Life Technologies) and stored at -80°C. The 5ml tubes were centrifuges at 1500rpm for 5 minutes,

140µl and 1000µl of the supernatant were transferred to eppendorf tubes and stored at -80°C for vRNA extraction and cytokine analysis respectively. The rest of the supernatant was removed and the cells were resuspended in 200µl of 1:400 diluted LIVE/DEAD and incubated at room temperature for 20 minutes in the dark. The cells were then washed with 2ml of FACS buffer and centrifuged at 1500rpm for 5 minutes and then the supernatant was removed. The cells were then resuspended in 200µl of BD Cytofix/Cytoperm for 10 minutes at room temperature.

After fixation, the cells were washed with 2ml of FACS buffer and centrifuged at 1500rpm for 5 minutes. The supernatant was removed and the cells were then permed with 500µl of 0.5% Triton X-100 (BDH VWR) in PBS for 10 minutes at room temperature. After permeabilisation the cells were washed with 2ml of FACS buffer and centrifuged at 1500rpm for 5 minutes, then the supernatant was removed. The cells were then incubated with 100µl of 10F0 anti-EV71 antibody at 4°C. after this incubation the cells were washed with 2ml of FACS buffer and centrifuged at 1500rpm for 5 minutes. The supernatant was removed and the cells were resuspended in 100µl of goat anti-mouse FITC (monocytes) and goat anti-mouse APC (CD4+ and CD8+ T cells) antibody at room temperature for 20 minutes. After secondary antibody staining the cells were washed with 2ml of FACS buffer and centrifuged at 1500rpm for 5 minutes and the supernatant was removed. The cells were then stained with a cocktail of surface marker antibodies made up to 100µl in FACS buffer, which consisted of:

Monocyte antibody panel

Antibody	**Colour**	**Manufacturer**	**Volume (µl)/reaction**
CD45	BV786	BD	2
CD14	BV650	BD	2
CD16	PerCP Cy5.5	Biolegend	2
CCR2	APC	Biolegend	2
CD11b	PE Cy7	BD	2
CD169	PE	Biolegend	2
HLA-DR	AF700	Biolegend	2
CD163	Texas Red	BD	2
CD33	APC Cy7	Biolegend	2

CD4+ and CD8+ T cell antibody panel

Antibody	**Colour**	**Manufacturer**	**Volume (µl)/reaction**
CD45	BV786	BD	2
CD3	PerCP Cy5.5	Biolegend	2
CD4	FITC	Biolegend	2
CD8	APC VCy7	BD	2
HLA-DR	AF700	eBiosciences	2
CD45RO	BV650	Biolegend	2
CD45RO	BV605	BD	2
CD56	PE	Miltenyi	2
CD25	PE Cy7	Biolegend	2
FoxP3	Pacific Blue	Biolegend	2

They were stained for 20 minutes at room temperature in the dark. After staining the cells were washed with 2ml of FACS buffer and centrifuged at 1500rpm for 5 minutes. The supernatant was removed and the cells were resuspended in 200µl of FACS buffer and then acquired via flow cytometry on a BD Fortessa analyser using BD FACS Diva software.

3.7.5 Flow cytometry analysis

All flow cytometry data acquired was analysed using FlowJo v.10 software and GraphPad prism x7.

3.8.0 Blood Brain Barrier Model

3.8.1 Setting up of the model

Cell culture dishes (60mm × 15mm) (Sigma) were coated with 25ng/ml fibronectin (Sigma-Aldrich) and incubated for 3 hours at 37°C before its removal for cell seeding. hCMEC/D3 (5×10^5) were then seeded and incubated at 37°C overnight. During infection, the media overlay is aspirated and replaced with a virus suspension that consists of EV71 at a virus concentration of multiplicity of infectivity 10 (MOI 10). The cells were then incubated at 37°C for 2 hours, with shaking at every 30 minutes. A mock infection was also prepared in parallel using hCMEC media for each time point. The virus overlay was then removed and replaced with hCMEC media. At 0, 6, 12, 24, 48, 72, 96, 120 and 144 hpi, supernatant was

removed for viral RNA (vRNA) extraction while the hCMEC/D3 were trypsinised and harvested for total RNA extraction and FACS analysis.

3.8.2 *In vitro* BBB model infection

0.4µm pore, semi-permeable, polystyrene transwell inserts in the wells of 12-well plates were coated with fibronectin and incubated for at least 3 hours at 37^{o}C then removed. hCMEC/D3 (1 x 10^{5}) were then seeded onto the inserts and incubated at 37^{o}C for 3 days. hCMEC media were also added to the luminal and abluminal region such that the hydrostatic pressure is kept constant throughout all replicates, as illustrated in (Fig 4).

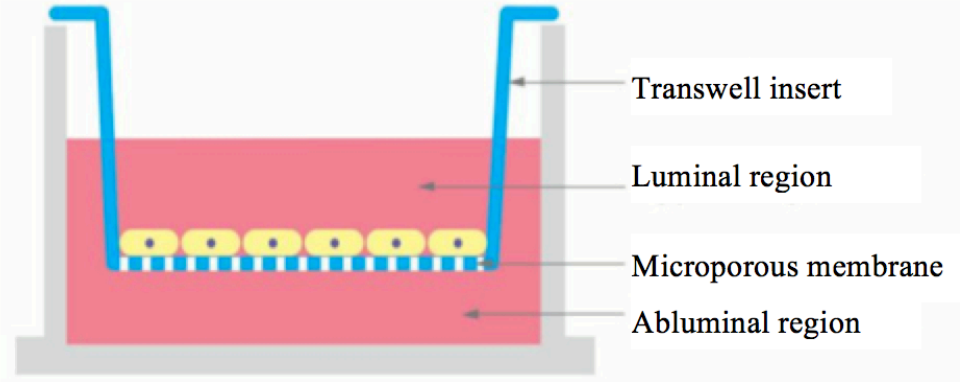

Figure 4. Layout of the BBB monoculture model, with a coat of a single confluent layer of hCMEC/D3 on the microporous membrane. This figure shows the cross-section of the BBB monoculture model, with the different aspects of the model labelled.

The luminal region represents the vascular side of the BBB while the abluminal region represents the brain parenchymal side of the BBB. Hydrostatic pressure of the luminal and abluminal region is kept constant throughout all replicates. (Adapted from Corning®)

The media in the luminal and abluminal region was then aspirated before a virus overlay that consists of CHIKV, ZIKV or EV-71 suspended in hCMEC media at MOI 10, was added to the luminal region. The cells were then incubated at 37^{o}C for 2 hours. Mock hCMEC/D3 was also prepared in parallel with the hCMEC media overlay instead for each time point. A blank well was also prepared in parallel, whereby there was no cells seeded onto the transwell insert. Fresh media was then added to the abluminal region while the virus overlay was also replaced with media, such that the hydrostatic pressure is kept constant throughout all replicates, as shown in (Fig 4). At 0, 24, 48, 72, 96, 120 and 144 hpi, the supernatant is removed

for vRNA extraction from both luminal and abluminal regions while the hCMEC/D3 monolayer was trypsinised and harvested for total RNA extraction and FACS analysis.

3.8.3 Trans-endothelial electrical resistance

Trans-endothelial electrical resistance (TEER) is measured using the STX2 electrode (World Precision Instruments) connected to a second-generation Epithelial Voltohmmeter ($EVOM^2$) (World Precision Instruments). The electrodes were sterilized in 100% ethanol before rinsing and equilibration with hCMEC media. TEER is measured as illustrated in (Fig 5). The electrodes are then positioned in the wells, as illustrated in (Fig 5), such that the shorter electrode is in the luminal region while the longer electrode is in the abluminal region. Readings were taken in triplicates. The electrodes were sterilized in formalin for 10 minutes after measurements for wells infected with the same virus were completed. TEER was also measured for the blank well and the calculated TEER (minus blank) values were derived by subtracting the average triplicate values of the blank well from the average triplicate values of the well of interest.

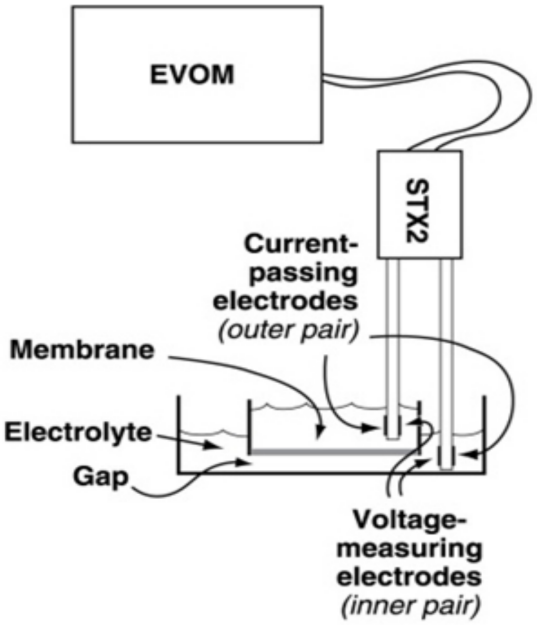

Figure 5. World Precision Instruments STX2 electrodes. This figure shows the cross-section of the WPI STX2 electrodes and how they measure resistance in a transwell cell system.

3.9.0 Viruses and Cells.

EV71 viral isolates 1-6 used in this study were originally isolated from 6 separate patients from the 2006 outbreak in Sarawak, Malaysia. Rhabdomyosarcoma (RD) cells (ATCC CCL-136) are grown and passaged in (DMEM; HyClone) supplemented with 10% FBS. Viruses are propagated in RD cells, pre-cleared by centrifugation then stored at -80°C.

3.10.0 Tissue culture infective dose 50 (TCID50) Assay

Viral titre was determined using TCID50 assay with RD cells. RD cells were seeded in 96 wells and infected with 80µl of serially diluted EV71 isolates in serum-free (SF) Dulbecco's Modified Eagle Medium (DMEM; HyClone) for 1.5h, with intermittent rocking. Then refreshed with 100µl of DMEM with 10% (vol/vol) foetal bovine serum (FBS; HyClone). Cells were then incubated for 4 days at 37°C. Cells were fixed with 10% formalin (Sigma Aldrich) before being stained with 0.5% crystal violet (Sigma Aldrich). Titre is calculated using the Reed-Muench method (201). Log_{10} 50% end point dilution = log_{10} of dilution showing a mortality next above 50% - (difference of logarithms × logarithm of dilution factor). Difference of logarithms = [(mortality at dilution next above 50%)-50%]/[(mortality next above 50%)-(mortality next below 50%)]

3.11.0 Phylogenetic Analysis

EV71 subgenogroup B phylogenetic tree generated by maximum-likelihood analysis of complete VP1 nucleotide sequences. The tree was rooted to the prototype genogroup A strain. Sequences are identified by

GenBank accession, country of origin and year of isolation. Viruses discussed in this study are underlined. The robustness of the tree was evaluated by bootstrap analysis using 1000 pseudoreplicate sequences. Bootstrap values >75% of major clades are indicated at relevant branch nodes. All branch lengths are drawn to scale and a measurement of relative phylogenetic distance is provided by the scale at the bottom of the tree

3.12.0 Infection in RD cells

EV71 *in vitro* infections in RD cells were performed at multiplicity of infection (MOI) 10, each infectious mix consisted of virus suspension prepared in SF DMEM. RD cells were incubated with the infectious mix in 60mm dishes at 37C for 1.5h with intermittent rocking before virus inoculum was removed and replaced with DMEM with 10% FBS. Cells were incubated at 37^{o}C and harvested at 0, 3, 6, 12 or 24 hours post infection (hpi). Controls were performed with cells undergoing the same infection condition in the absence of infectious EV71 virus. These controls are referred to as mock-infected samples.

3.13.0 Infection in human peripheral blood mononuclear cells

Peripheral blood mononuclear cells (PBMCs) were isolated from a blood apheresis cone by gradient centrifugation using Ficoll-Hypaque (GE Healthcare) as previously described(202, 203). EV71 *ex vivo* infections in PBMCs were performed at multiplicity of infection (MOI) 5, each infectious mix consisted of virus suspension prepared in SF Iscove's Modified Dulbecco's Medium (IMDM; HyClone). PBMCs were incubated with the

infectious mix in 60mm dishes at 37^{o}C for 2h with intermittent rocking before virus inoculum was removed and replaced with IMDM with 10% human serum (HS; Innovative Research Inc.). Cells were incubated at 37^{o}C and harvested at 0, 6, 12 or 24hpi. Controls were performed with cells undergoing the same infection condition in the absence of infectious EV71 virus or with heat inactivated virus. Heat-inactivated samples were inactivated by being incubating viruses at 80^{o}C for 30 min. These controls are referred to as mock-infected and heat-inactivated samples respectively.

3.14.0 Infection in Monocytes, CD4+ and CD8+ T Cells

PBMCs were isolated as described above, and then monocytes, CD4+ and CD8+ T cells were isolated from these PBMC using STEMCELL Human Monocyte Enrichment Kit Without CD16 Depletion, Human CD4+ T Cell Isolation Kit and Human CD8+ T Cell Isolation Kit respectively, following the manufacturer's instructions. Infection was then performed as in PBMCs above and cells were harvested at 6 and 12 hpi.

3.15.0 Viral RNA extraction and viral RNA quantification

Viral RNA was extracted using QIAamp® Viral RNA Mini Kit (QIAGEN) according to manufacturer's instructions. VP1-targeted qRT-PCR was adapted from Tan et al; 2008(200) with forward and reverse primers (GAGAGCTCTATAGGAGACAGT and GAGAGCTCTATAGGAGACAGT respectively), and an additional novel lab-designed FAM-labeled molecular beacon probe (ACCCACAGGTCAAAACACACA) taken from consensus

sequence of the 6 isolates. To assemble the RT-PCR reaction, 1µl of RNA template was mixed with the following reagents: 4.375µl of nuclease-free H2O, 6.25µl of 2x premix, 0.5µl of forward and reverse primers (final concentration 400nM) and 0.25µl of each Taqman probe (final concentration 200nM), and 0.125µl RT mix to a final reaction volume of 12.5µl. The thermal cycling conditions were a 30-minute reverse transcription step at 50°C, followed by the initial activation at 95°C for 15 minutes. This was then followed by the 2-step cycle of 1 cycle at 94°C for 15 seconds followed by 45 1 minute cycles at 55°C. Assay exclusivity of EV71-VP1 was confirmed by testing viral RNA extracted from the following viruses, and no cross-reactions were identified: Dengue viruses (DENV serotype 1-4), Chikungunya virus (CHIKV) and O'nyong-nyong virus (ONNV). Analytical sensitivity was also determined using quantitated EV71 RNA transcripts and the lower limit of detection was estimated as 10 copies for the VP1 gene target. Copy numbers of EV71 RNA were determined by using the Ribogreen RNA specific Quantitation Kit (Invitrogen, Carlsbad, USA). RNA transcripts ranging from 10^9 to 10 copies were performed in pentaplicates to construct standard curve for the qRT-PCR assay to estimate the copy number of EV71 in samples. All qRT-PCR assays were performed on Applied Biosystems (ABI) 7900HT Fast Real-Time PCR System using the Quantitect Probe RT-PCR Kit (Qiagen, Hilden, Germany).

3.16.0 Flow cytometry analysis

Cells from the *in vitro* infections in RD cells were stained with AmCyan LIVE/DEAD Fixable Aqua Dead Stain. Subsequently, cells were fixed with 1X FACS lysing solution (BD Biosciences). Permeabilisation was achieved with 1X FACS permeabilisation solution 2 (BD Biosciences) before staining with the EV71 VP1 protein specific mouse monoclonal antibody (Abcam). Stained cells were counter-stained with a fluorophore-tagged secondary goat anti-mouse IgG (H+L) antibody (Invitrogen). Cells were subsequently acquired with Canto II flow cytometer (BD Biosciences) with BD FACSDiva software (BD Biosciences). Cells from the *ex vivo* infections in PBMCs were stained with AmCyan LIVE/DEAD Fixable Aqua Dead Stain. Subsequently, cells were fixed with 1X FACS lysing solution (BD Biosciences). Permeabilisation was achieved with 0.5% Triton X-100 (Sigma Aldrich) before staining with the EV71 VP1 protein specific mouse monoclonal antibody (Abcam). Stained cells were counter-stained with a fluorophore-tagged secondary goat anti-mouse IgG (H+L) antibody (Invitrogen). Cells were subsequently acquired with Fortessa flow cytometer (BD Biosciences) with BD FACSDiva software (BD Biosciences). Cell surface staining was then performed with mouse anti-human CD45, CD3, CD19, CD14, CD16 (Biolegend), CD56, CD11c and HLA-DR (Miltenyi). Cells were subsequently acquired with Fortessa flow cytometer (BD Biosciences) with BD FACSDiva software (BD Biosciences). The threshold for EV71 positive cells was determined from the gating of mock-infected control at the same time point. Junk cells and doublets were excluded in all FSC/SSC gating. Amount of EV71 antigen

positive cells was determined in total CD45+, T, B, NK cells, monocytes and DCs. All analyses were performed using FlowJo version 9.3.2 software (Tree Star, Inc.).

3.17.0 Total RNA extraction

Total RNA was extracted using RNeasy Micro Kit (QIAGEN) according to manufacturer's instructions. The extracted total RNA was subsequently quantified with the Nanodrop 1000 spectrophotometer (Thermo Scientific).

3.18.0 RNASeq

The RNA samples were DNase treated using Ambion Turbo DNA-free Kit, and subsequently purified using Ampure XP beads. 2ug of the DNase treated RNA was then put through a Ribozero treatment using the Epicentre Ribo-Zero Gold Kit (Human/Rat/Mouse) and purified again with Ampure XP beads. Successful depletion was then quality tested using Qubit and Agilent 2100 Bioanalyzer and all of the depleted RNA was used as input material for the ScriptSeq v2 RNA-Seq Library Preparation protocol. Following 14 cycles of amplification, the libraries were purified using Ampure XP beads. Each library was quantified using Qubit and the size distribution assessed using the AATI Fragment Analyser. These final libraries were pooled in equimolar amounts using the Qubit and Fragment Analyser data. The quantity and quality of each pool was assessed by the Fragment Analyser and subsequently by qPCR using the Illumina Library Quantification Kit from Kapa on a Roche Light Cycler LC480II according to manufacturer's instructions. The template DNA was denatured according

to the protocol described in the Illumina cBot User guide and loaded at 12 pM concentration. To improve sequencing quality control 1% PhiX was spiked-in. The sequencing was carried out on three lanes of an Illumina HiSeq 2500 with version 4 chemistry generating 2 × 125 bp paired end reads.

3.19.0 Bioinformatics Analysis

Base calling and de-multiplexing of indexed reads was performed by CASAVA version 1.8.2 (Illumina) to produce 30 samples from the 5 lanes of sequence data, in fastq format. The raw fastq files were trimmed to remove Illumina adapter sequences using Cutadapt version 1.2.1(204). The option “-O 3” was set, so the 3' end of any reads which matched the adapter sequence over at least 3 bp was trimmed off. The reads were further trimmed to remove low quality bases, using Sickle version 1.200 with a minimum window quality score of 20. After trimming, reads shorter than 50 bp were removed. If both reads from a pair passed this filter, each was included in the R1 (forward reads) or R2 (reverse reads) file. If only one of a read pair passed this filter, it was included in the R0 (unpaired reads) file. The reference genome used for alignment was the human reference genome assembly GRCh38. The reference sequence was downloaded from the Ensembl ftp site (ftp://ftp.ensembl.org/pub/release77/fasta/homo_sapiens/dna/Homo_sapiensGRCh38.dna_sm.primary_assembly.fa.gz). The reference annotation was also downloaded from the Ensembl ftp site (ftp://ftp.ensembl.org/pub/release-

77/gtf/homo_sapiens/Homo_sapiens.GRCh38.77.gtf.gz). The annotated file contained 63,152 genes. R1/R2 read pairs were mapped to the reference sequence using TopHat2 version 2.1.0 (205) which calls the mapper Bowtie2 version 2.0.10 and then compiled using CuffDiff software (206).

3.20.0 Data Analysis

All statistical analyses were performed using either GraphPad Prism 6 or R software. Analyses between groups were performed using 2-way ANOVA analysis with Bonferri's multiple comparison test sand Kriskal-Wallis analysis (GraphPad) and Friedman's analysis (R software). A *p* value of less than 0.05 is considered to be statistically significant.

Chapter 4

Results

4.1.0 *In Vitro* Model of EV71 Infection

4.1.1 Aims

Before establishing any primary cell models, I first needed to find out if the clinical specimens could be propagated, and then needed to examine if there were any differences in the infection and replicative profiles of the different samples. I propagated the samples in RD cells, up to what I deemed an acceptable titre and then measured their viral kinetics over a 24-hour period. This was done using flow cytometry analysis to detect infectivity and qRT-PCR analysis to determine replication.

4.1.2 EV71 clinical isolates

To examine the impact of different EV71 genotypes on infection, six viruses isolated from patients with differing levels of severity of disease during an EV71 outbreak in Sarawak, Malaysia were sent to us for analysis. The patients, from whom these samples were isolated had EV71 related diseases ranging from mild HFMD, to neurological complications, to a fatality (82) (Table 1). These six isolates all belonged to the B5 subgroup of EV71.

Isolate	Genotype cluster	Date taken	Sample type	Clinical symptoms
1	B5-1	09/08/06	Throat swab	Herpangina
2	B5-1	13/0606	Vesicle swab	HFMD
3	B5-2	03/07/06	Throat swab	HFMD with Acute meningoencephalitis
4	B5-2	16/04/06	Vesicle swab	HFMD
5	B5-3	01/04/06	Rectal	Fatal
6	B5-3	20/03/06	CSF	HFMD with CNS involvement

Table 1. EV71 virus isolates from 2006 outbreak in Sarawak, Malaysia. This tables shows the viral isolates we received from the 2006 EV71 outbreak in Sarawak, Malaysia. Information includes, EV71 genotype, date the sample was taken, region of the body the sample was isolated from, and the symptoms the patient displayed during their infection

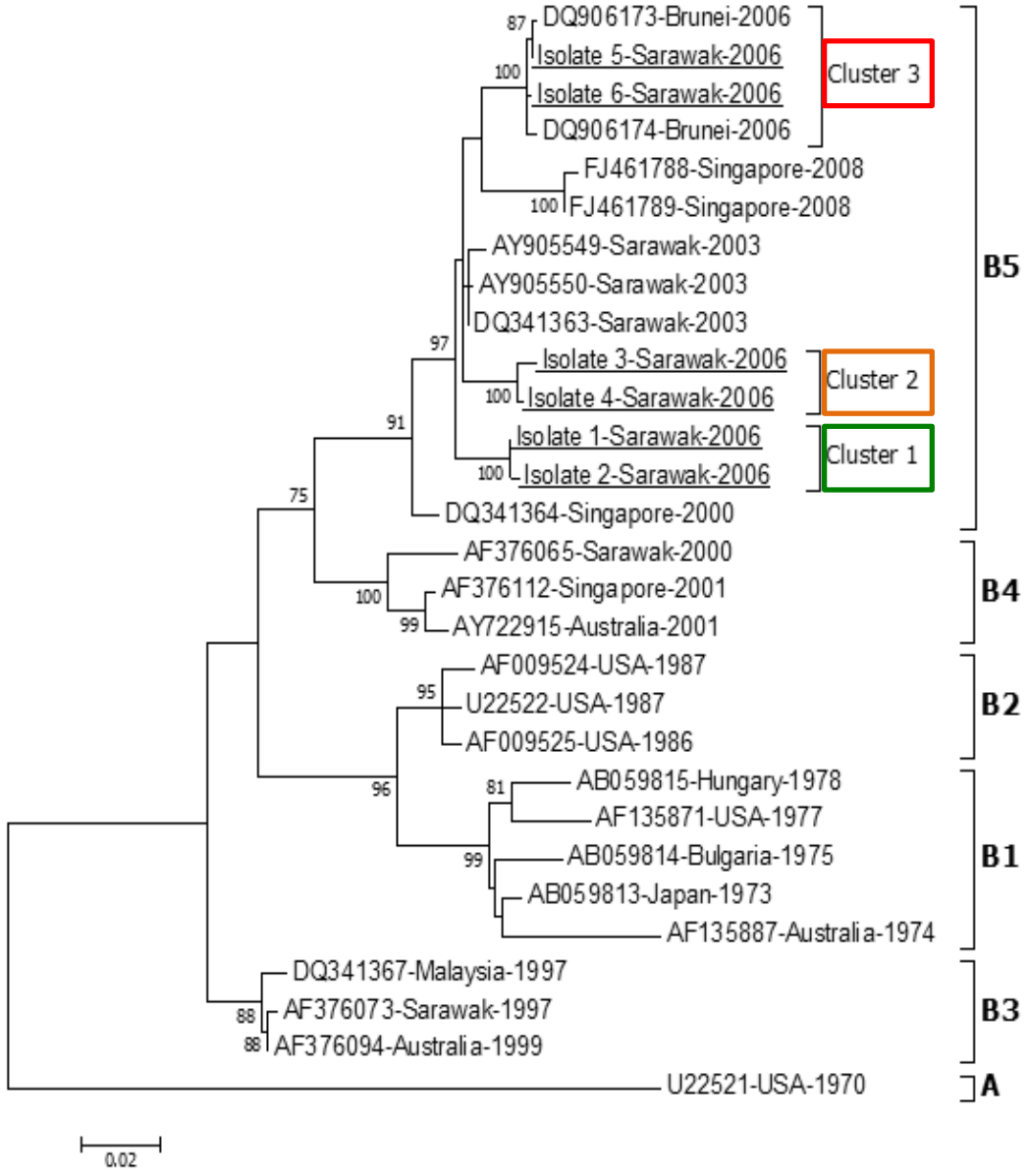

Figure 6. Phylogenetic tree of EV71 virus including the 6 isolates received from 2006 outbreak in Sarawak, Malaysia.
EV71 subgenogroup B phylogenetic tree generated by maximum-likelihood analysis of complete VP1 nucleotide sequences. The tree was rooted to the prototype genogroup A strain. Sequences are identified by GenBank accession, country of origin and year of isolation. Viruses discussed in this study are underlined. The robustness of the tree was evaluated by bootstrap analysis using 1000 pseudoreplicate sequences. Bootstrap values >75% of major clades are indicated at relevant branch nodes. All branch lengths are drawn to scale and a measurement of relative phylogenetic distance is provided by the scale at the bottom of the tree.

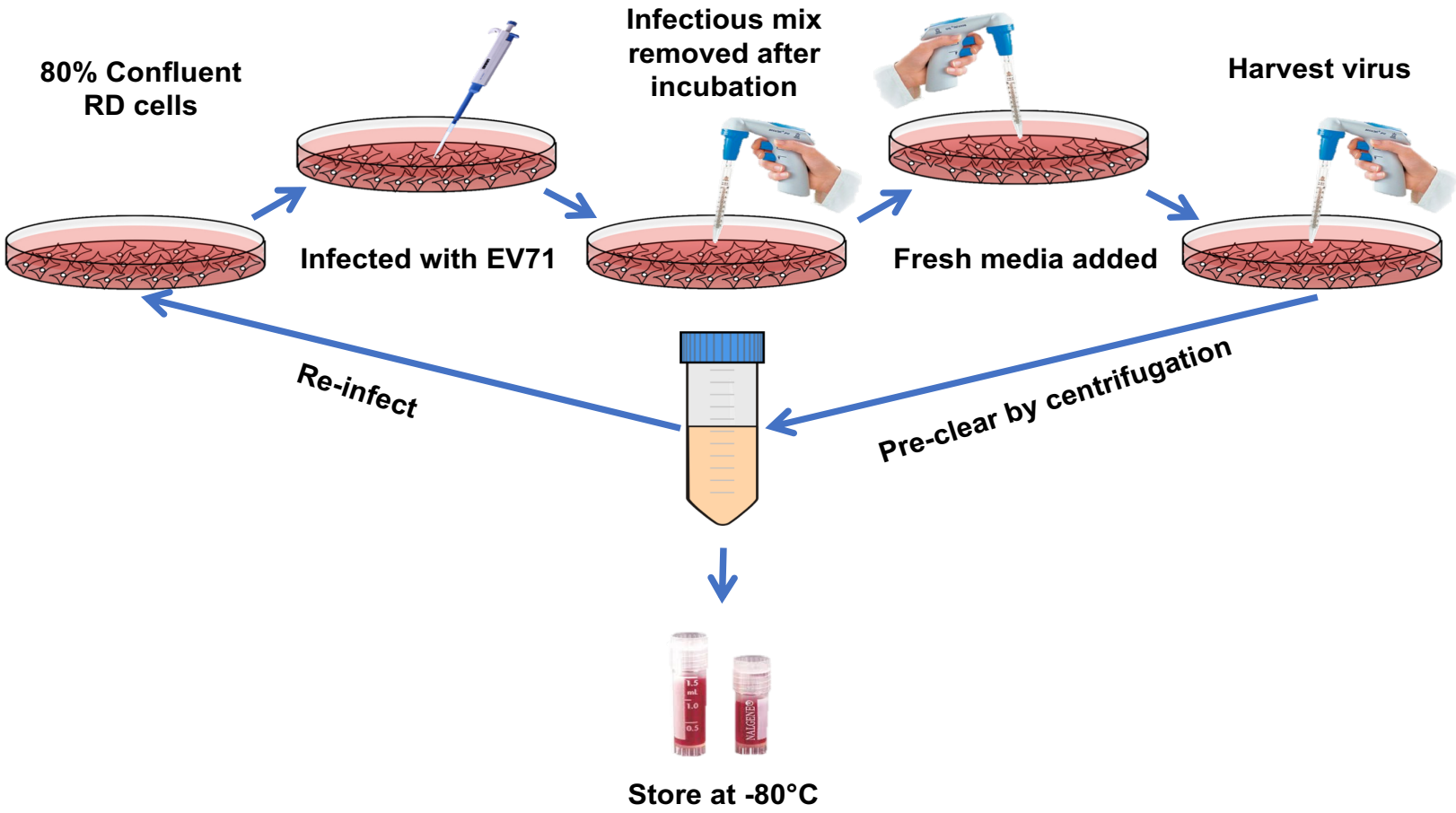

Figure 7. Diagram of viral propagation method.
RD cells were seeded T150 flasks and infected with a 1:5 ratio of EV71 to media mix once the cells had reached 80% confluency. The cells were then incubated for 2 hours at 37°C with 5% CO_2. After these two hours, the virus mix was removed and fresh media was added. The infected cells were then closely monitored and once 85% CPE was observed the supernatant was removed via aspiration, pre-cleared via centrifugation at 1500rpm for 5 minutes, before either being used to re-infect fresh cells for further propagation, or stored at -80°C.

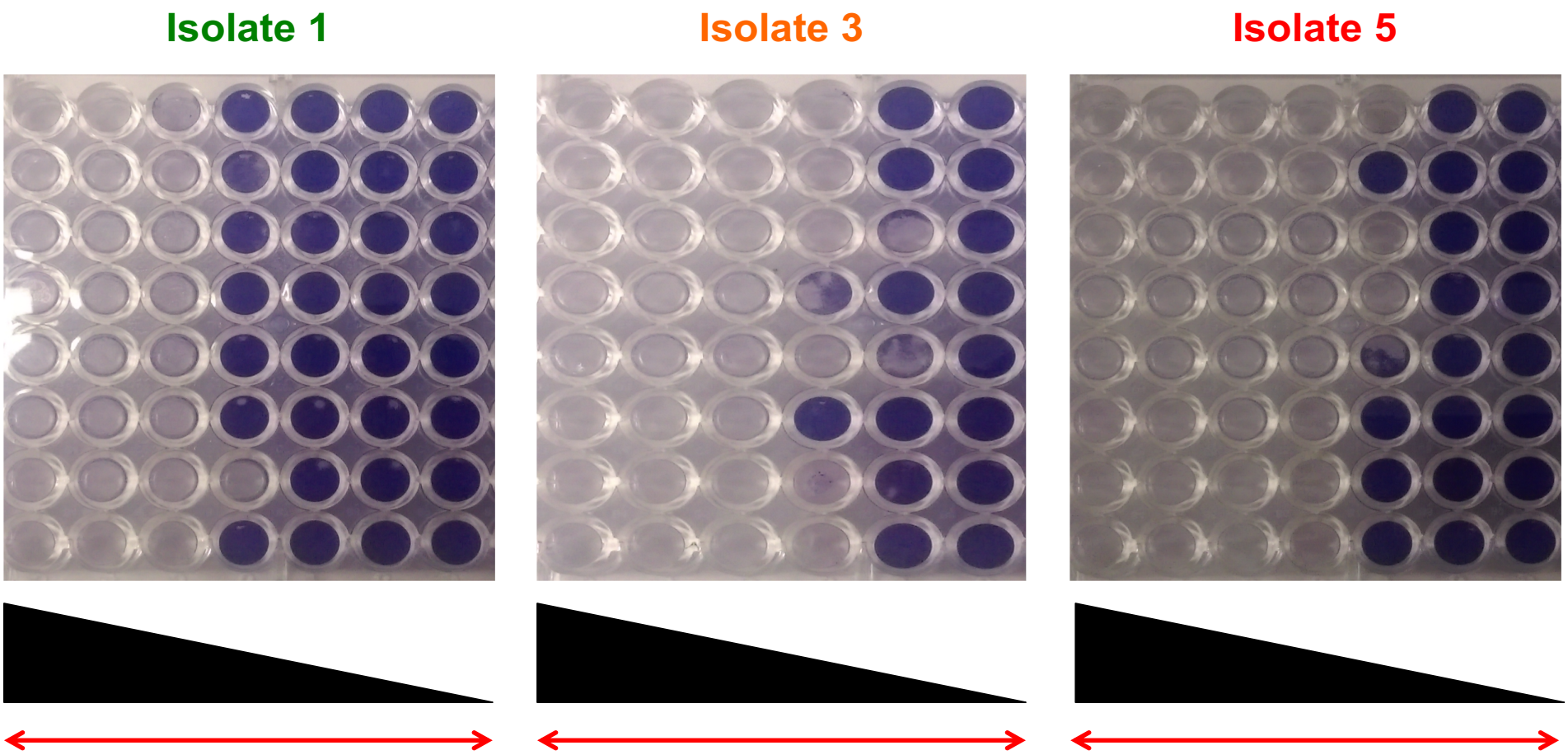

Figure 8. Titration of EV71 isolates using TCID50 assay.
This figure shows representative images of the viral titration of the EV71 isolates. A 96 well plate of RD cells seeded at 25E4 cells/well were infected with serially diluted EV71 for 96 hours. Image taken at 96hpi after fixation with 10% formalin and staining with 0.5% crystal violet. The values were deduced from this assay using the Reed-Muench method and then converted in to PFU/ml.

4.1.3 Phylogenetic analysis of EV71 clinical isolates

The isolates were then phylogenetically analysed by a phylogenetic tree, generated by maximum-likelihood analysis of complete VP1 nucleotide sequences. The tree was rooted to the prototype genogroup A strain. Sequences are identified by GenBank accession, country of origin and year of isolation. Viruses discussed in this study are underlined. The robustness of the tree was evaluated by bootstrap analysis using 1000 pseudoreplicate sequences. Bootstrap values >75% of major clades are indicated at relevant branch nodes (Fig 6). The isolates which caused the least severe disease (1 and 2) were grouped together in the phylogenetic tree (Fig 6), the two viruses that caused moderate disease (3 and 4) were grouped together, separate from isolates 1 and 2 (Fig 6). The severe disease-causing isolates, including the fatal isolate (5 – fatal and 6) were again together but then separate from the other four isolates (Fig 6).

Viral isolate propagation and titring

After receiving the isolates from Sarawak, I first propagated each virus to passage 2 (P.2) in RD cells. After propagation, the cells were titred using a tissue culture infective dose 50 (TCID50) assay. The cells were infected for 96 hours then fixed using 10% formalin and stained with 0.5% crystal violet (Fig 8). Titres were then deduced using the Reed-Muench method and converted to PFU/ml. All isolates reached a titre of at least 1E7 PFU/ml.

Novel qRT-PCR System

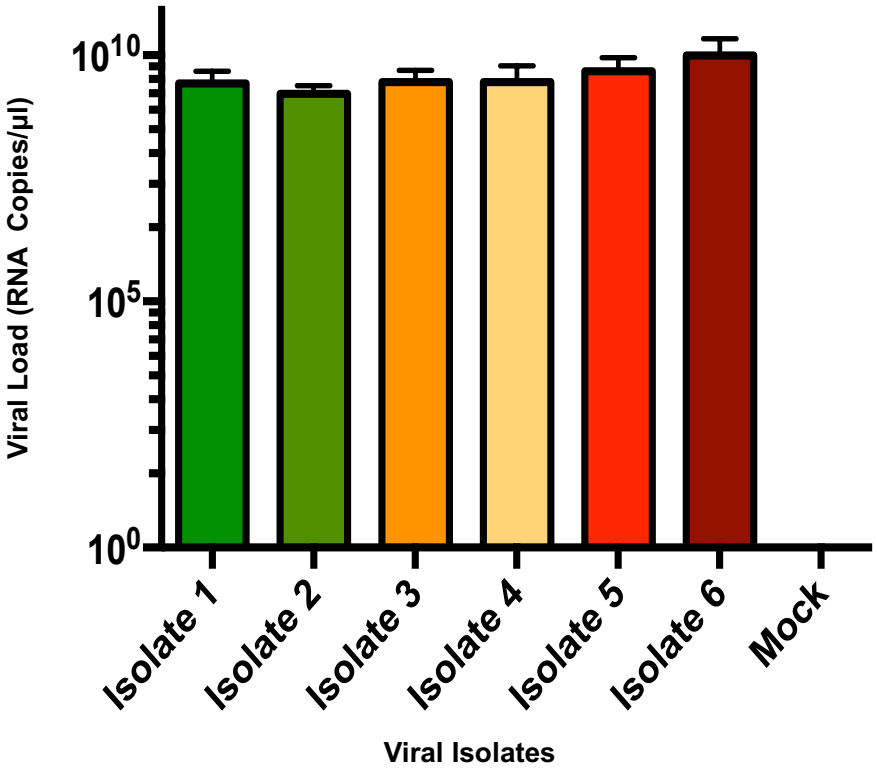

Figure 9. Novel qRT-PCR system for measuring the viral copy number of EV71 isolates.
EV71 isolates were propagated in RD cells up to P.2 to increase viral load/titre. Viral RNA was then extracted from the supernatant of the propagation media and then ran through a novel qRT-PCR system. This figure shows the viral load of the P.2 virus stocks

4.1.4 Measurement of viral replication using qRT-PCR

I also created a novel qRT-PCR assay and used it to measure the viral copy number. The viral genome was sequenced and the VP1 region of the virus was subsequently aligned and analysed using MegAlign software (Lasergene, DNA Star). Novel forward and reverse primers and a Fam-labelled molecular beacon probe were created from a consensus sequence of all six isolates; the primers and probe were a perfect match for all six isolates. RNA standards were created using a Ribogreen assay and were serially diluted from $1x10^{11}$ to create standards from $1x10^{9}$ to $1x10^{1}$ RNA copies/µl. This was used to measure the viral load of the propagated viruses to ensure high enough level of viral copy number (Fig 9).

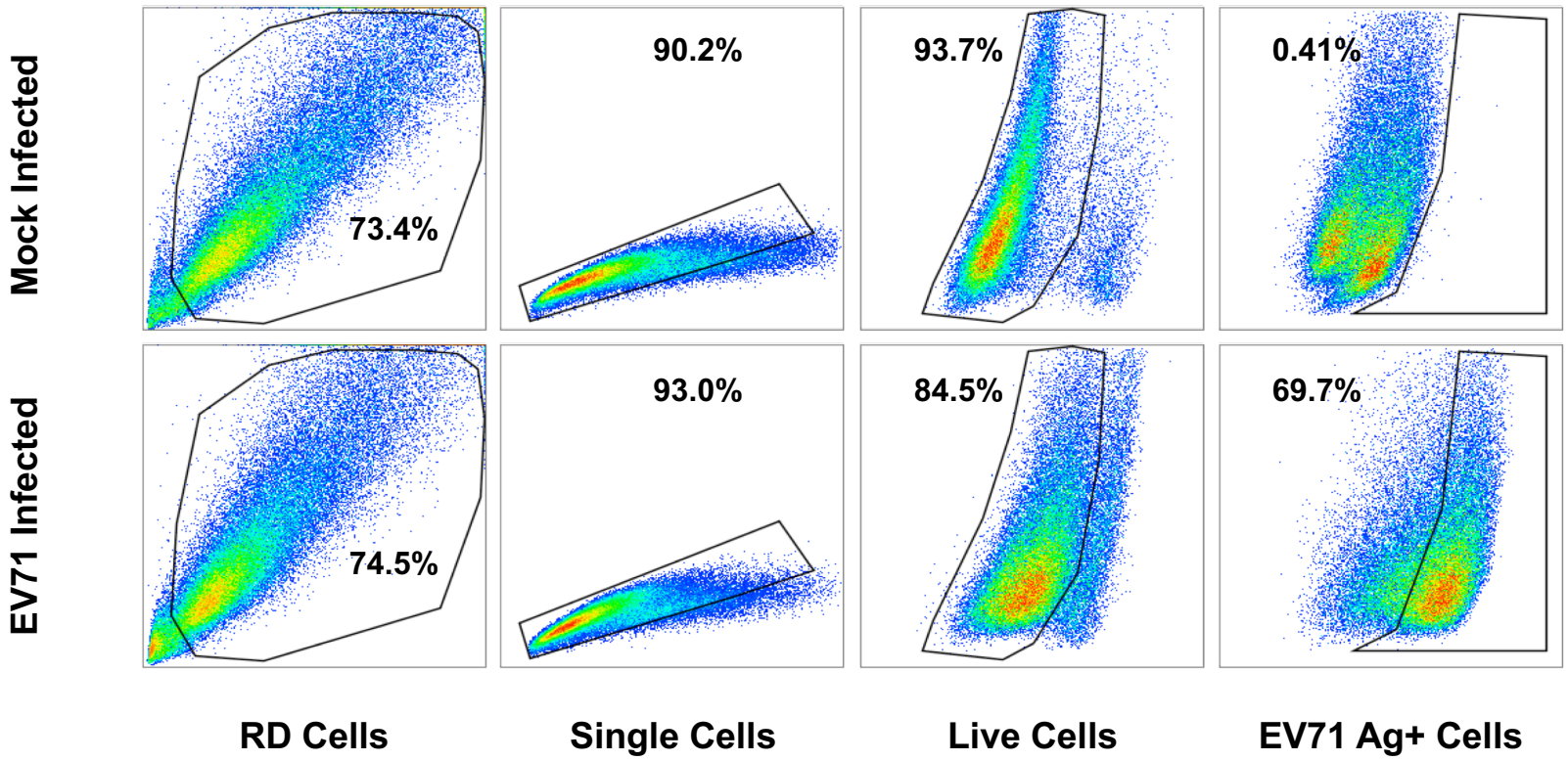

Figure 10. Gating strategy for flow cytometry analysis of viral kinetics of EV71 isolates in Rhabdomyosarcoma (RD) cells.
This figure shows a representative illustration of the flow cytometry gating strategy of EV71 infected RD cells, using 10F0 (Abcam) mouse monoclonal antibody recognizing the EV71 VP1 antigen (taken at 24hpi). RD cells were infected with EV71 isolates one to six as well as mock-infected, at MOI 10 and harvested at 0, 3, 6, 12 and 24 hours post infection (hpi). All infected cells were compared against a mock-infected control at each timepoint.

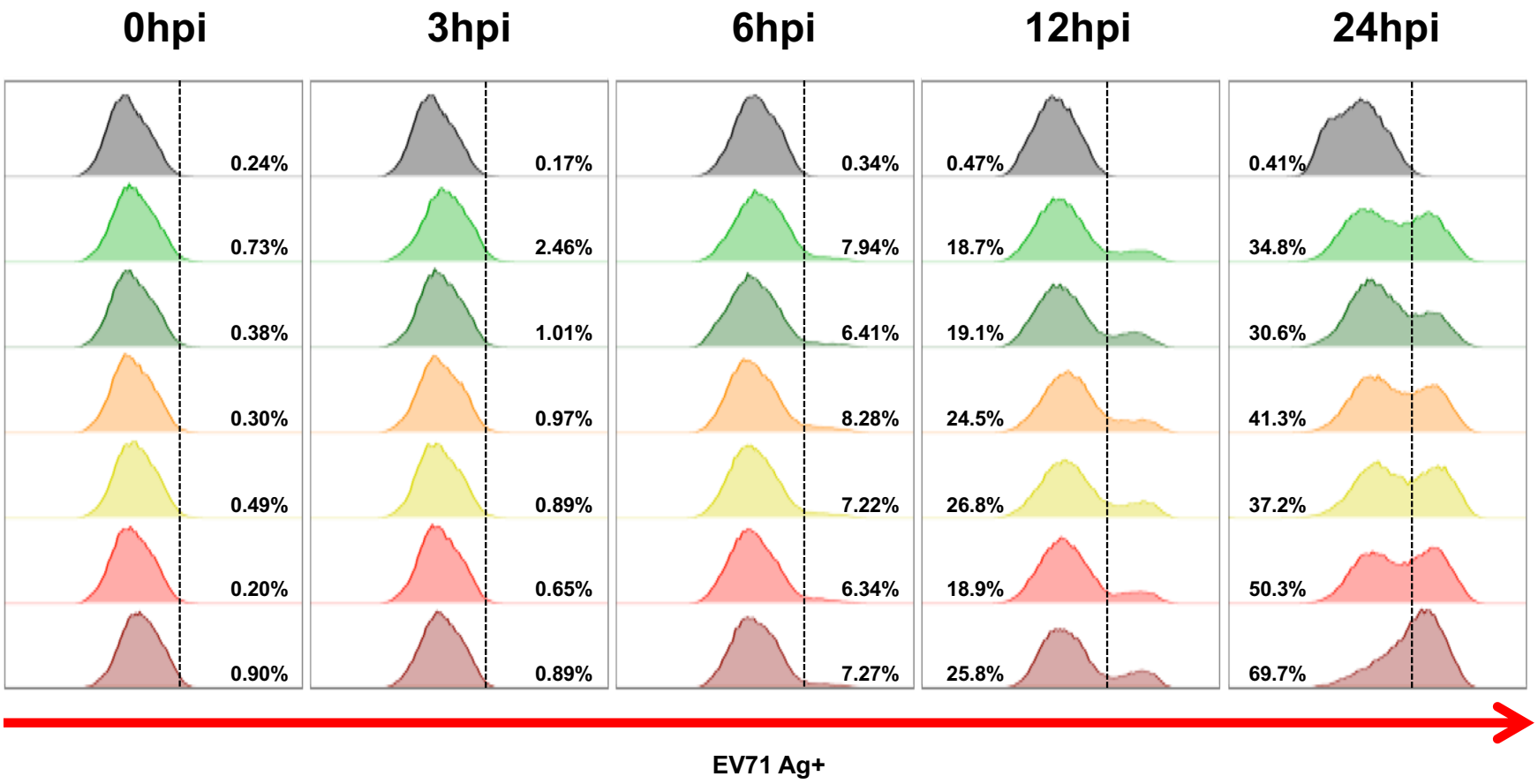

<u>Figure 11.</u> Viral kinetics of EV71 isolates in Rhabdomyosarcoma (RD) cells over 24 hours.
Representative histograms of EV71 isolates 1-6 infected RD cells at 0, 3, 6, 12 and 24hpi, collected via flow cytometry and analysed using FlowJo software. RD cells were infected with EV71 isolates 1-6, at MOI 10 and harvested at 0, 3, 6, 12 and 24 hours post infection (hpi). All infected cells were compared against a mock-infected control at each timepoint. Each isolate is identified via it's colour, used in table 1. Mock-infected is coloured black

EV71 Infectivity in RD Cells

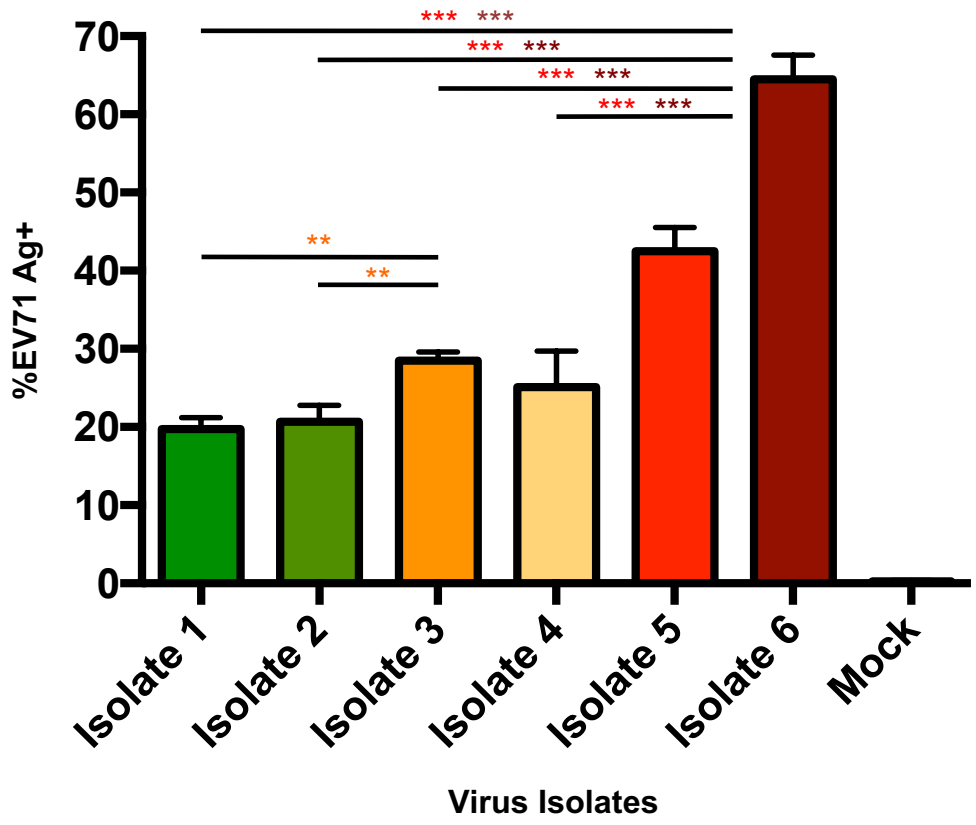

Figure 12. Severe EV71 isolates show higher levels of infectivity in RD cells over 24 hours.
RD cells were infected with the six different isolates of EV71 over 24 hours. The infected cells was taken at each respective timepoint, fixed, permed and incubated with an anti-EV71 antibody conjugated with a fluorophore. The infectivity was then measured via flow cytometry using a mock-infected sample at each timepoint as a control. This figure shows the graph of infection kinetics of EV71 isolates one to six at 24hpi in RD cells at MOI 10 (n=3). Data on this graph was compared against other isolates using 2-way ANOVA with Bonferroni's multiple comparisons (*$p<0.05$, **$p<0.01$ and ***$p<0.001$).

4.1.5 Examining the infectivity of EV71 clinical isolates

Once an acceptable titre had been reached across all isolates, the viral kinetics of the isolates were assessed over a 24-hour time period, at 0, 3, 6, 12 and 24 hours post infection, measuring infectivity via flow cytometry and replication via qRT-PCR. Infectivity was assessed by infecting RD cells with all isolates, separately, at MOI 10.

An MOI of 10 was chosen for this experiment after inspecting the surrounding literature and performing a series of optimisation experiments using different MOI's and time points. MOI's of 1 and 10 were trialled along with time points of 0, 6, 12, 24 and 48 hours post infection These MOIs and time points were selected as they have been previously used in experiments in similar literature papers (91, 207) .

Cells were harvested at 0, 3, 6, 12, and 24hpi. Virus infectivity was determined by measuring the level of intracellular EV71 VP1 antigen (Ag) detected by an anti-EV71 VP1 monoclonal antibody via flow cytometry. The threshold for EV71 positive cells was determined from the gating of mock-infected control at the same time point (Fig 10). Once this was established, infection kinetics experiments were performed by infecting RD cells with all isolates at MOI 10 across a time course of 0, 3, 6, 12 and 24hpi (Fig 11). Interestingly, significantly higher levels of EV71 Ag+ cells were detected in isolates 5 and 6 infections at 24hpi when compared with the other isolates and the mock infected. Isolate 3 also had a significantly

higher percentage of EV71 Ag+ cells when compared to isolates 1 and 2 at 24hpi (Fig 12).

EV71 Replication in RD Cells

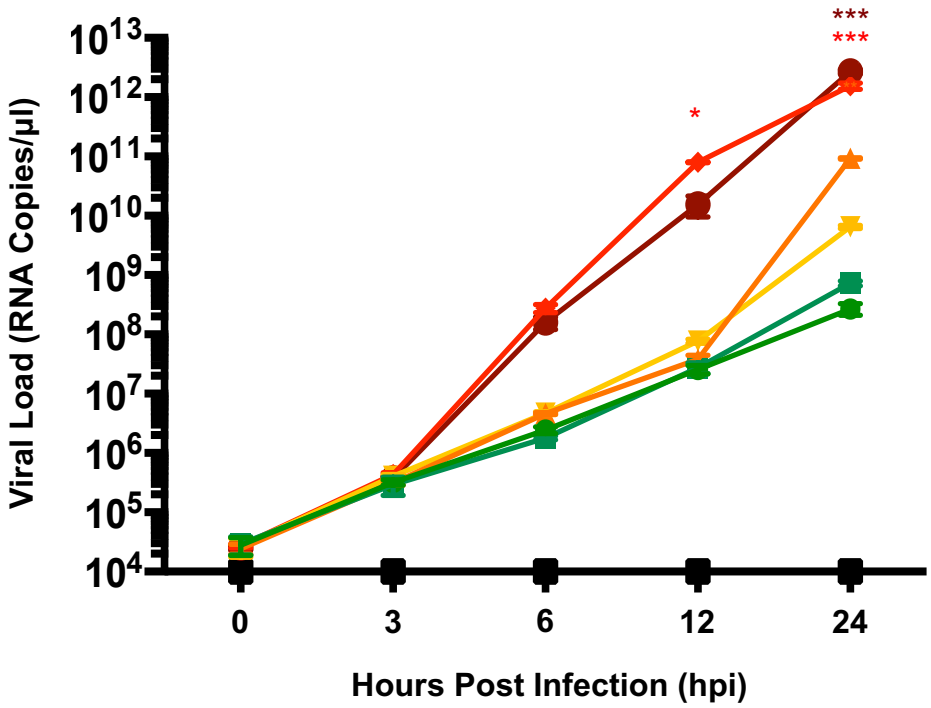

Figure 13 Severe EV71 isolates show higher levels of replication in RD cells over 24 hours.
RD cells were infected with the different isolates of EV71 over 24 hours. The infectious supernatant was taken at each respective time point, the vRNA was extracted and then ran through our novel qRT-PCR assay. This graph shows the level of EV71 isolates one to six viral load, taken at 0, 3, 6, 12, and 24hpi, and measured using qRT-PCR (n=3). Data on this graph was compared against other isolates using 2-way ANOVA with Bonferroni's multiple comparisons (*$p<0.05$, **$p<0.01$ and ***$p<0.001$).

4.1.6 Examining the replication of EV71 clinical isolates

To determine virus replication, viral RNA was extracted from the supernatant followed by qRT-PCR. Expectedly, similar trends were observed in the replication kinetics with significantly higher numbers of negative sense VP1 RNA copies observed at 24hpi for isolates 5 and 6 compared to all the other isolates and the mock-infected sample. Again isolate 3 showed significantly higher levels of negative sense VP1 RNA copies as compared to isolates 1, 2 and the mock infected sample (Fig 13).

4.2.0 *Ex vivo* human blood EV71 infection model

4.2.1 Aims

Once it was found that there was a difference in the viral kinetics of these isolates. I next wanted to examine the effect of these viruses in a model that was more relatable to the actual disease. Primary human peripheral blood mononuclear cells were chosen for this model. As leukocytes are the main players in the immune response, I wanted to use a primary source of leukocytes. This would help me examine the infectivity and immune reaction of EV71 on the host immune system, as well as giving me a view into deciphering the pathways and roles of the immune response. Using fresh PBMCs, which contain no plasma or serum, gives the added advantage (e.g. over whole blood) that the donor's antibodies will not play any role during the experiments. There will also be minimal levels of any other factors that may interfere with the experimental process such as cytokines and chemokines.

Due to the limited amount of primary PBMC donors, 3 virus isolates that representing the best range of symptoms were selected for further studies. A mild (HFMD only - Isolate 1), moderate (HFMD and meningoencephalitis - Isolate 3) and severe (fatal - Isolate 5) strain of EV71 were chosen. Viral load, infectivity, immunophenotyping and RNASeq analysis was subsequently performed on the samples.

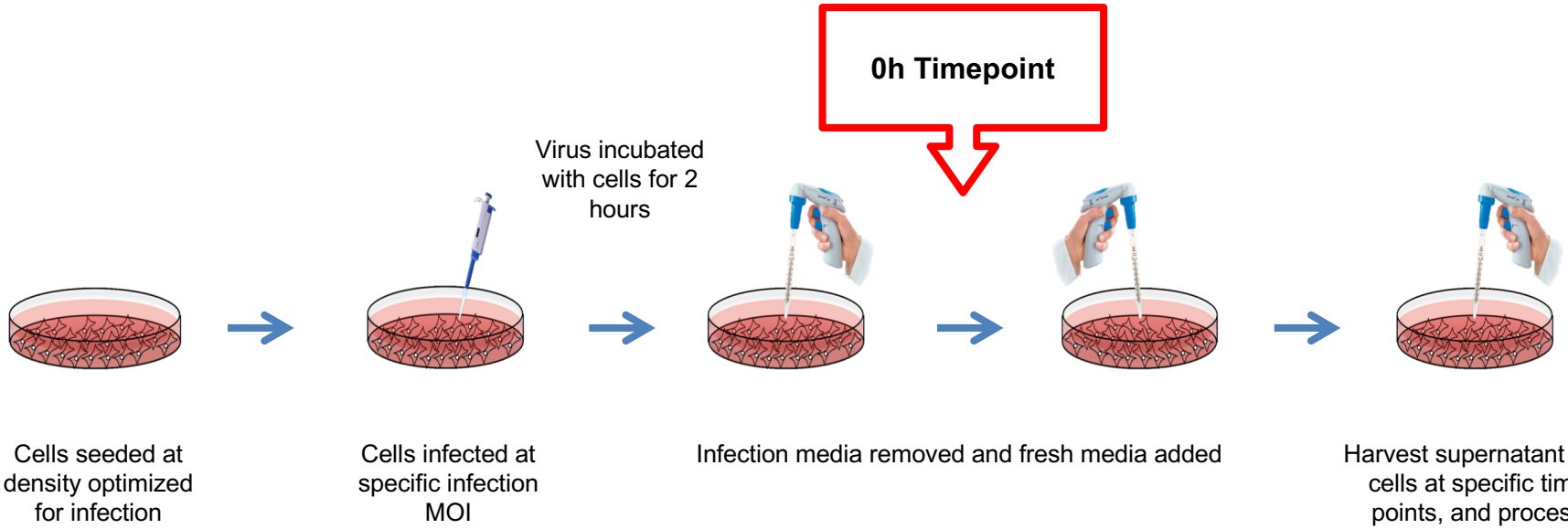

<u>Figure 14.</u> Diagram of infection protocol for all infection experiments.
Cells were seeded at their optimal density depending on which infection experiment was being carried out. The cells were then infected with the specific virus at the specific MOI respective to that experiment. The cells were then incubated for 2 hours at 37°C with 5% CO_2. After these two hours, the virus mix was removed and fresh media was added. Once the fresh media was added, this is the 0h time point. Just to note, at 0h post infection the virus has been in contact with the cells for 2 hours, so this is why infection and viral load can be seen at 0h post infection.

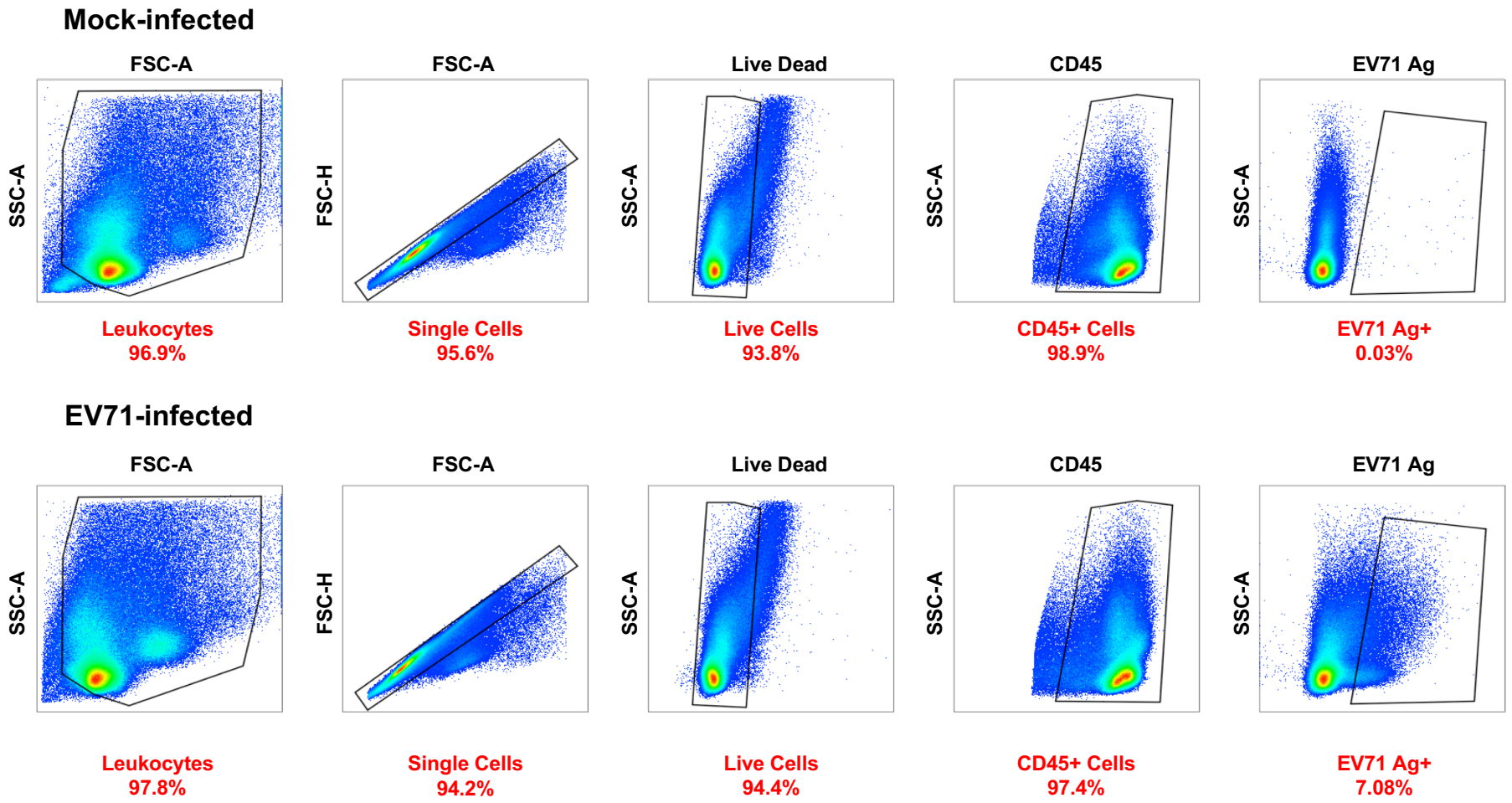

<u>Figure 15.</u> Gating strategy for flow cytometry analysis of CD45+ EV71 infected cells.
PBMCs were infected with EV71 isolates 1, 3 and 5, as well as heat inactivated EV71 and a mock-infected control, at MOI 5 over 24 hours. The PBMCs were harvested at each respective timepoint, then fixed, permed and stained with an anti-EV71 antibody and respective cell surface marker antibodies, then analysed using flow cytometry. This figure shows a representative illustration of the flow cytometry gating strategy of EV71 infected PBMCs, taken at 6hpi.

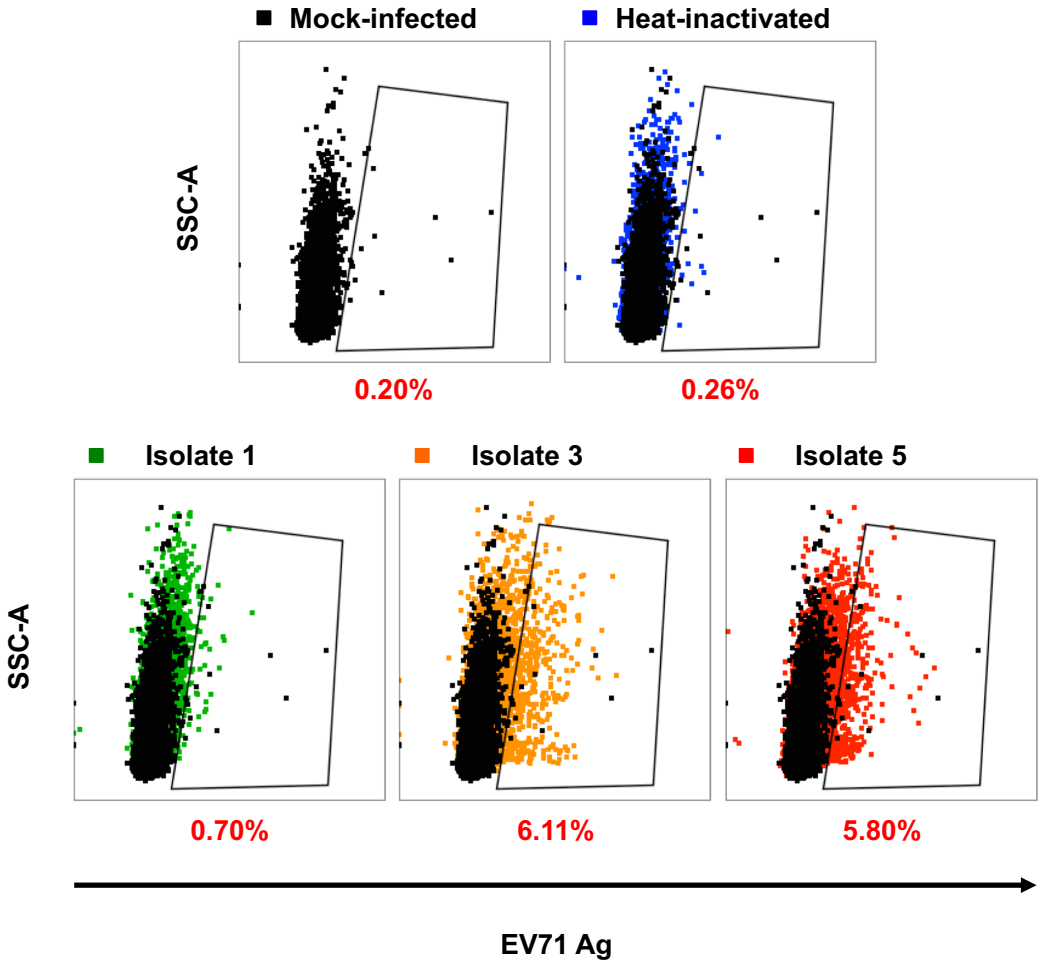

Figure 16. Infection percentages of CD45+ gated cells from PBMCs infected with EV71 isolates of differing severity.
PBMCs were infected with EV71 isolates 1, 3 and 5, as well as heat inactivated EV71 and a mock-infected control, at MOI 5 over 24 hours. The PBMCs were harvested at each respective timepoint, then fixed, permed and stained with an anti-EV71 antibody and respective cell surface marker antibodies. The cells were gated in to CD45+ cells, and then EV71 Ag+ percentage was compared to the mock-infected control at the specific timepoint. This figure shows a representative dot plots of the EV71 Ag gate of CD45+ EV71 infected PBMCs (taken from 6hpi).

4.2.2 EV71 infection in primary human peripheral blood mononuclear cells

PBMCs were isolated from human blood apheresis cones and infected with EV71 isolates 1, 3 and 5, along with heat-inactivated and mock-infected controls at MOI 5 across a time course of 0, 6, 12 and 24hpi.

An MOI of 5 was chosen for this experiment after inspecting the surrounding literature and performing a series of optimisation experiments using different MOI's and time points. MOI's of 1, 5 and 10 were trialled along with time points of 0, 12, 24, 48 and 72 hours post infection These MOIs and time points were selected as they have been previously used in experiments in similar literature papers (130, 131).

At each time point the PBMCs were harvested, fixed, stained for dead cells, permed, stained with a mouse anti-EV71 antibody, then stained with an anti-mouse antibody conjugated with a fluorophore, then finally stained with antibodies against certain cell surface markers. This was then analysed using flow cytometry. Infectivity in the PBMCs was determined by initially gating out the dead and duplet cells using a fixable Live/Dead stain and an FSC-W/FSC-H gate respectively, before gating the CD45+ cells and measuring the level of intracellular EV71 VP1 Ag. The threshold for EV71 positive cells was determined from the gating of the mock-infected control at the same time point (Fig 15). Each infection was completed to n=10. The neurovirulent isolates (isolates 3 and 5) were shown to be more infectable in PBMCs as compared to the non-neurovirulent isolate (isolate

1) (Fig 16). Significantly higher levels of EV71 VP1 Ag were detected in the neurovirulent isolates of EV71 (3 and 5) as compared with the non-neurovirulent strain (isolate 1), the heat-inactivated virus and the mock-infected controls (Fig 13). All the data within these graphs were compared using Friedman analysis (*$p<0.05$, **$p<0.01$ and ***$p<0.001$).

EV71 Infectivity in PBMCs

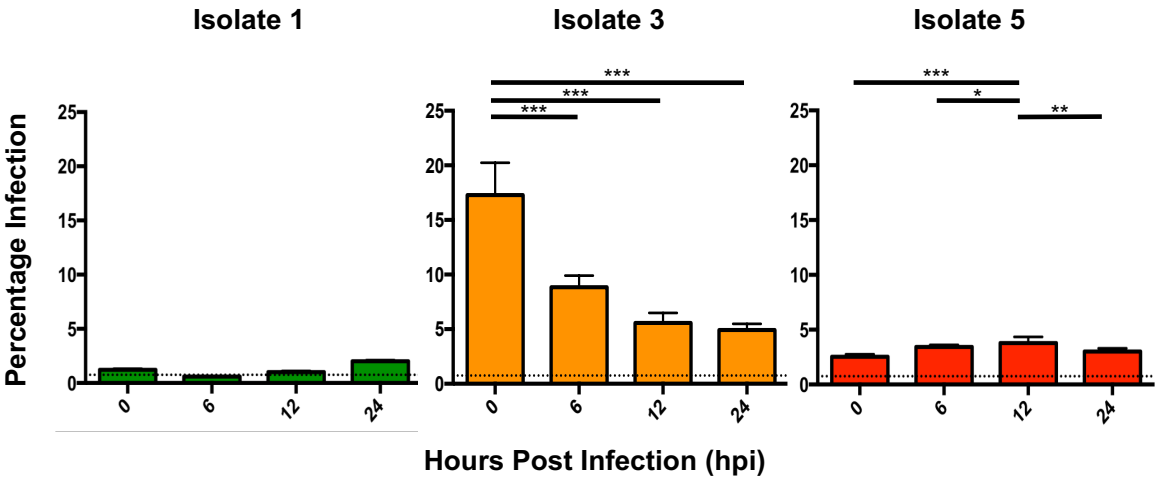

Figure 17. Infection percentages of EV71 isolates of differing severities in CD45+ cells from PBMCs over 24 hours.
PBMCs were infected with EV71 isolates 1, 3 and 5, as well as heat inactivated EV71 and a mock-infected control, at MOI 5 over 24 hours. The PBMCs were harvested at each respective timepoint and analysed via flow cytometry. The cells were gated in to CD45+ cells, and then EV71 Ag+ percentage was compared to the mock-infected control at the specific timepoint. This figure shows the summary graphs of the infection percentages of CD45+ cells infected by the different EV71 isolates (n=10). Dotted line represents mock-infected control. Data within these graphs were compared using Friedman analysis (*$p<0.05$, **$p<0.01$ and ***$p<0.001$).

4.2.3 Examining the infection kinetics in primary human PBMCs

Differing trends were seen across the isolates over the time-course of infection in PBMCs. Isolate 1 showed limited infectivity across all time points during the PBMC infection, barely passing the background baseline set by the mock-infected control. There was a non-significant increase from 6 to 24hpi, however this still did not exceed 2% infection (Fig 17).

Isolate 3 showed high levels of initial infectivity, peaking after the initial incubation period at 0hpi. However, it then had steadily decreasing levels of EV71 VP1 Ag detected as the time course progressed, with 0hpi having significantly higher levels of infection over 6, 12 and 24hpi (Fig 17). As previously shown in Fig 14 at 0hpi the cells have already been incubated with the virus for two hours, which is enough time for EV71 to begin binding to its receptors and start the internalisation process. This is why these levels of infection can be seen at 0hpi.

Isolate 5 was the only isolate to show increasing levels of infectivity across the time points. With initially low levels of infectivity at 0hpi, there was a non-significant increase between 6hpi. Infectivity peaked at 12hpi, with a significantly higher point of infection than any other time point. Before decreasing at 24hpi to a level below the 6hpi level of infectivity (Fig 17).

EV71 Replication in PBMCs

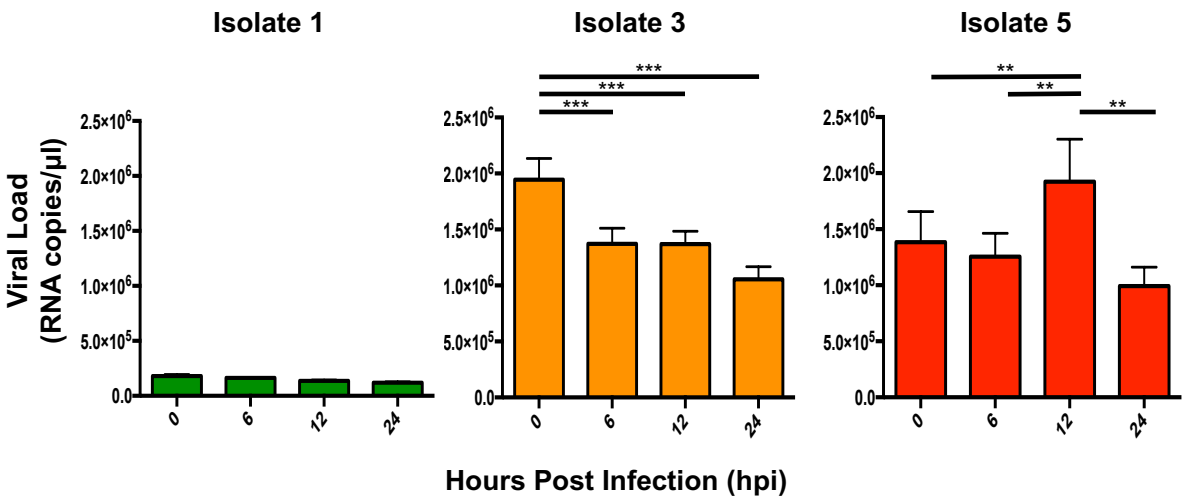

Figure 18. Viral load of EV71 isolates of differing severities in CD45+ cells from PBMCs over 24 hours.
PBMCs were infected with EV71 isolates 1, 3 and 5, as well as heat inactivated EV71 and a mock-infected control, at MOI 5 over 24 hours. The infectious supernatant was collected at each time point from each isolate. The vRNA was extracted and then analysed via a novel qRT-PCR assay. This figure shows the summary graphs of the viral loads of PBMCs infected by the different EV71 isolates (n=10). Data within these graphs were compared using Friedman analysis (*$p<0.05$, **$p<0.01$ and ***$p<0.001$).

4.2.4 Examining the replication kinetics in primary human PBMCs

As well as harvesting the cells, the supernatant was also taken from the infectious mix at each time point. The viral RNA was extracted from this supernatant and then the level was measured using a novel qRT-PCR assay. Similar trends to the infectivity kinetics were also observed in the viral load from the PBMC infection. Isolate 1 showed significantly lower levels of VP1 RNA copies detected across all time points as compared with isolates 3 and 5. They were significantly higher than the mock-infected sample at each time point, but there was no significant increase across any of the time points (Fig 18).

Isolate 3 again showed significantly high initial levels of VP1 RNA copies, peaking at 0hpi. There was a significant decrease between 0 and 6hpi. The viral load then plateaued between 6 and 12hpi, before decreasing again at 24hpi. This decrease across all time points shows that there was limited replication during the isolate PBMC infection (Fig 18).

Isolate 5 was the only isolate that seemed to show replicative capacity during this PBMC infection. There was no increase between 0 and 6hpi, however there was then a significant increase in viral load between 6 and 12hpi. Showing that isolate 5 has the capacity to replicate in human PBMCs. There was then a significant decrease in viral load between 12 and 24hpi, suggesting 6-12hpi is the peak time for replication in PBMCs for this isolate (Fig 18).

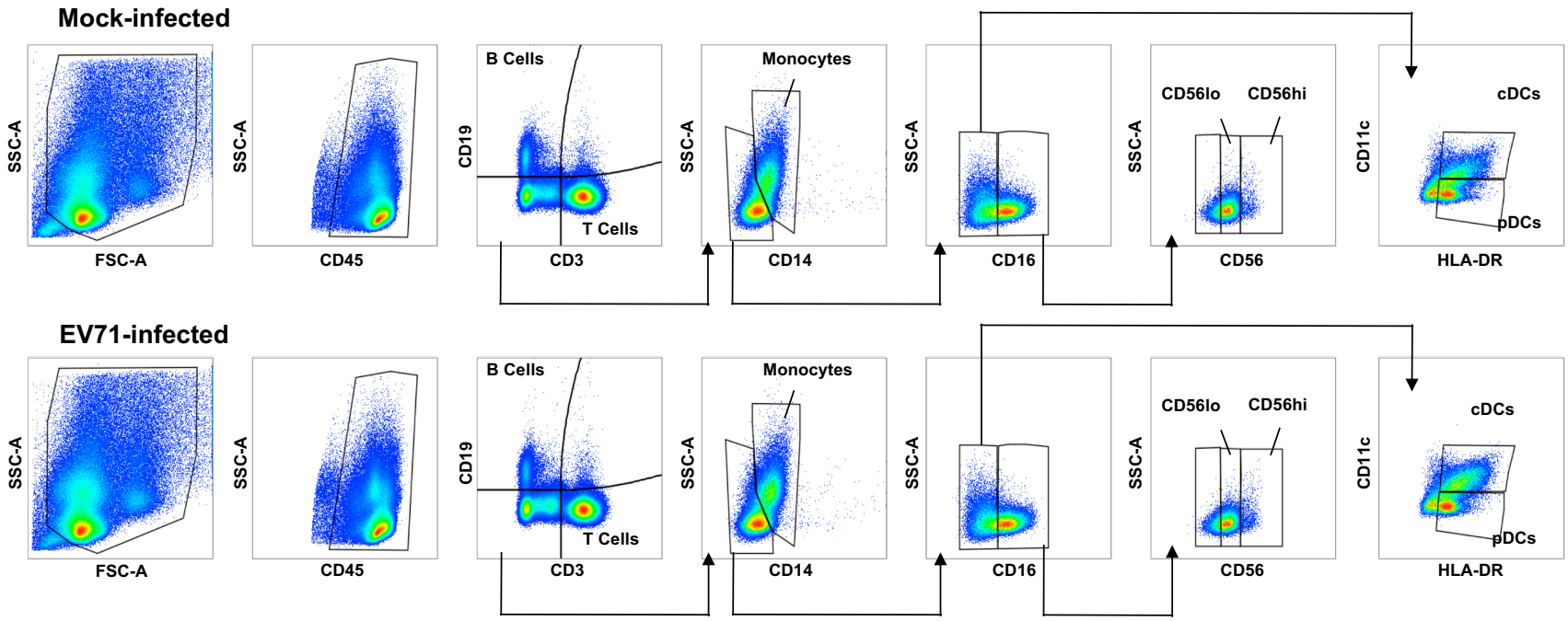

<u>Figure 19.</u> Flow cytometry gating strategy for immunophenotyping PBMCs after EV71 infection.
After infection with EV71 and harvesting at specific time points, the PBMCs were fixed, permed, stained with antibodies for EV71 and then stained with antibodies for cell surface markers. The cells are gated on size and granularity to remove debris. Then gated for single cells and Live/Dead (shown on Figure 7). The leukocytes are then gated using CD45+ cells. From these cells T cells and B cells are gated using a CD3/CD19 gate. T cells are CD3+/CD19-. B cells are CD3-/CD19+. The rest of the panel is gated from the CD3-/CD19- gate. Monocytes are gated from this using CD14/SSC-A, CD14+ cells are the monocytes, these can be further gated into CD14+/CD16- or CD14+/CD16+ monocytes (not shown). The CD14-/SSC-A gate is then gated using CD16/SSC-A. CD16+ cells are further gated using CD56/SSC-A in to CD56lo and CD56high NK cells. The CD16- gate is further gated using a HLA-DR/CD11c gate. With HLA-DR+/CD11c+ cells being cDCs and HLA-DR+/CD11c- cells being pDCs. This figure shows a representative image of the gating strategy used to isolate the immune cell subsets after EV71 infection in PBMCs via flow cytometry (taken at 12hpi)

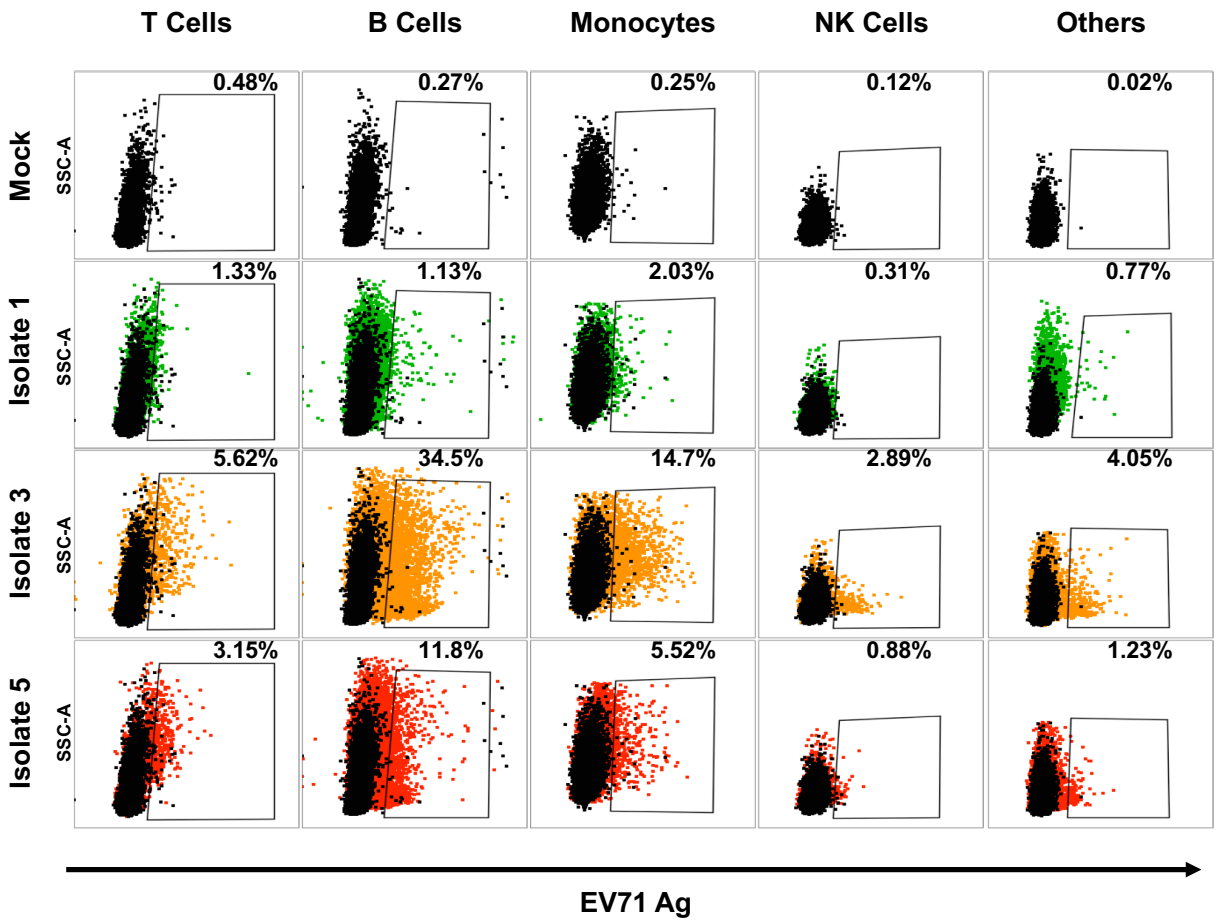

<u>Figure 20.</u> Infection levels in leukocyte subsets of PBMCs after infection with EV71 isolates over 24 hours.
EV71 infected PBMCs were harvested, fixed, permed and stained with EV71 and surface marker antibodies, and then analysed via flow cytometry. They were then gated as shown in figure 11. Each subset was then gated against the EV71 Ag and the percentage infectivity was analysed, as compared to the mock-infected. This figures show representative dot plots of the infection levels for the T cells, B cells, monocytes, NK cells and the other cells, gated from EV71 infected PBMCs. Image taken from 6hpi.

4.2.5 Non-virulent and virulent strains of EV71 isolates generate different immunophenotype infectability profiles

To further examine the role of PBMCs in EV71 infection severity, immunophenotyping was performed on the infected PBMCs. This allowed for an in-depth analysis of the infection profiles and kinetics of the immune subsets. The cells were further gated from the CD45+ leukocyte population (Fig 15) into the subset populations of PBMCs using the cell surface markers, CD3, CD19, CD14, CD16, CD56, CD11c and HLA-DR. These markers separate the cells into:

- T cells - CD45+/**CD3+**/CD19-
- B cells - CD45+/CD3-/**CD19+**
- Monocytes - CD45+/CD3-/CD19-/**CD14+**
    - CD45+/CD3-/CD19-/**CD14+/CD16+**
    - CD45+/CD3-/CD19-/**CD14+/CD16-**
- NK cells - CD45+/CD3-/CD19-/CD14-/**CD16+/CD56+**
    - CD45+/CD3-/CD19-/CD14-/**CD16+/CD56lo**
    - CD45+/CD3-/CD19-/CD14-/**CD16+/CD56hi**
- cDCs - CD45+/CD3-/CD19-/CD14-/CD16-/**HLA-DR+/CD11c+**
- pDCs - CD45+/CD3-/CD19-/CD14-/CD16-/**HLA-DR+/CD11c-**

Important respective cell surface markers are in bold (Fig 19).

EV71 Infectivity in PBMC Leukocyte Subsets

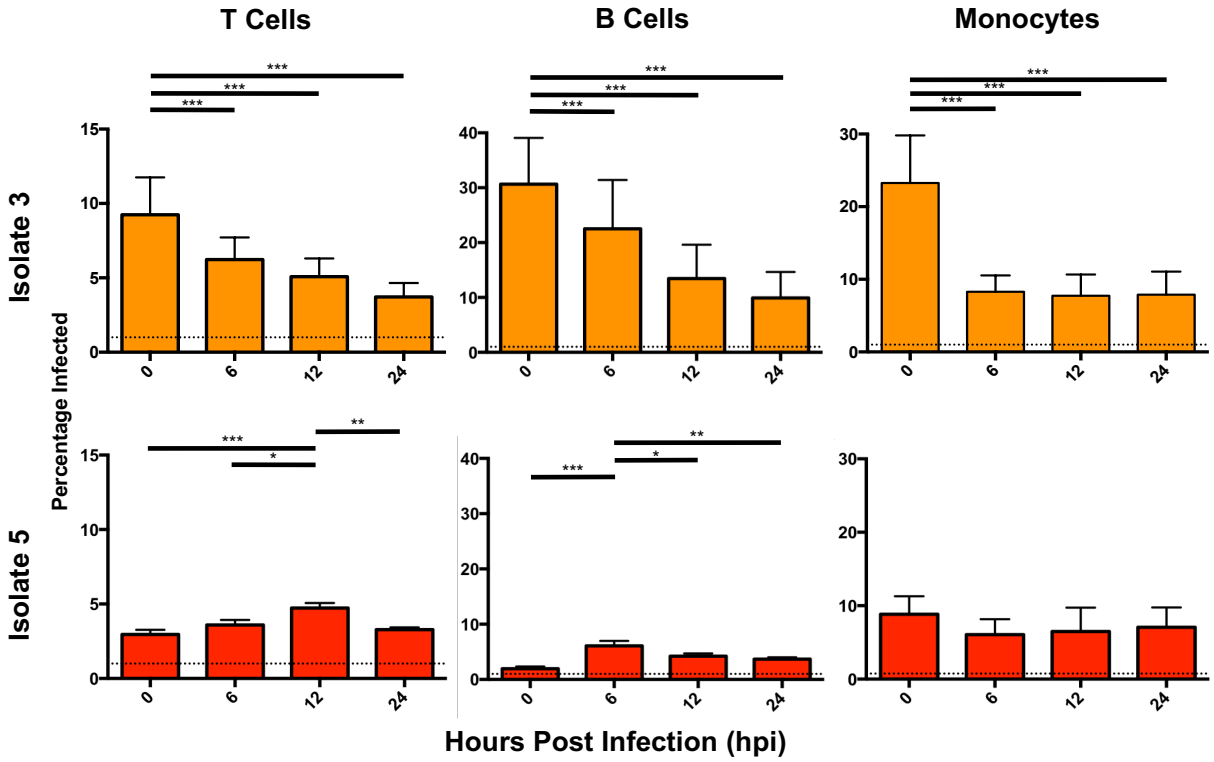

Figure 21. Infectivity in leukocyte subsets of PBMCs after infection with EV71 isolates over 24 hours.
EV71 infected PBMCs were harvested, fixed, permed and stained with EV71 and surface marker antibodies, and then analysed via flow cytometry. They were then gated as shown in figure 11. Each subset was then gated against the EV71 Ag and the percentage infectivity was analysed, as compared to the mock-infected. This figure shows summary graphs of the level of infection in T cells, B cells and monocytes gated from PBMCs infected with the EV71 isolates (n=10). Dotted line represents mock-infected baseline. Isolate 1 not shown as no infection seen. Data within these graphs was compared using Friedman analysis (*$p<0.05$, **$p<0.01$ and ***$p<0.001$).

From this more in-depth gating, it was observed that there are three main infectable subsets within the PBMCs; T cells, B cells and monocytes (Fig 20), which show higher levels of infection compared to the other subsets. These other subsets such as DCs and NK cells were infectable but showed lower/limited levels of infectability (Fig 20). It is also seen that isolate 1 (non-virulent) shows limited infection across all of the immune cell subsets, when compared with the virulent strains (isolate 3 and 5). It has a profile closer to the heat inactivated and mock-infected samples (Fig 20).

Isolate 3 showed a similar infectivity trend in T cells as in the total PBMCs. There was a significantly high initial level of EV71 VP1 Ag+ cells detected at 0hpi. There was then a steady decrease to 6hpi then 12 and 24hpi (Fig 21). This trend was also seen in the other lymphocyte population, the B cells. Again, with significantly high levels of EV71 Ag+ cells being detected at 0hpi, and then a steady decline over the 24 hours (Fig 21). Isolate 3 infected monocytes; however, showed a slightly different pattern to that of the isolate 3 infected lymphocytes and infected PBMCs. Although a similar initial high infectivity at 0hpi was observed, there was a larger decrease in EV71 Ag+ cells between 0 and 6hpi, and then plateau with a similar/constant level of infectivity across the remaining time points (Fig 21).

Each of the leukocyte subsets showed different infection profiles after infection with EV71 isolate 5, as well as showing completely different trends from the other isolates. The isolate 5 infected T cells subset showed a

similar pattern of infection to isolate 5 infected total PBMCs. This was a steady, significant increase in infection from 0hpi to 12hpi, where the infection peaked, before a decrease in infection at 24hpi (Fig 19). The B lymphocyte subset showed an earlier increase in infectivity than T cells. With low levels of infection at 0hpi, suddenly peaking to significantly higher levels at 6hpi, before steadily decreasing at 12 and 24hpi (Fig 21). EV71 isolate 5 infected monocytes showed a completely different trend to either of the lymphocyte subsets. It maintained a constant, relatively high, level of infectivity across the 24-hour time course (Fig 21). Both isolate 3 and isolate 5 showed significantly higher levels of infection in T cells, B cells and monocytes as compared to the heat inactivated virus and the mock-infected control.

EV71 Infectivity in Monocytes

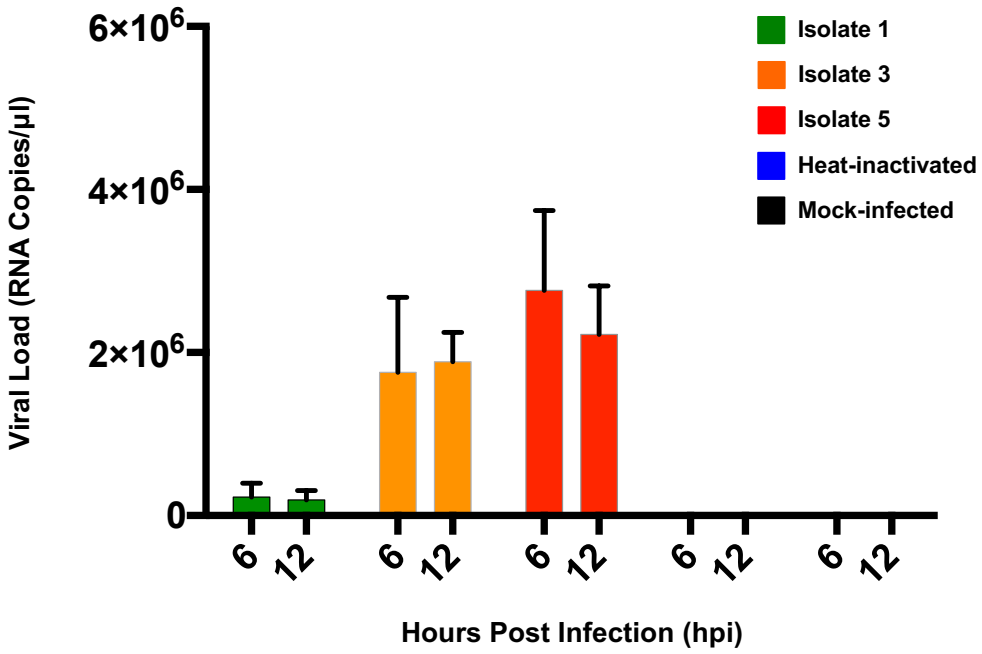

Figure 22. Replication of EV71 isolates of differing severities in monocytes isolated from PBMCs over 24 hours.
Isolated human primary monocytes were infected with EV71 isolates 1, 3 and 5, as well as heat inactivated EV71 and a mock-infected control, at MOI 5 and harvested at 6 and 12hpi. This figure is a summary graph of viral load taken from EV71 isolate 1, 3 and 5, heat inactivated and mock infected human monocytes at 6 and 12hpi (n=4). Data within this graph was compared using Friedman analysis (*$p<0.05$).

EV71 Infectivity in CD8+ T Cells

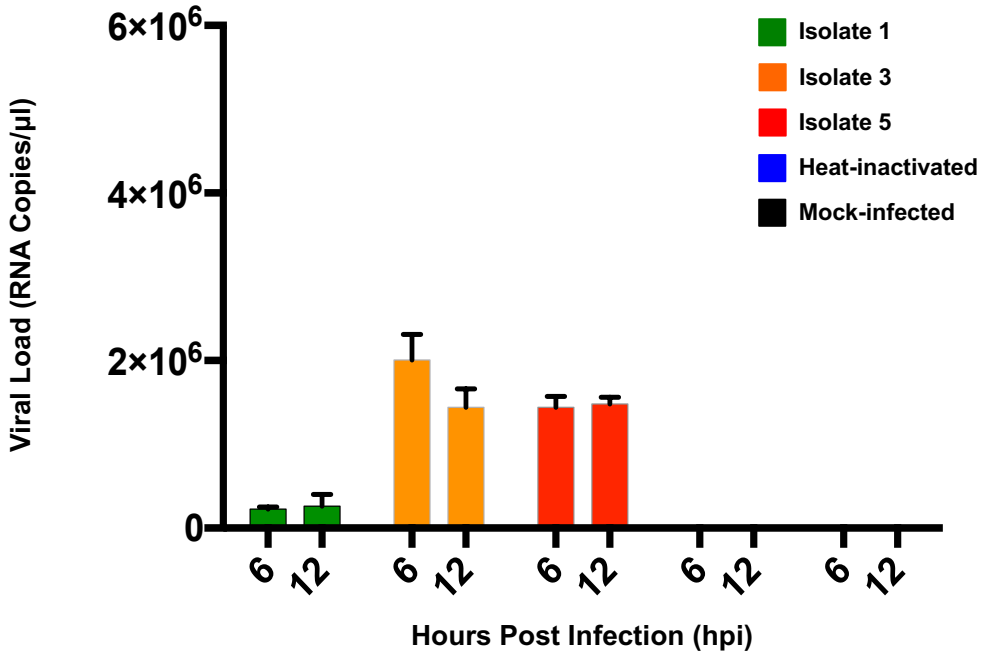

Figure 23. Replication of EV71 isolates of differing severities in CD8+ T cells isolated from PBMCs over 24 hours.
Isolated human primary CD8+ T cells were infected with EV71 isolates 1, 3 and 5, as well as heat inactivated EV71 and a mock-infected control, at MOI 5 and harvested at 6 and 12hpi. This figure is a summary graph of viral load taken from EV71 isolate 1, 3 and 5, heat inactivated and mock infected human CD8+ T cells at 6 and 12hpi (n=4). Data within this graph was compared using Friedman analysis (*$p<0.05$).

EV71 Infectivity in CD4+ T Cells

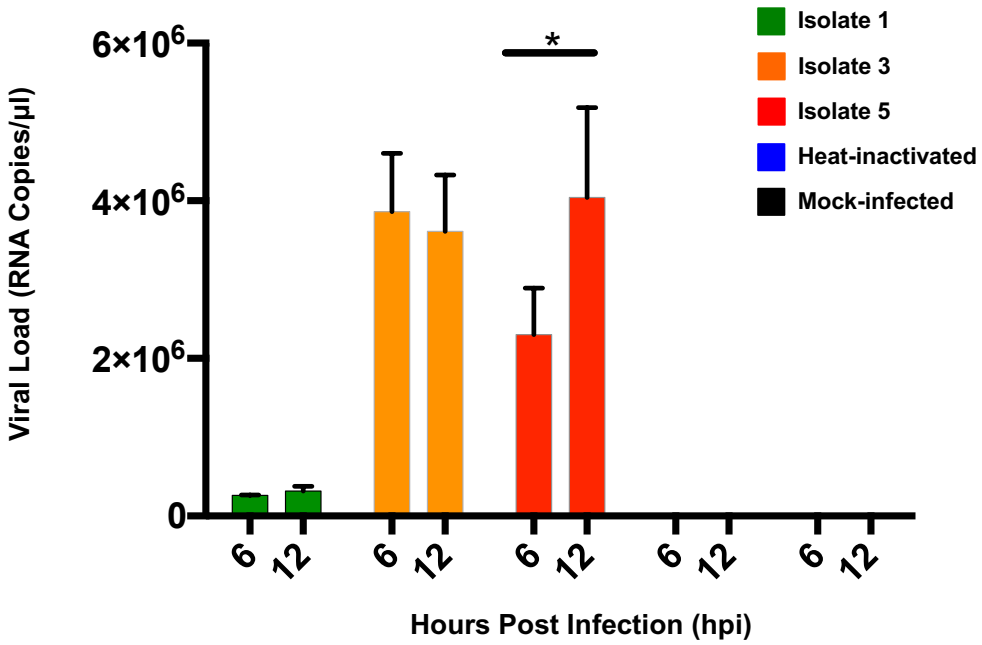

Figure 24. Replication of EV71 isolates of differing severities in CD4+ T cells isolated from PBMCs over 24 hours.
Isolated human primary CD4+ T cells were infected with EV71 isolates 1, 3 and 5, as well as heat inactivated EV71 and a mock-infected control, at MOI 5 and harvested at 6 and 12hpi. This figure is a summary graph of viral load taken from EV71 isolate 1, 3 and 5, heat inactivated and mock infected human CD4+ T cells at 6 and 12hpi (n=4). Data within this graph was compared using Friedman analysis (*$p<0.05$)

4.2.6 Differential replication kinetics seen across individual primary peripheral blood cell subsets

To deeper explore the role of the individual immune cell subsets a further infection using isolates 1, 3 and 5 as well as heat inactivated virus and a non-infected mock control, was performed on isolated monocytes, CD4+ and CD8+ T cells. Viral RNA was isolated from the supernatant of these infections at 6 and 12hpi and then analysed through qRT-PCR.

After examination of the viral load taken during infection, isolate 1 again showed significantly lower levels of VP1 RNA copies across the time points when compared with the other two isolates in monocytes (Fig19), CD8+ T cells (Fig 23) and in CD4+ T cells (Fig 24). Isolate 3 showed no significant change in viral load across the between 6 and 12 hours post infection during the isolated monocyte infection. However, the level was significantly higher than the mock-infected, heat inactivated and isolate 1 infections (Fig 22). There was also no significant change in viral copy number during the isolate 3 infection of isolated CD8+ T cells (Fig 23), this was again, however, significantly higher than the isolate 1, heat inactivated and mock-infected samples. A similar trend is also seen in the isolate 3 infected CD4+ T cells, with no significant change across the time points but being significantly higher than isolate 1 and the controls (Fig 24). These outcomes substantiate the results seen in the whole PBMC infection.

Isolate 5 showed limited replication in monocytes across the 6 and 12h time points (Fig 22). This lack of significant change in viral copy number is

also seen in the CD8+ T cells (Fig 23). Both are significantly higher than isolate 1 and the controls however. The CD4+ T cell infection is where isolate 5 differs from the other isolates. There was a significant increase in EV71 VP1 RNA copies in isolate 5 infected CD4+ T Cells between 6 and 12hpi (Fig 24), which was not seen in any of the other subsets. This significant change points to the CD4+ T cells being the major players in EV71 replication in PBMCs. This increase in replication is also at the same time point as the isolate 5 infection in whole PBMCs (Fig 16).

4.3.0 *In Vitro* Human Blood-Brain Barrier Model

4.3.1 Aims

As EV71 can be a neurotropic virus, and the mechanism of entry to the brain is not fully clarified, I wanted to examine the ability of the different isolates to cross/breakdown the blood-brain barrier, to see if this could play a possible role in EV71 pathogenicity. I also wanted to examine the genes and pathways that could play a role, to figure out why EV71 can cross the blood brain barrier, and to do this I needed a non-neurotropic virus to which I could compare EV71, for this I chose Chikungunya virus.

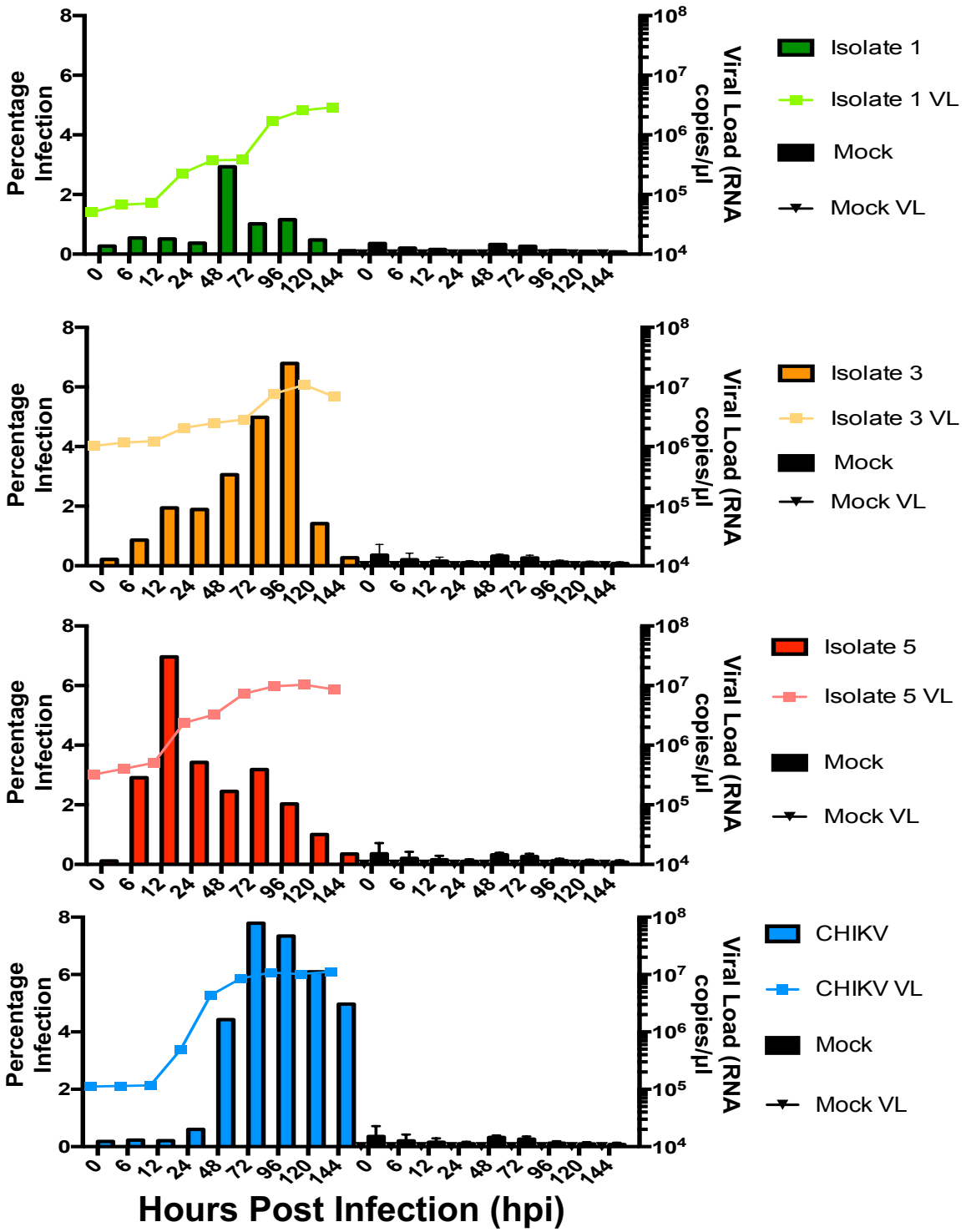

<u>Figure 25.</u> EV71 infection and replication in a 60mm dish *in vitro* infection of HCMEC/D3 cells.
HCMEC/D3s were seeded in 60mm dishes and infected with the different isolates of EV71 at MOI 10. At each time point the cells were harvested and analysed for level of infection via flow cytometry. The cell supernatant was also harvested and the viral RNA was extracted and the viral load was assessed via qRT-PCR. All samples were compared to a mock infected sample at the same time point.

4.3.2 Cerebral microvascular endothelial cell susceptibility to EV71 infection and replication.

Before I began to test on a BBB model, I first wanted to know if HCMEC/D3 cells were susceptible to EV71 infection. The cells were seeded in 60mm dishes and infected with isolates 1, 3 and 5 of EV71 at MOI 10 and incubated for up to 144 hours. At each time point the cells were harvested and analysed for level of infection via flow cytometry. Isolate 1 showed limited infectivity during this infection, with most time points being similar to the mock infected sample, and the peak of infectivity only just reaching over 2% infectivity at 48hpi (Fig 25). Isolate 3 had a much greater level of infection however. The level of infection gradually increased across the time points, reaching a peak at 96hpi, suggesting it has a much greater ability to infect these cells (Fig 25). Isolate 5 reached a similar level of infectivity to isolate 3, however it achieved this infection level at a much faster rate peaking at 12hpi, suggesting an even greater suitability to these cells (Fig 25).

As well as harvesting the cells from the infection, I also harvested the supernatant from and extracted the viral RNA so I could analyse the viral load of these infections. The results showed a similar trend to the infection profiles. Isolate 1 showed limited replication compared with the other two isolates, with one main peak just after 48hpi (Fig 25). Isolate 3 showed a higher level of replication, gradually increasing and peaking just after 96hpi (Fig 25). Isolate 5 showed a similar level of replication to isolate 3, but with its large increase in replication seen just after 12hpi (Fig 25).

TEER in a HCMEC/D3 BBB Model

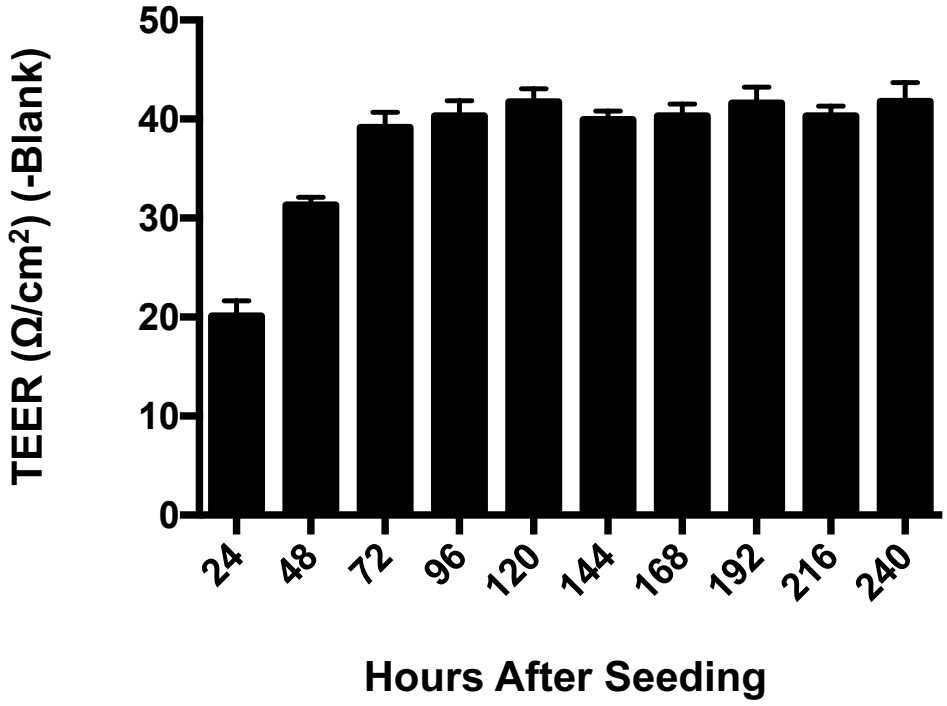

Figure 26. Setting up of monolayer HCMEC/D3 *in vitro* blood brain barrier model.
Human cerebral microvascular endothelial cells were seeded on a 12-well transwell semi-permeable membrane insert at 1E5 per insert. They were left to grow and the TEER was measured every 24 hours. This is a summary graph showing the TEER level after the blank value had been deducted.

4.3.3 *In vitro* blood-brain barrier model optimisation

The next step in this experimental procedure was to optimise the BBB model I would be using. The model needed to be able to withstand the amount of time the infection would run for, without the barrier losing integrity, as this would compromise the results. HCMEC/D3 cells were seed on 12-well transwell inserts, which were then placed into a 12 well plate. The cells were then left to grow, and the transendothelial electrical resistance (TEER) was measure every 24 hours (Fig 26). The BBB did not reach optimal strength until 72 hours after initial seeding, which meant that the infection should not take place before this time point. The TEER value did not significantly change from this point onwards, until the experiment was stopped at 240 hours after the initial seeding (Fig 26). From 72h to 240h would be enough time for all the time points I wanted to use for these experiments.

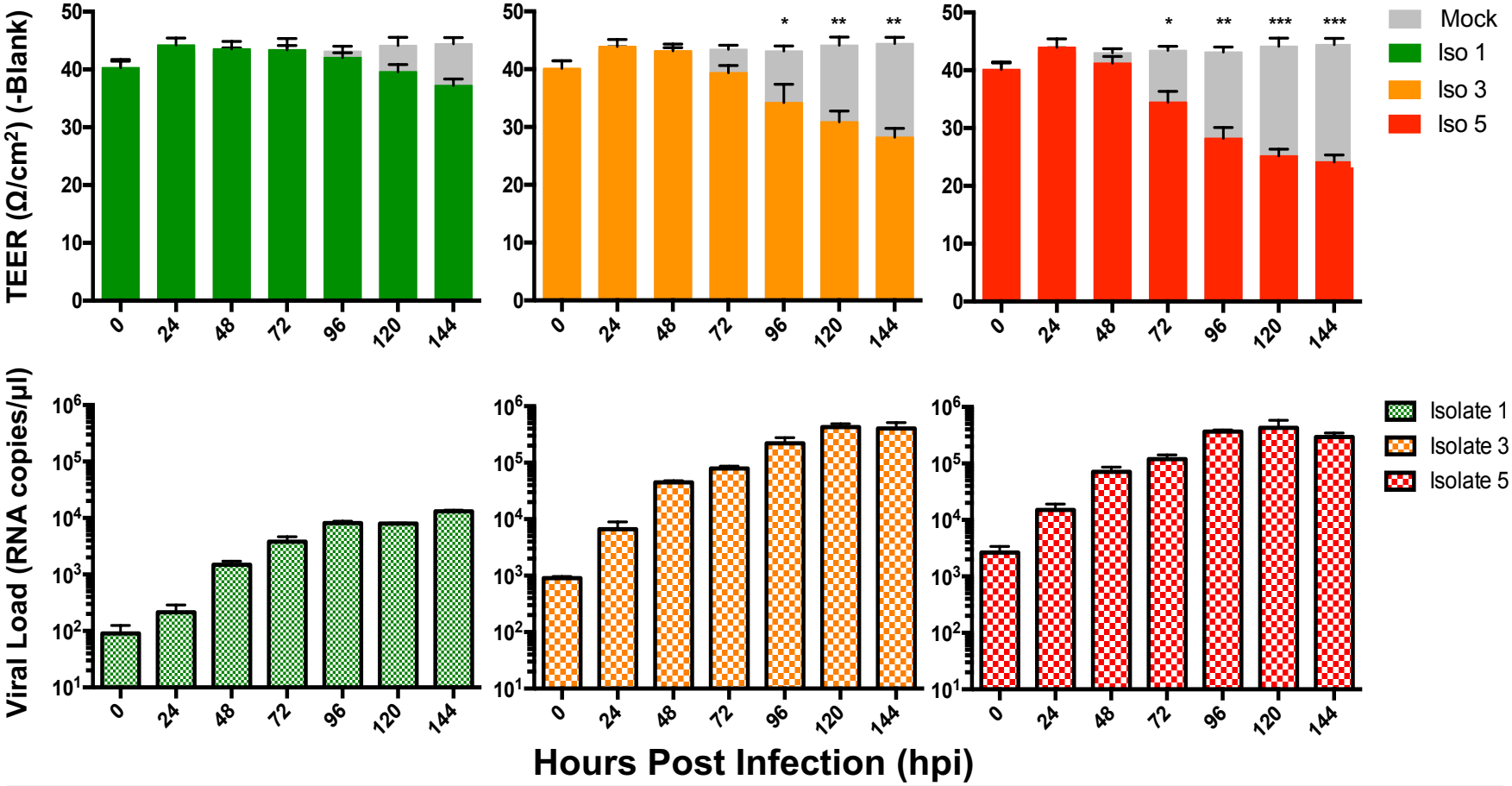

Figure 27. EV71 isolate infection of a HCMEC/D3 *in vitro* blood brain barrier model.
Human cerebral microvascular endothelial cells were seeded on a 12-well transwell semi-permeable membrane insert at 1E5 per insert. They were left for 72 hours to adhere and form a barrier. They were then infected with different isolates of EV71 and measured for TEER and viral load every 24 hours. All TEER measurements are shown after blank value has been deducted, and are then compared to mock infected value. All viral load shown were taken from the abluminal side. Mock viral load was undetectable. Data within these graphs was compared using students test (**p<0.05, **p<0.01 and ***p<0.001*).

4.3.4 EV71 isolate infection in an *in vitro* blood-brain barrier model

After the optimisation of the BBB, I again seeded HCMEC/D3 cells on a 12-well transwell semi-permeable membrane insert at 1E5 per insert. They were left for 72 hours to adhere and form a barrier. I then infected the barrier with different isolates of EV71 and measured for TEER and viral load every 24 hour up to 144hpi. The level of TEER is an indicator of the barrier's strength and integrity, whilst the viral load (taken from the abluminal side) measures the ability of the virus to pass through the BBB.

During infection with isolate 1, the BBB suffers very little damage; and there is no reduction in TEER seen up to 96hpi (Fig 27). At 120hpi and 144hpi there is a small decrease in TEER however it is not a significant drop (Fig 27), suggesting isolate 1 does not cause any serious breakdown of the BBB. This is mirrored in the viral load analysis with a very low level of virus being able to pass through the BBB (Fig 27), suggesting that its integrity is still intact.

Isolate 3 causes much more damage to the BBB. The decrease in TEER starts at 72hpi, with a significant decrease seen at 96hpi onwards (Fig 27). This suggests that the barrier is losing its integrity and is losing some of its barrier function. This can also be seen in the viral load, with a much greater level of vRNA being detected in the abluminal side of the isolate 3 infection, compared with isolate 1.

The highest level of damage is seen during the infection with isolate 5. A significant decrease in TEER was seen at 72hpi, which continued until 144hpi, at which point the barrier was almost completely destroyed (Fig 27). This deterioration in barrier function can also be seen in the viral load data, with extremely high levels of vRNA detected early on in the infection (Fig 27). Suggesting severe detrimental damage to the BBB has been inflicted.

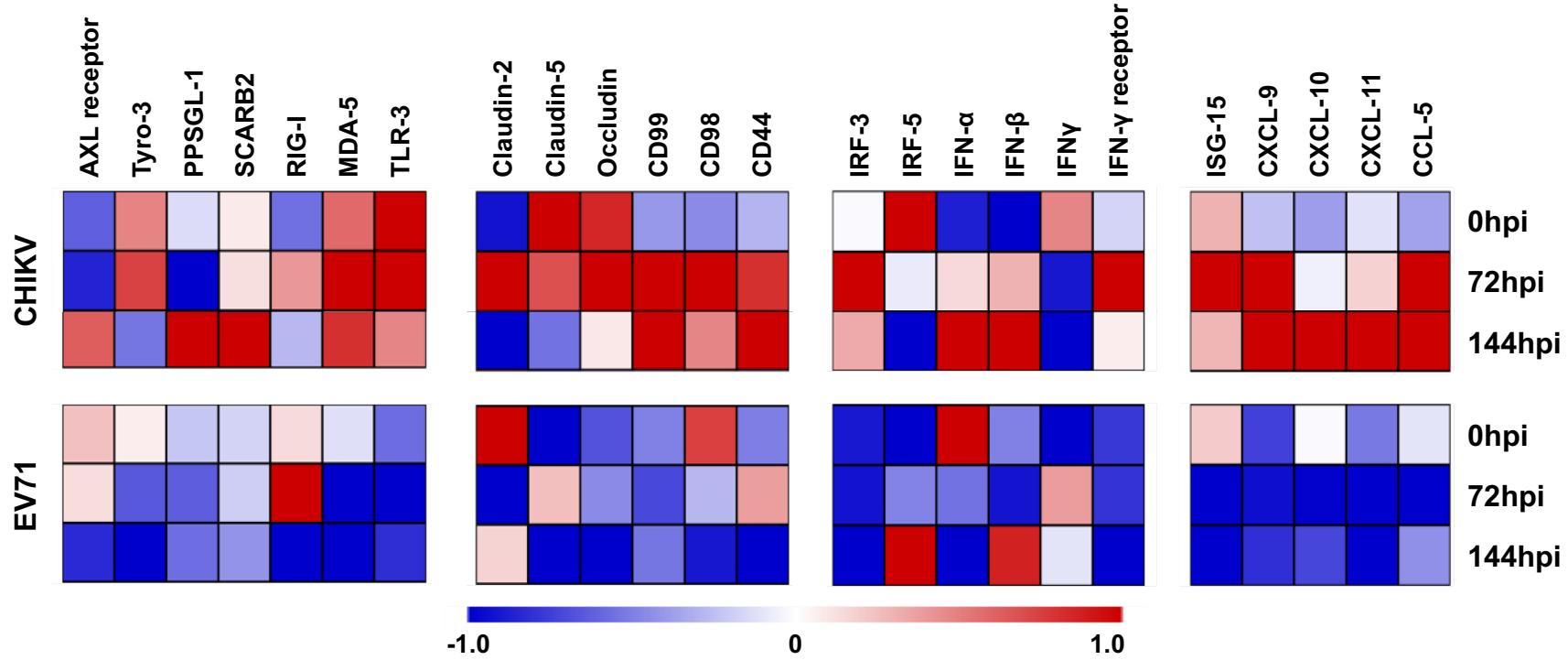

<u>Figure 28.</u> Heatmap gene expression analysis of total RNA taken from CHIKV and EV71 infected *in vitro* HCEMC/D3 BBB model.

The *in vitro* BBB was infected with CHIKV or EV71, at each timepoint cells were harvested and the total RNA was extracted from them. They were then analysed for there gene expression and compared against mock infected and a house keeping gene β-actin. The time points chosen here represent initial infection (0hpi), first drop in TEER (72hpi) and peak TEER drop (144hpi). A total of 24 genes were screened, including 7 receptor genes (AXL receptor, Tyro-3, PSGL-1, SCARB2, RIG-I, MDA-5 and TLR-3) 6 genes encoding for tight junction proteins (Claudin-2, Claudin-5, Occludin) and adhesion factors (CD99, CD98 and CD44), 6 IFN production genes (IRF-3, IRF-5, IFN-α, IFN-β, IFN-γ and IFN-γ receptor) and 5 IFN-associated genes (ISG-15, CCL-5, CXCL9, CXCL10 and CXCL11) at the selected time points using the Quantifast™ SYBR-Green assay. Fold change in the mRNA expression level is then derived using GADPH as the house-keeping gene and normalized to mock population, calculated using the ΔΔ Ct method. A heatmap was generated, based on the fold change values and viewed in MeV 4.9.0 . Any up-regulation of gene expression is indicated in red while any down-regulation of gene expression is indicated in blue. Scale is normalized from -1 to 1 in MeV 4.9.0.

4.3.5 Gene expression in the endothelial cells of the BBB during neurotropic and non-neurotropic infections

To investigate the pathways involved in the disruption of the BBB during EV71 infection, I examined the gene expression profiles of important infection immune response or BBB tight junction related genes during an EV71 infection. Namely virus receptors and PRRs AXL receptor, Tyro-3, PSGL-1, SCARB2, RIG-I, MDA-5 and TLR-3, 6 genes encoding for tight junction proteins (Claudin-2, Claudin-5, Occludin) and integrin-mediated inter-endothelial adhesion factors (CD99, CD98 and CD44), 6 IFN production genes (IRF-3, IRF-5, IFN-α, IFN-β, IFN-γ and IFN-γ receptor) and 5 IFN pathway associated genes (ISG-15, CCL-5, CXCL9, CXCL10 and CXCL11). To compare the EV71 neurotropic infection, I used a non-neurotropic viral infection (Chikungunya virus; CHIKV) and a mock infected control.

EV71 and CHIKV infections produced two very distinct gene expression profiles when the hCMEC/D3 *in vitro* BBB model was infected by the viruses. CHIKV upregulated many of the different gene classes across all the time points during the infection, to cause a sustained pro-inflammatory response (Fig 28). However, conversely, EV71 down-regulated the mRNA expression level of many pro-inflammatory genes screened when TEER first significantly decreases at 72hpi (Fig 28). EV71 also sustained the down-regulation and suppression of the pro-inflammatory response all the way until 144hpi (Fig 28).

4.3.6 Reduced expression of BBB junction proteins coincided with the initial reduction in TEER

To determine if the drop in TEER in the BBB model represents a genuine breach in the integrity of the barrier function, key BBB proteins such as integrin-mediated inter-endothelial adhesion factors CD99, CD98 and CD44, and tight junction proteins Claudin-2, Claudin-5 and Occludin, were screened to identify any changes in their expression levels.

During EV71 infection there was a down-regulation of the mRNA expression levels of key tight junction proteins and adhesion factors during the first TEER drop at 72hpi and 144hpi respectively. Particularly, EV71 infection resulted in the down-regulation of Occludin, Claudin-2, CD99 and especially CD98. Although there was a slight up-regulation of Claudin-5 and CD44 from 0hpi to 72hpi (first TEER drop), they were down-regulated again at 144hpi (Fig 28). CHIKV had a contrasting expression profile of these genes. There was a sustained or increased level of gene expression of the adhesion factor and tight junction proteins Claudin-5, Occludin, CD99, CD98 and CD44, at 72h after CHIKV infection. EV71 continued to down-regulate all of the BBB proteins except Claudin-2 at 144hpi. These results from the mRNA expression level of blood-brain barrier proteins during an EV71 infection suggest that the initial breach in BBB integrity may be due to a virus-induced down-regulation of BBB adhesion and tight junction proteins, which is likely to be sustained during EV71 infection.

4.3.7 Suppression of IFN response associated with down-regulated BBB proteins

A consistently low mRNA expression level of IFNs, its transcription factors and downstream IFN-associated cytokines was seen during EV71 infection, from 0 through 72 and 144hpi (Fig 28). Specifically, IFN-α, IFN-β, IFN-γ, IFN-γ receptor, IRF-3, IRF-5, ISG-15, CCL-5, CXCL9, CXCL11 and CXCL10, were all down-regulated at 72hpi. This pattern of suppressed IFN responses was sustained until 144hpi, except for a slight up-regulation in IRF-5 and IFN-β (Fig 28). This result of down-regulated IFN responses is juxtapose to CHIKV infection, where a potent IFN-mediated pro-inflammatory response was induced across all the time points, including the up-regulation in expression levels of IRF-3, IFN-α, CXCL-9, IFN-β, ISG-15, CXCL-11 and CCL-5 at both 72hpi and 144hpi (Fig 28). This suggests that the down-regulation of the IFN response coincides with increased BBB permeability.

4.3.8 Reduction in host PRR expression levels could be associated with BBB permeability

Genes encoding for host PRRs, that could mediate downstream IFN responses, were screened to see if the suppression of IFN response due to EV71 infections could be due to upstream factors of the IFN response.

Upon EV71 infection, the mRNA expression level of two host PRRs, namely MDA-5 and TLR-3, was down-regulated across the time points,

72hpi and 144hpi (Fig 28). However, the mRNA expression level of RIG-I was slightly up-regulated at 72hpi but became significantly down-regulated at 144hpi (Fig 28). Again, these results contrast with the expression level of the PRRs during CHIKV infection, which are up-regulated across the time points.

4.4.0 Immune Response Pathways Involved in EV71 Pathogenesis

4.4.1 Aims

During any infection, multiple pathways are activated, either by the host in response to the pathogen, or by the pathogen itself trying to extend its own survival. Whilst these pathways are usually activated with host survival in mind, they can often cause more and larger complications. I wanted to examine the different pathways used by EV71 during infection, and to see if there is any difference between the pathways activated during infection with the isolates of differing severity.

4.4.2 Examining the pathways via RNASeq gene expression

To examine any possible differences in pathways involved in EV71 pathogenesis I needed to use a high-throughput, wide ranging technique to cover as many options as possible, before narrowing in on the interesting results. Otherwise I could be at risk of missing out possible key pathways as they aren't included in my experimental scope. To cover these bases, I decided to use RNASeq analysis to examine the pathways.

Primary human PBMCs were infected with the different EV71 isolates at MOI 5 and incubated for 0, 6, 12 or 24hpi, as described in previous chapters. At each time point, the cells were harvested, and their total RNA was extracted. After the RNASeq was ran, the data was analysed using TopHat and CuffDiff analysis tools. This combined and compared the data from the four separate donors used for each isolate, at each specific time point. From this the fold changed compared with the mock was deduced, and the fold increase or decrease analysed for any noteworthy results. Results were deemed of interest if the fold change was greater than 1.5 or less than -1.5 compared with the mock.

Unfortunately, due to time and resource constraints only a very basic level of initial analysis after the TopHat and CuffDiff analysis was able to be performed. The results from the analysis were collated for each time point for all isolates in a tabular format. The "no results" were removed from the results, and the remaining genes were filtered on their level of fold change

(greater than 1.5 or less than -1.5). Before removal of any no results, or filtering based on fold change was performed, the number of genes analysed was approximately 16, 000.

After the initial filtration of results and the individual time points, the genes that scored above and below 1.5 and -1.5 fold change respectively were then compared across the different time points to find any patterns or data of interest. The genes that were seen to have high/low levels across all the time points, or showed an interesting trend across the time points were picked for further analysis and interpretation. This analysis narrowed the initial search down to 33 genes of interest.

If extra time and resources allowed, extra high throughput analysis would have been performed on this data to reveal more information of interest in this research area. I would have initially run a volcano plot on the different time points to find the most statistically significant data and analyse this across the time points. This could have been followed up with DAVID analysis, or ingenuity pathway analysis (IPA), which could have helped to identify new markers of interest, potential biomarkers or biological pathways that could lead to new areas of interest in EV71 severity studies.

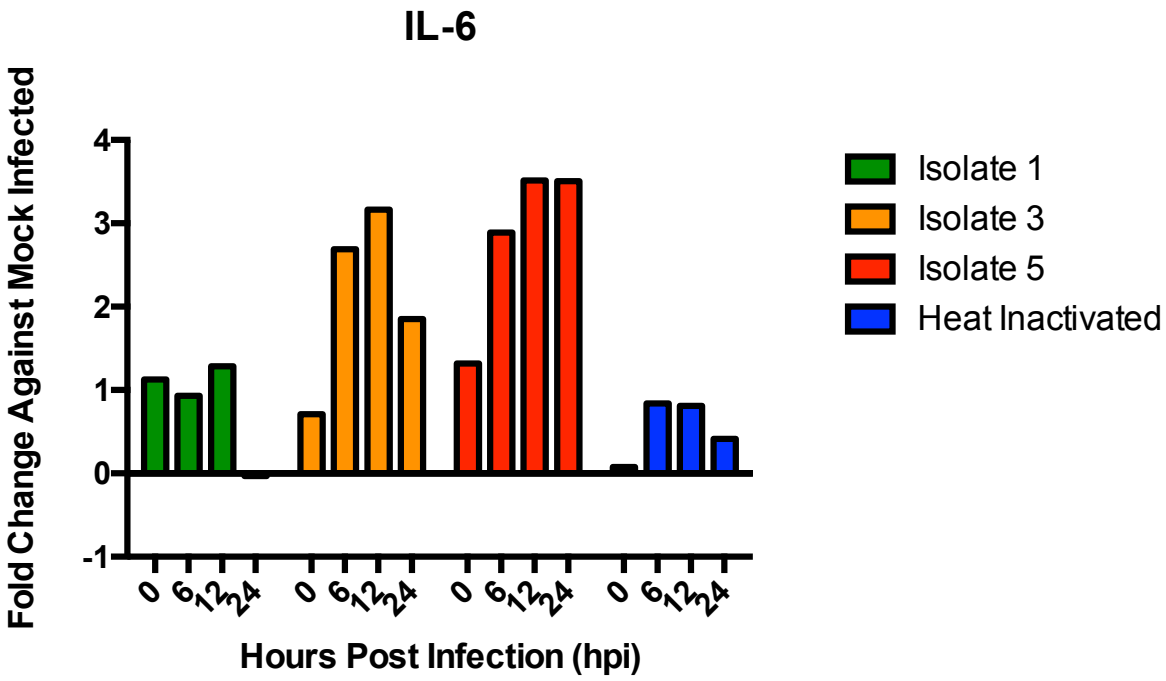

Figure 29. Gene expression level of the IL-6 gene during EV71 infection, measured as fold change against the mock infected sample.
Isolated human primary PBMCs were infected with EV71 isolates 1, 3 and 5, as well as heat inactivated EV71 and a mock-infected control, at MOI 5 and harvested at 0, 6, 12 and 24hpi. The total RNA was extracted and RNASeq was ran on this RNA. The results were then analysed using TopHat and CuffDiff. The gene expression level was compared with the mock infected sample at the respective time point and the fold changed was calculated.

4.4.3 Genes of interest – IL-6

One of the first genes of interest I found was interleukin-6. This well-known pro-inflammatory cytokine has been previously associated with the development of encephalitis, when seen in high levels, in patients infected with EV71. Isolate 1 shows little increase in IL-6 across all time points (Fig 29.), there was a slight increase above the mock level, but only on similar terms with the heat inactivated virus (Fig 29).

On the other hand, the more severe isolates, 3 and 5, show much greater levels of IL-6 gene expression, increasing almost 3-fold over the first 6h (Fig 29). There was a further small increase at 12hpi for both isolates (Fig 29). This was where isolate 3 peaks and before returning to a lower level of fold increase (Fig 29). Isolate 5, however, kept a consistent fold increase across 12 and 24hpi (Fig 29). This extended, increased level of IL-6 upregulation, could play an important role in the increased pathogenesis of this isolate.

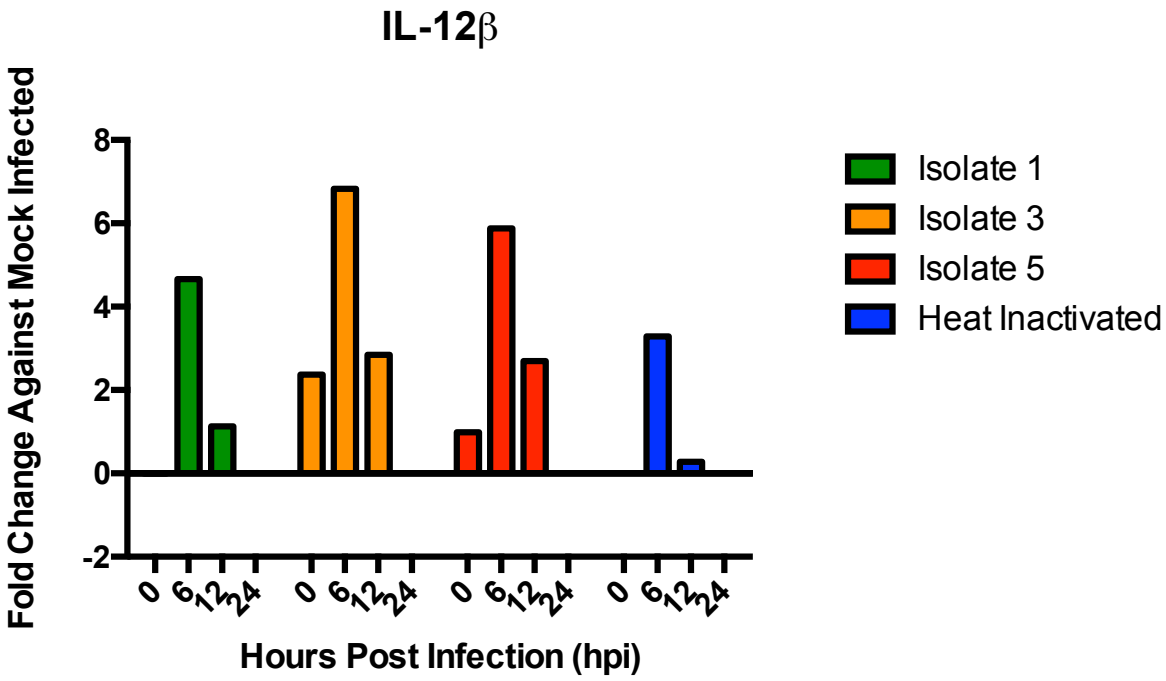

Figure 30. Gene expression level of the IL-12β gene during EV71 infection, measured as fold change against the mock infected sample.
Isolated human primary PBMCs were infected with EV71 isolates 1, 3 and 5, as well as heat inactivated EV71 and a mock-infected control, at MOI 5 and harvested at 0, 6, 12 and 24hpi. The total RNA was extracted and RNASeq was ran on this RNA. The results were then analysed using TopHat and CuffDiff. The gene expression level was compared with the mock infected sample at the respective time point and the fold changed was calculated.

4.4.4 Genes of interest – IL-12β

IL-12β is the beta subunit of IL-12, which is a cytokine that has been shown to induce the differentiation of T cells, and stimulate the production of IFN-γ and TNF-α. During EV71 infection with the different isolates, there was large increase in IL-12β seen in all of the isolates at 6hpi, most notably in isolates 3 and 5 (Fig 30). At 12hpi there was still a notable fold change in IL-12β gene expression in isolates 3 and 5, however it is much lower than at 6hpi. There was no fold increase for any note seen at 12hpi for isolate 1 (Fig 30). The fold change was completely depleted at 24hpi for all isolates (Fig 30).

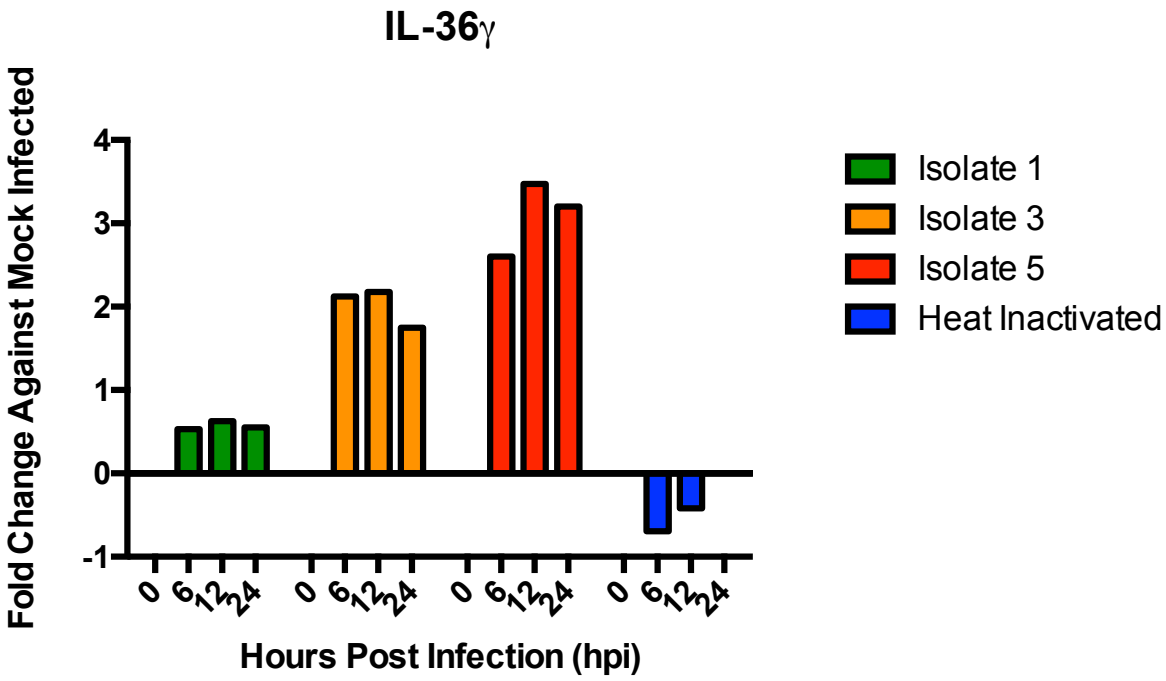

Figure 31. Gene expression level of the IL-36*γ* gene during EV71 infection, measured as fold change against the mock infected sample.
Isolated human primary PBMCs were infected with EV71 isolates 1, 3 and 5, as well as heat inactivated EV71 and a mock-infected control, at MOI 5 and harvested at 0, 6, 12 and 24hpi. The total RNA was extracted and RNASeq was ran on this RNA. The results were then analysed using TopHat and CuffDiff. The gene expression level was compared with the mock infected sample at the respective time point and the fold changed was calculated.

4.4.5 Genes of interest – IL-36γ

IL-36γ belongs to the IL-1 cytokine family, and has be reported to be stimulated by IFN-γ, TNF-α and IL-1β. Interestingly, the expression of this cytokine has been linked with psoriasis like lesion. Expression of this could therefore be linked to the HFMD sores seen in patients, and an increase in the expression of this cytokine could provide evidence as to why certain patients suffer from a more sever for of HFMD.

There was a small increase in fold change in IL-36γ during isolate 1 infection, starting at 6hpi, this level of increase was consistent across all the time points, from 6hpi onwards (Fig 31). This limited level of increase could indicate why the patient only suffered a mild case of HFMD, and did not produce any more severe symptoms.

Isolate 3 showed a greater level of fold change compared with isolate 1, this increased level of gene expression was seen at 6hpi (Fig 31). This higher fold increase stayed consistent for the rest of the time course. This adds further evidence that IL-36γ could play an important role in the severity of HFMD and its relating complications.

Isolate 5 showed the highest level of fold change across the 3 isolates, again, starting at 6hpi, then increasing and peaking at 12hpi, before plateauing at 24hpi (Fig 31). This adds further evidence that IL-36γ could be implicated in the severity of EV71, especially concerning HFMD.

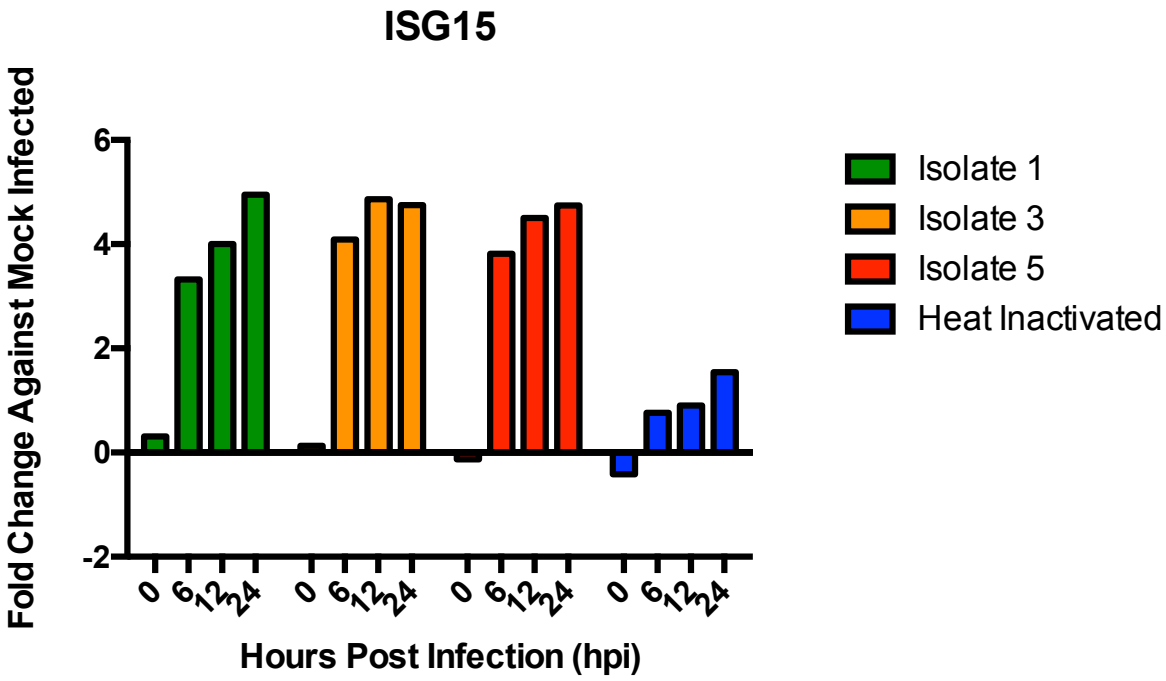

Figure 32. Gene expression level of the ISG15 gene during EV71 infection, measured as fold change against the mock infected sample.
Isolated human primary PBMCs were infected with EV71 isolates 1, 3 and 5, as well as heat inactivated EV71 and a mock-infected control, at MOI 5 and harvested at 0, 6, 12 and 24hpi. The total RNA was extracted and RNASeq was ran on this RNA. The results were then analysed using TopHat and CuffDiff. The gene expression level was compared with the mock infected sample at the respective time point and the fold changed was calculated.

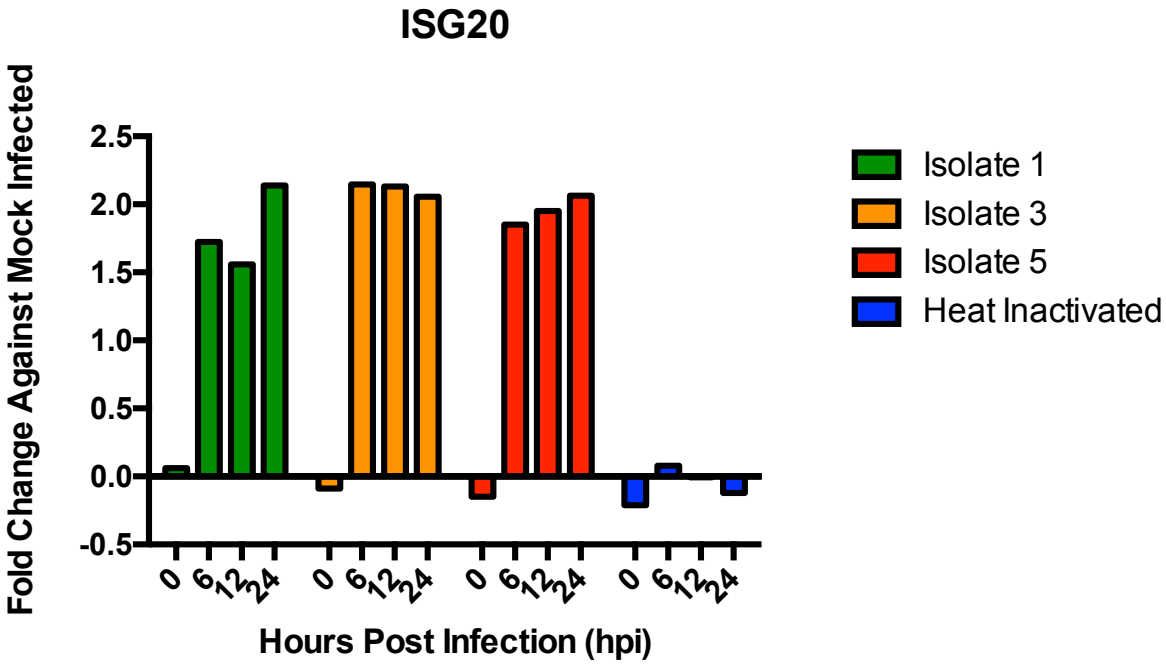

Figure 33. Gene expression level of the ISG20 gene during EV71 infection, measured as fold change against the mock infected sample.
Isolated human primary PBMCs were infected with EV71 isolates 1, 3 and 5, as well as heat inactivated EV71 and a mock-infected control, at MOI 5 and harvested at 0, 6, 12 and 24hpi. The total RNA was extracted and RNASeq was ran on this RNA. The results were then analysed using TopHat and CuffDiff. The gene expression level was compared with the mock infected sample at the respective time point and the fold changed was calculated.

4.4.6 Genes of interest –ISG15 and ISG20

ISG15 and ISG20 belong to a family of genes known as the interferon stimulated genes. Their expression is induced in response to type I IFNs. Type I IFNs are usually an antiviral response mounted by the innate immune system. As such, a high and increasing level of ISG15 and ISG20 should be expected in response to the increasing level of type I IFN. Whilst an initial increase was seen across all isolates at 6hpi, a continued large increase was not (Fig 32 and Fig 33). However, as mentioned earlier, EV71 has mechanism and methods to restrict and inhibit the release and activation of IFN and its downstream receptors. This theory could well be coming in to play again here, containing the level of ISG15 and ISG20.

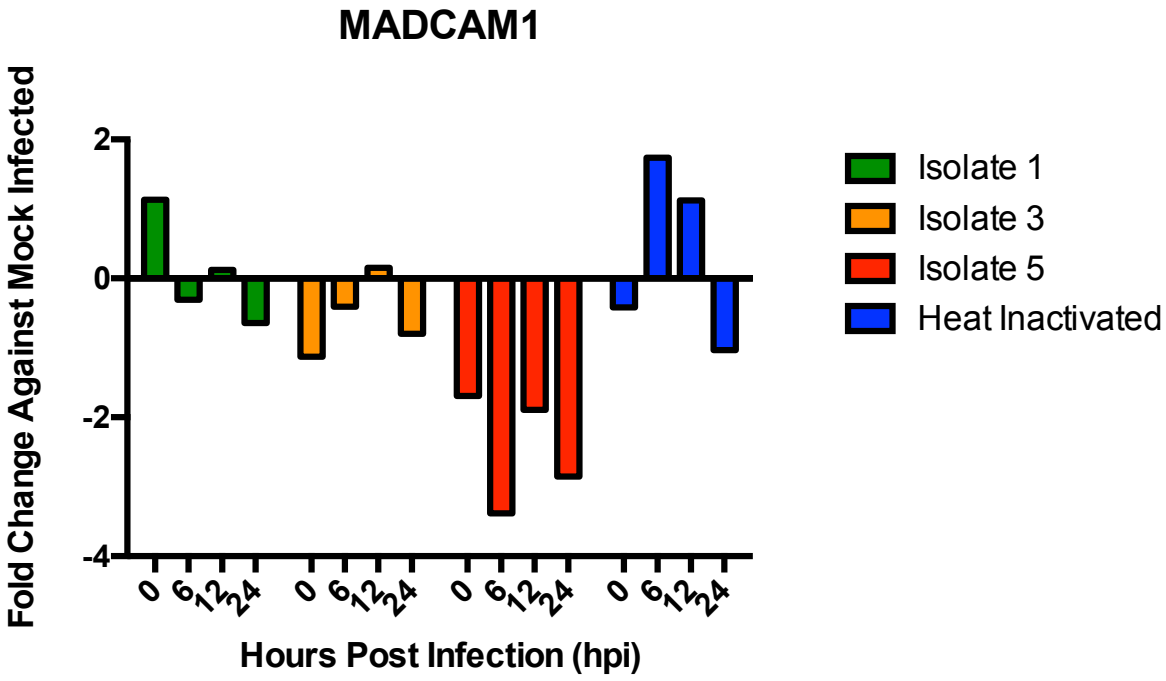

Figure 34. Gene expression level of the MADCAM1 gene during EV71 infection, measured as fold change against the mock infected sample.
Isolated human primary PBMCs were infected with EV71 isolates 1, 3 and 5, as well as heat inactivated EV71 and a mock-infected control, at MOI 5 and harvested at 0, 6, 12 and 24hpi. The total RNA was extracted and RNASeq was ran on this RNA. The results were then analysed using TopHat and CuffDiff. The gene expression level was compared with the mock infected sample at the respective time point and the fold changed was calculated.

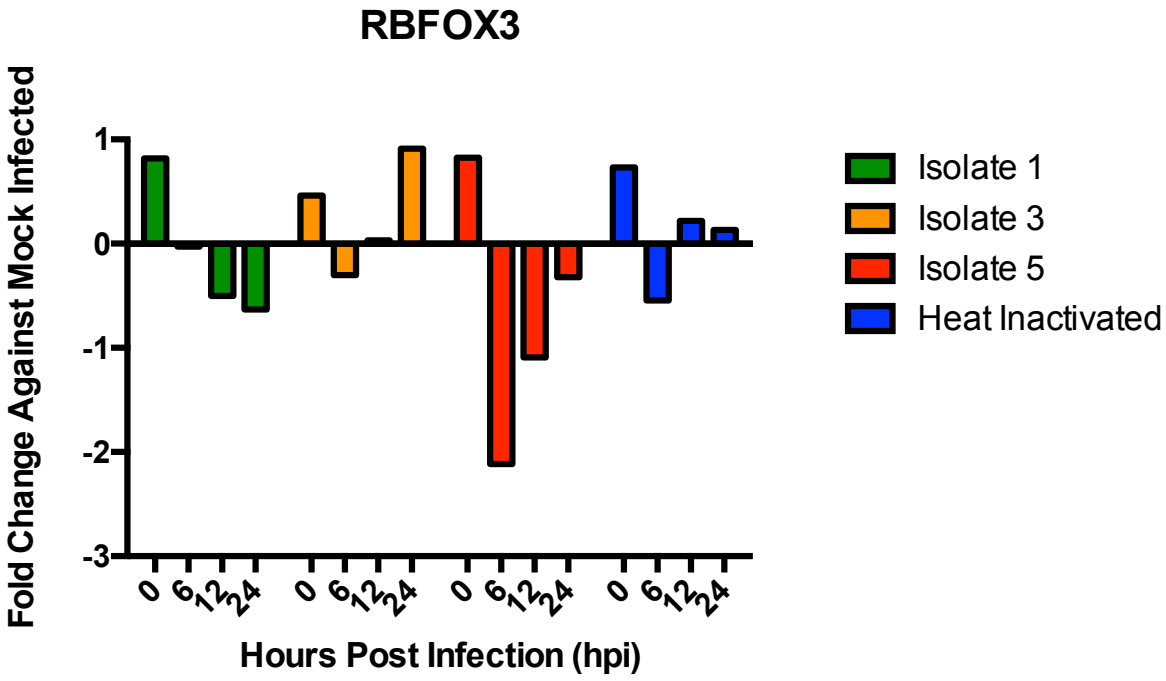

Figure 35. Gene expression level of the RBFOX3 gene during EV71 infection, measured as fold change against the mock infected sample. Isolated human primary PBMCs were infected with EV71 isolates 1, 3 and 5, as well as heat inactivated EV71 and a mock-infected control, at MOI 5 and harvested at 0, 6, 12 and 24hpi. The total RNA was extracted and RNASeq was ran on this RNA. The results were then analysed using TopHat and CuffDiff. The gene expression level was compared with the mock infected sample at the respective time point and the fold changed was calculated.

4.4.7 Genes of interest – MADCAM1

MADCAM1 codes for the protein addressin, these proteins are ligands for the homing receptors of lymphocytes. Their function is to direct lymphocytes into inflamed and mucosal tissues. Isolates 1 and 3 show little change in the expression of their MADCAM1 levels, they stay consistently between 1 and -1-fold increase (Fig 34). However, isolate 5 largely downregulated the expression levels of MADCAM1 across all time points (Fig 34). This could possibly suggest that isolate 5 uses this downregulation as an immune evasion technique to avoid detection by leukocyte, thus giving it more time for replication and a greater chance of survival and spread.

Genes of interest – RBFOX3

RBFOX3 is an alternative splicing factor, which regulates the cells of the immune system, mostly related to neuronal regulation. This was seen to have no significant change across isolates 1 and 3, both keeping between 1 and -1-fold change across the whole time course (Fig 35). However, isolate 5 was majorly downregulated at 6hpi, and continued to be largely downregulated at 12hpi (Fig 35). This suppression may be part of the pathway that is linked with neurogenic dysregulation, which lead to the systemic failure of the patient's cardio and respiratory systems.

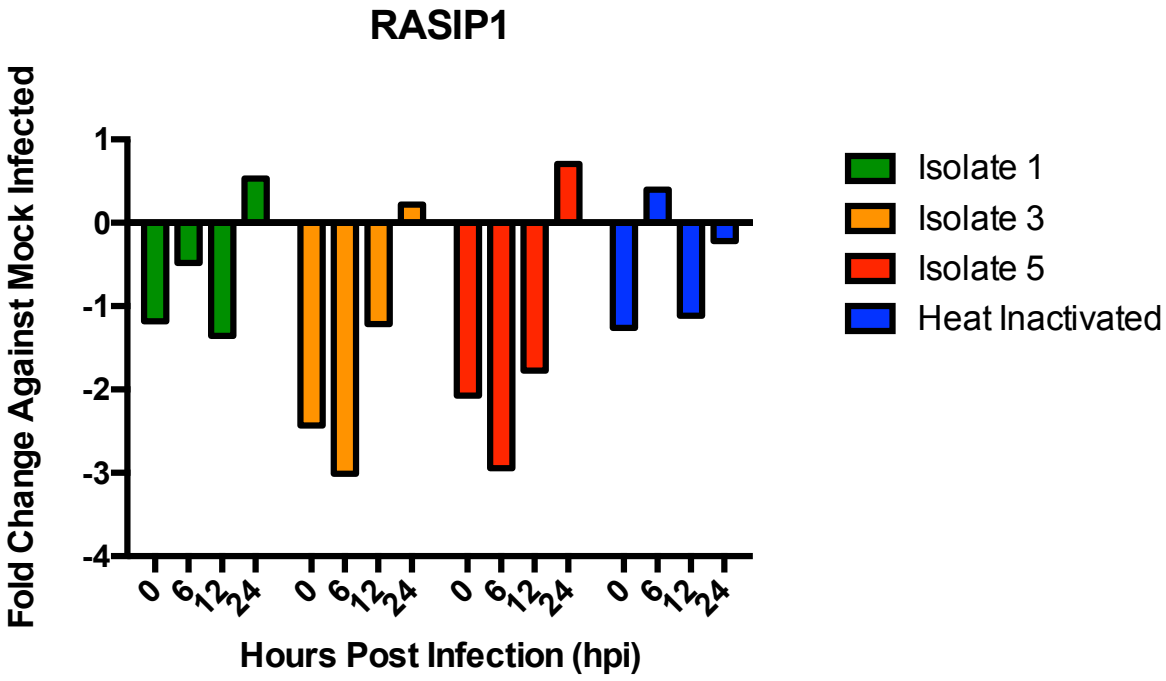

Figure 36. Gene expression level of the RASIP1 gene during EV71 infection, measured as fold change against the mock infected sample. Isolated human primary PBMCs were infected with EV71 isolates 1, 3 and 5, as well as heat inactivated EV71 and a mock-infected control, at MOI 5 and harvested at 0, 6, 12 and 24hpi. The total RNA was extracted and RNASeq was ran on this RNA. The results were then analysed using TopHat and CuffDiff. The gene expression level was compared with the mock infected sample at the respective time point and the fold changed was calculated.

4.4.8 Genes of interest – RASIP1

RASIP1 is the Ras-interacting protein1 gene. It acts as a regulator of GTPase signalling, and adhesion. It is also important in supressing RhoA signalling. RhoA has been linked to instability in endothelial cell tight junctions, and it has been suggested that it can interfere with the stability and integrity of the BBB.

Isolate 1 showed a slight downregulation in the level of gene expression for RASIP1 however, it was not a significant downregulation, and was almost on par with the heat inactivated control (Fig 36). Isolate 3 however showed high early levels of downregulation, starting at 0hpi and increasing to 6hpi before it decreased in downregulation at 12hpi to a non-significant level (Fig33). Isolate 5 showed a similar pattern to isolate 3, with an increased level of downregulation at 0hpi. However isolate 5 showed a higher level of downregulation all the way through to 12hpi before it decreased in downregulation and significance (Fig 36).

This downregulation in the two isolates that caused neurological complications, lends itself to the theory that sever EV71 infection can lead to an increase in RhoA activation, leading to a decrease in BBB stability and integrity.

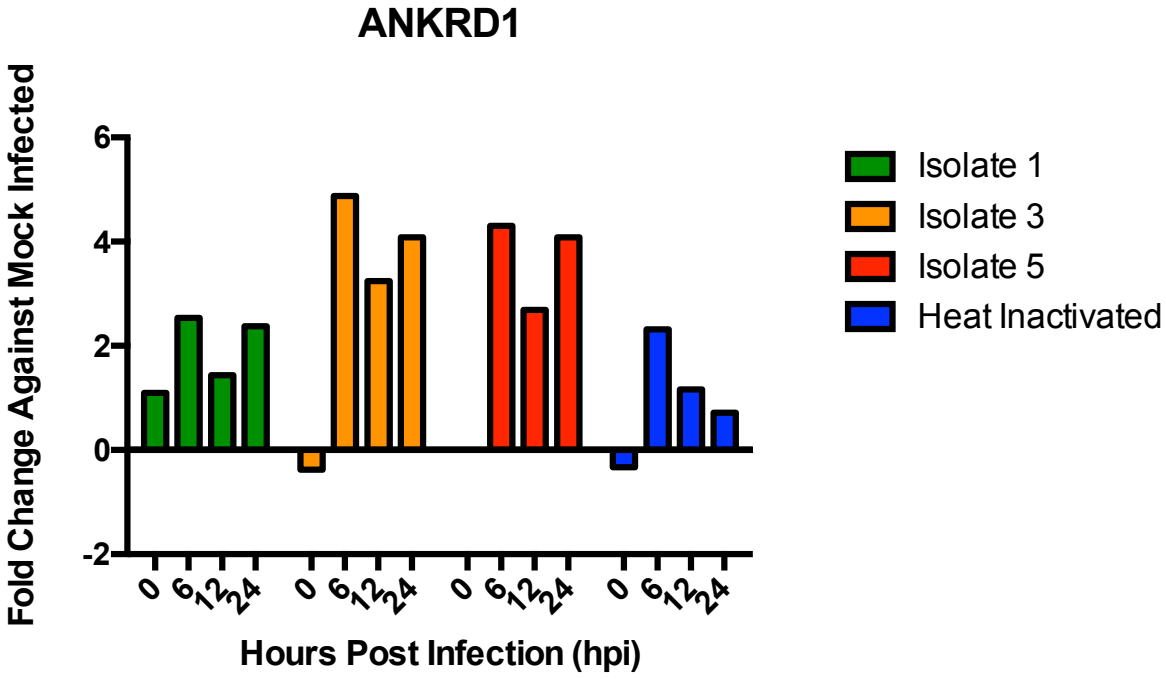

Figure 37. Gene expression level of the ANKRD1 gene during EV71 infection, measured as fold change against the mock infected sample. Isolated human primary PBMCs were infected with EV71 isolates 1, 3 and 5, as well as heat inactivated EV71 and a mock-infected control, at MOI 5 and harvested at 0, 6, 12 and 24hpi. The total RNA was extracted and RNASeq was ran on this RNA. The results were then analysed using TopHat and CuffDiff. The gene expression level was compared with the mock infected sample at the respective time point and the fold changed was calculated.

4.4.9 Genes of interest – ANKRD1

ANKRD1 is the gene that encodes the protein cardiac adriamycin-responsive protein (CARP) which is a transcription involved in conditions of stress. It is thought that CARP may have a negative effect on contractile function. The more severe viral isolates, 3 and 5, showed increased levels of the ANKRD1 gene expression compared with isolate 1 (Fig 37). This increase could be linked to the pathway which is connected to EV71 related heart failure.

Chapter 5

Discussion

5.1.0 The Effect of Viral Infectivity and Replication on Severity During an EV71 Infection

5.1.1 Phylogenetic analysis of EV71 isolates show clustering according to severity

In vitro infections have long been used to examine the infection and replication kinetics of viruses (208, 209). As there is currently limited knowledge on why there is such a difference in pathogenicity in EV71 infections, I wanted to discover whether the different isolates of the virus had any role in this.

After sequencing the virus isolates taken from the outbreak of EV71 in Sarawak, Malaysia in 2006 (32) used in these experiments, it can clearly be seen that different groups are emerging (Fig 6). Patterns between the severity of the outcomes in the patients can be seen in the phylogenetic tree, with patient who suffer milder symptoms due to EV71 infection are seen grouped together. Further phylogenetic evidence could show or suggest areas that could be further explored as areas relating to the severity of the patient's disease.

It is not only the mild symptom groups that can be seen grouped in the phylogenetic tree. Patients who suffered from "moderate" symptoms, which include more severe cases of HFMD and slight neurological complications, are also grouped together. This suggests that there is viral element to the

severity of disease during EV71 infection, that it is not just simply down to the host response to the virus.

To add further evidence to this, the severe symptoms group, which includes severe neurological complications, cardiopulmonary issues and fatalities were also found to be clustered together after analysis. This signifies that the virus could play a pivotal role in the patients' outcome severity.

This data is a starting point that could be used to further understand the areas of the EV71 genome that may be important in pathogenesis. Obviously, the initial information has a few flaws. This data was only collected from one outbreak in one country, and during this outbreak only subgroup B5 was seen. The other subgroups may have different areas/regions in the genome that convey pathogenesis. A much broader phylogenetic investigation would need to be carried out in order to test if any differences or patterns could be found across all the subgroups.

Another possible route to take, rather than diversifying the investigation, would be to look deeper into the genetic analysis of these six isolates and find regions or motifs that may be responsible for the differences in pathogenesis seen in these six patients.

5.1.2 EV71 virus isolates that cause mild symptoms in patients have low levels of infectivity and limited levels of replication in an *in vitro* infection model

As the virus' ability to infect and replicate can play an important role in the efficacy to colonise the host I looked at each isolates ability to infect, and replicate in, human cells in a controlled *in vitro* viral kinetics assay.

EV71 isolates 1 and 2, which both produced mild symptoms in the respective patients during the 2006 outbreak, were both seen to have limited infectivity over the 24h time course. This inability to produce an effective infection in an environment where there is no competition gives us an insight into a possible reason for the mild symptoms seen in the patients. If the virus only produces a limited infection in this system then it is predicted that it will also have a poor infection efficacy *in vivo*. This inability to infect has a twofold effect on viral pathogenesis (210).

Firstly, if the virus cannot enter the cell then it cannot replicate, as all viruses require their host's replicative machinery to proliferate. Without access to this apparatus, there will be no increase in viral load. Lack of virus will lead to lessened immune response meaning a decrease in adverse effects and symptoms. The second part to this limitation is, the virus' inability to enter the host's cells will lead to an increase in exposure to endogenous cells, cytokines or particles that can destroy the virus. The longer the virus is out in the open, the more likely it is to be destroyed. An increase in viral clearance leads to a faster resolution of symptoms.

5.1.3 An increase in viral infection and replication was seen in EV71 isolates that cause moderate symptoms in patients, compared to those that cause mild symptoms

Both of the moderate isolates show an increased level of infectivity as compared to the isolates that cause mild disease. This further substantiates the theory that the infection capacity of the virus is linked to the severity of the disease in patients.

The level of replication, shown via viral load, also shows a significant increase between the two groups. The higher level in replication could be down to two factors. The increase in infectivity would lead to an increase in virus presence in the cells, meaning an increase in the virus interacting with the host machinery. Naturally more cells hijacking and using the replicative machinery of the host would translate in to an increase in viral replication. The second factor is that it could be a more effective replication from the moderate virus due to subtle mutations between the isolate groups. This could lead to a greater viral load, which could in turn lead to a higher level of infectivity as there is a higher number of viruses. More viruses mean a greater virus to cell ratio, which leads to an increased chance in the virus entering the cell.

It is likely that both these factors play a role as there is a similarly significant increase in both replication and infection between mild and moderate isolates, suggesting there isn't one specific factor driving the other (210).

5.1.4 The severe isolates show the highest levels infection and replication across all groups

This theory is further demonstrated by the viral kinetics of the most severe isolates. Isolate 5 and 6 show significantly higher levels of both infection and replication than all the other isolates. This significant elevation in viral load could be the reason that there is increased pathogenesis *in vivo*. An increased viraemia in patients can lead to significant, systemic infection and severe complications. Higher levels of viraemia means that the virus is more likely to come into contact with different tissues and organs with in the host. When this is combined with an increased ability to infect the host cells, the probability of severe infection is likely to be hugely increased. This increased level of infectivity and replication could be the reason infections with these isolates lead to neurological complications (210, 211).

5.1.5 Further studies proposed for this area

As there seems to be such a distinctive grouping between the isolates of different severity I would look to further this area of study by taking a more in depth look at the genome sequences of the different clades, and the individual isolates. Then try to map these to either the known gene epitopes or a 3D structure of the EV71 virus to see if there are any major mutations between the groups. Any changes in protein sequences or structure could point to a reason why there is such a difference in severity between these isolates. As well as that it could lead to a possible drug target that may help reduce the severity of the symptoms in patients.

The regions I would initially want to look at if I continued with this area of research would be: the VP1 region, which has already shown, specific regions of interest for receptor binding and infection levels (95). I would also look at the VP1/VP2/VP3 canyon as this has been shown to play an interesting role in receptor binding and integration (155).

The other areas I would be interested in looking at would be the 2A and 3C viral protease regions. As these have been shown in several studies to be able to have a large effect on the virus's immune evasion strategies (67, 68, 102, 110, 115, 139, 212). Any mutations or patterns in this region could prove crucial to the virus's ability to minimise detection and therefore continue to proliferate and cause damage to the host.

If the link between the virus and the severity of the outcome can be found this could not only lead to huge improvement in the ability to predict the most at risk patients. It could also provide us with possible avenues that could be explored in the realms of drug targets and therapeutic treatments to limit the severity of conditions the virus can cause.

5.2.0 EV71 and Leukocyte Interaction During an *Ex Vivo* PBMC Infection

5.2.1 EV71 infection in primary human peripheral blood mononuclear cells

As I had established an infection in an *in vitro* setting, and found significant differences in between the virus isolates, I wanted to look at more representative model of infection. Many studies have shown that leukocytes are the key players in host defence response, so I decided to use an *ex vivo* model to further study the intricate differences between these viruses. During the isolation procedure for PBMCs, all plasma and serum is removed, thus eliminating any chance of reactive antibodies from the donors interfering with the results. There will also be minimal levels of any other factors that may interfere with the experimental process such as cytokines and chemokines.

As there was a limited number of donor's blood cones received per week, and a limited number of cells that could be retrieved from each cone, combined with the number of cells needed per sample and the number of conditions (time points, plus samples, plus controls) meant only three viruses could be selected. To get the best coverage of the three severities, I chose isolates 1 (mild; herpangina), isolate 3 (moderate; HFMD with meningoencephalitis) and isolate 5 (fatal). I wanted to see if PBMCs could be infected by the different isolates, and if there were any distinct differences between the infection profiles of the isolates. To examine these differences, I decided to use flow cytometry to measure the infectivity of

the isolates in PBMCs and qRT-PCR to measure the replication of the virus.

5.2.2 Viral infection kinetics of EV71 in an *ex vivo* PBMC system

After isolating the PBMCs from fresh apheresis cones, they were infected with the different isolates. At the respective time point, the samples were harvested, the cells kept for flow cytometry and total RNA extraction, and the supernatant for vRNA and cytokine analysis. The initial area I wanted to investigate was the infectability of the total PBMC population. Using flow cytometry, the cells were gated on their size and granularity to remove any debris, then on their height to width ratio to remove any doublet cells which may affect the results. Dead cells were then removed via a live/dead stain. The cells that remained should be whole, live, single cells. These cells were then gated on the CD45 cell surface marker, which is also known as the common leukocyte antigen. It is found on all white blood cells and is a way to separate them out from other cells such as red blood cells and platelets. The CD45 positive cells for finally gated on their positivity for the anti-EV71 ab.

Isolate 1 showed very limited infectivity after gating. It was almost comparable with the mock infected and heat inactivated virus in terms of infectability. This was unsurprising as isolate 1 had a poor infectability in the immortalised cell line RD cells, which are known for being highly susceptible to EV71 infection. So, infecting primary cells such as fresh PBMCs would be quite unlikely, as these are known to be much more

difficult to infect compared to immortalised cell lines. This limited ability to infect either immortalised or primary cells could be a strong indicator as to why this isolate only caused a mild onset of disease symptoms during the initial patient infection. This may be due to an inability to bind to the receptors efficiently which would cause a marked decrease in the virus's ability to infect the cells. If less virus can enter the cell, this would also lead to a decrease in viral replication and viral replication speed compared to other isolates as there would be less viral RNA available for transcription and translation.

A different pattern of infection was seen in PBMCs during isolate 3 infection. This isolate managed to have a high level of initial infection, which decreased across the time course. This suggests that the virus isolate does not struggle to enter the cell, however it cannot efficiently replicate once inside. If it cannot replicate than it cannot increase its viral copy number, and will also struggle to leave the cell. If the virus is then trapped inside the cell, it is likely to be subject to the cells innate defences and degraded. This would then lower the viral load and, in time, the effectiveness of the virus. This could be the explanation why this virus caused a moderate and not a severe illness (210). The viruses lessened ability to replicate meant that it could cause initial problems for the patient, however it could not reach the severe systemic effects of other isolates (213).

Isolate 5 showed a different trend again to both isolates 3 and 5. There was an initially low infection which steadily increased peaking at 12hpi before

decreasing. This was the first isolate to show signs of an increase in infectivity across the time points. This increase in infectivity could suggest that isolate 5 shows an ability to replicate in these cells. Which could give an indication as to why it caused severe symptoms in the patient. The ability to replicate inside the cells not only means that the virus can increase its own number, it also gains control over the host cell's replication centre. Giving it the ability to limit host RNA synthesis, as well as increasing its only RNA synthesis which can lead to the supress and downregulation of certain crucial immune factors (109). It can also lead to upregulation of pathways and factors that are beneficial to the virus's survival (109).

This data would suggest that the infection of the cell may not be the be all and end all to pathogenesis with EV71. As the moderate isolate (isolate 3) is seen to be much more infectious, however it showed lower severity in the patient. This may be due to the replication ability of the virus. It could also be due to the receptor which this isolate preferentially binds to enter the cell. It has previously been shown that PSGL-1 has a greater efficiency for binding to EV71 (91). However, the virus cannot undergo the initiation of uncoating as efficiently and therefore cannot enter the replication cycle as proficiently compared to binding with SCARB2 (91). This would be an interesting area of further study. I would look at knocking down/inhibiting SCARB2 and PSGL-1 in PBMCs (or an immortalised cell line first), and see what effect this would have on the infection and replication levels of the different isolates. This could be combined with phylogenetic analysis of the virus to identify any areas of sequencing difference in the receptor motifs.

5.2.3 Viral replication kinetics of EV71 in an *ex vivo* PBMC system

I next assessed the isolates' replication capacity via qRT-PCR. Isolate 1's replication profile tallied with its infection profile. There was limited replication across the time points. This adds further evidence as to why it only produced a mild set of symptoms in the patient during the initial infection. As stated previously a limited ability to infect and replicate would inhibit the virus from spreading easily throughout the body, especially into areas that are normally extremely difficult for pathogens to enter, e.g. the brain. This would lead to only local symptoms being able to present, and preventing the chance of a systemic infection.

This result adds further volume to the theory that the virus and not only the host response is responsible for the severity of EV71 infection, as each infection was carried out with cells from the same donor. This means there should be no donor to donor variation across the isolations during the infection, and the only difference in response seen should be due to the virus.

The lack of replication seen in isolate 1, added to the lack of infectivity would suggest that there may be two (or possibly be more) areas in the genome where this isolate varies from the more severe isolates. The initial areas I would be interested in would be the binding sites for PSGL-1 and SCARB2, as I believe slightly mutations in this area may be the reason for the limited level of infection. For the second area, I would look at the viral

proteases 2A and 3C. Mutations in these sequences may lead to the protease having limited/diminished cleavage abilities, which would not only limit the virus's ability to process its proteins and form the necessary additional machinery required for viral replication. It would also decrease the virus's mechanisms in its immune evasion strategies, meaning it would be an easier target for immune discovery and destruction.

One other area I would also think about exploring would be the viral protein 3D, which is the virus's RNA polymerase. If there was a mutation or defect in this gene it could lead to a lesser amount of the viral RNA being transcribed, therefore less protein being translated and less viral particles being produced inside the cell. This would inevitably lead to a lower level of infectivity. If this were found to be the case, this could explain why there is not only lower levels of infectivity and replication seen for isolate one in the PBMC model, but in the *in vitro* RD cell viral kinetics model as well.

The replication profile of isolate 3 was also similar to its infection profile. With a high initial viral load, which slowly decreased across the time points. This again points to the virus's ability to infect the cells but not replicate within them efficiently. This result furthers the evidence that the isolates ability to proficiently infect cells but not replicate in them could be the cause of the limited capacity of this virus to cause a full systemic and potentially fatal attack.

As mentioned previously the high level of infection but low level of replication seen in the isolate 3 PBMC infection could be due to a number of factors. The one I would be most interested in pursuing would be looking at the mutations in the proteases 2A and 3C. This may be the reason there is a slow decrease in the level of infection across the time course. However, as there is still a higher level of infection, this would suggest that the mutation is not as severe as with isolate 1.

As with the other two isolates, isolate 5 showed large similarities between its infection and its replication kinetics. Again, it was the only isolate to show an increase across the time points. This, proving that it is the only isolate to show positive replication in PBMCs. As mentioned earlier, this ability is likely to be a causative factor in the proficiency of this virus. Increasing the viral load, as well as controlling host replication is very likely to enhance this virus's ability to spread throughout the body, and increase its pathogenesis.

5.2.4 Infectivity of EV71 in PBMC subsets

To further investigate the effect of EV71 on the leukocyte population, and how this relates to severity, I used flow cytometry to examine different PBMC cell subsets during EV71 infection. Using specific, cell surface markers, I separated the CD45 positive cells into: T Cells, B cells, monocytes, NK cells, cDCs and pDCs. These subset populations were then gated on the EV71 antigen positivity. This allowed me to pick out the

specific populations that seemed most susceptible to EV71 infection, and those which are most likely to have the biggest effect on outcome severity.

Isolate 1 barely gets higher than the mock infected and heat inactivated virus samples. The adds more evidence to the previous theory that this is a leading cause behind its limited pathogenesis. It also highlights that there are no specific cell subsets that are majorly susceptible to infection with isolate 1.

In both isolate 3 and isolate 5 there seems to be 3 main subsets that are responsible for the majority of the infection. T cells, B cells and monocytes seem to be the leukocyte subtypes that are most susceptible to EV71 infection. NK cells, cDCs and pDCs still show some level of infection however it is not as high as the other subsets. Within these subsets different patterns can be seen, both between the individual subsets and between the isolates. During infection with isolate 3, T cells and B cells showed the same infection pattern as the total PBMCs, which was a high initial infection, and then a slow steady decrease in infection levels across the time points. A slightly different trend was seen in the monocytes infected. They show the same high initial infection, but then have a sudden large decrease at 6hpi, and then stay at this level for the rest of the time course. This was probably not reflected in the total PBMC infection result as monocytes only make up approximately ten percent of the total number of PBMCs, whereas T and B cells usually make up about seventy percent. This information justifies the process of further splitting the cells into

subsets, as it is something that wouldn't have been seen in the total population but due to this drilling down, it can be seen.

Three separate patterns can be seen during isolate 5 infection of PBMCs. T cells show a similar pattern to the total PBMC infection, with a gradual increase in infection until 12hpi, then a decrease at 24hpi. T cells are the highest cell population within PBMCs, usually accounting for 40-60 percent of the total cell number. So, the fact that the total infection pattern and this subset profile are so similar is not surprising. B cells show their own distinctive infection profile during isolate 5 infection. They have a much lower initial infection percentage, but then peak at 6hpi before decreasing across 12 and 24hpi. This different infection level could indicate that B cells have an earlier role to play in the infection process. This profile however doesn't compare with the replication kinetics of isolate 5, which would suggest that B cells don't have a major role in the replication of EV71 in PBMCs. It could be argued that because of their lower total number that a change would be less detectable as it would be masked by any T cell profile. However, given that B cells make up 20-30 percent of the total cell number, and that there is large increase in infection between 0 and 6hpi, you would expect to see an increase in the replication between this time points. Yet, there is no increase, in fact there is a slight, although not significant, decrease in the replication between these time points. Which suggests that there is only a limited amount of replication occurring in the B cells.

Monocytes during isolate 5 infection show a completely different trend to both T and B cells. They show a much higher early level of infection, which is then slightly decreased at 6hpi, but stays constant for the rest of the time course. This may suggest one of two things. Firstly, the virus, may be entering the cell, not be able to replicate, but also not be destroyed, almost entering a state of dormancy. On the other hand, it could be that the virus is replicating just enough to keep a steady infection of the monocytes, without drastically increasing its population, or being eradicated in large numbers.

5.2.5 Individual leukocyte subset infections with EV71 isolates

To have a more in-depth assessment of the infection profile of the EV71 isolates, I wanted to look further into the specific subsets that seem to be key to EV71 infection and pathogenesis. As T cells and monocytes seem to be the most infectable and most replicative, they were the ones I focussed on. First the PBMCs were isolated in the same way as previous, then the individual subsets were isolated via negative selection with magnetic beads. The T cells were isolated into CD4 positive and CD8 positive cells respectively. These isolated cells were then subjected to the same infection procedure under the same conditions as the initial PBMC infection.

Isolate 1 again showed limited level of replication in these cells, which confirms with the infection data, that it is not very capable of mounting a sustainable infection in PBMCs, and this could be a major factor in why it

has a limited level of pathogenesis within the patient, and only produced a mild onset of symptoms. Isolate 3 showed no significant change in the level of viral load. Suggesting a limited level of replication in monocytes. The further backs up the evidence that despite its ability to infect cells in the host, its lessened replication capabilities prevent it from maximising it pathogenicity, and stops it from progressing to a severe systemic disease. Isolate 5 also has a limited level of replication in monocytes, this adds to the infection data seen in the total PBMC infection, and adds more evidence to the theory that whilst monocytes are able to sustain an infection with isolate 5, they are not the main proponents of EV71 infection in a severe outcome patient.

In CD8 positive T cells, isolate 1 again continues the trend of limited replication, and isolate 3 shows a much higher viral load than isolate 1, but still there was a decrease across the time points, again suggesting limited replication within these cells. Isolate 5 shows a different pattern than expected here, compared with the total PBMC infection. Both the viral load of the total PBMCs and infection profile of the total T cell subset shows that there is an increase and a peak at 12hpi. However, this is not seen during the CD8 positive T cell only infection. There could be two reasons for this, one is that the CD8 T cells need other factors from other cells to stimulate infection and replication. Yet, the more likely reason is that CD8 T cells are not the main subset of T cells involved in EV71 isolate replication. As there is only a plateau in replication this would suggest that CD4 T cells are the main players in replication.

In fact, CD4 positive T cells do show a significant increase in replication across the time points. Isolate 5 infected T cells were the only cell subset tested to show a significant positive replication of EV71 across the time course. This suggests that the more severe virus isolates have developed an ability to replicate within these cells. This ability could be one of the reasons why they have an increased pathogenic ability. Whether, it is form controlling the hosts ability to synthesise its own mRNA, thus reducing its ability to eliminate the virus, or cause a large increase in the production of cytokines. Or whether it can use the cell as a Trojan horse, to enter parts of the host's system, that it previously could not enter.

5.2.6 Further studies proposed for this area

I would like to see the subset infection expanded to see more time points, and to include the B cell subset, as I believe it would be interesting to see if there was any replication in B cells, and why there was such a significant increase at the earlier time point. I also think an interesting area to explore would be to examine the pathways affected in the different subsets by this infection. Especially during significant increases in replication, just to see exactly which pathways are becoming affected. This could give an indication in to possible pathways that are increasing the severity of the disease, and offer either a possible biomarker for severity, or a pathway in which we could disrupt to lessen the severity for the patient.

As well as expanding the infection to include extra time points and a B cell infection, I would also try to confirm the infective nature of the virus in the individual subsets. I did originally attempt this using flow cytometry; however, the cells were too sensitive to the permeabilisation buffer, and analysis via flow cytometry was not possible. To assess the infectivity level of EV71 in these subsets I would run a Western blot on the infected cells to detect the virus particles as proof of infection. Although this would not be able to give the same level of quantification of infection as flow cytometry, it will serve as proof of infection and should be able to offer some level of measurement of viral infection across the isolates based on the band thickness and intensity.

5.3.0 EV71 Infection and the Blood-Brain Barrier

5.3.1 BBB disruption in an *in vitro* model

The blood brain barrier is a physical, highly selective, diffusion barrier, that can prevent components carried by the blood, such as pathogens, and neurotransmitters from entering the brain. A major component of this barrier is the high abundance and density of tight junction proteins populating the endothelial cells of the cerebral blood vessels and capillaries. These proteins have been well established and characterised in upholding the integrity of the BBB and limiting the paracellular passage of these dangerous components through. However, during severe infection and stress, the BBB is known allow some of these neurotropic pathogens to gain access to the brain and CNS, to cause potentially fatal neurological

complications. For example, EV71 has been shown to cause a wide range of neurological complications, from encephalitis and meningitis to acute flaccid paralysis and neurogenic pulmonary oedema in certain cases. How these pathogens cross this tightly regulated barrier still remains unclear.

To attempt to understand how EV71 can enter the brain and cause these neurological complications, I set up an *in vitro* blood brain barrier model. The aim of which was to study, assess and try to identify the crucial factors or genes relevant in the viral transverse or barrier breakdown of the BBB. This was then compared with a non-neurovirulent virus, which was infected on the same model. The two viruses were then compared both in their ability to disrupt the BBB via TEER measurement and in their gene expression of specific markers. TEER reflects the ionic conductance of the paracellular pathway in an endothelial monolayer by measuring the resistance in Ohms (Ω) (214). Consequently, a decrease in resistance (TEER) indicates a higher ionic conductance of the paracellular pathway and hence implies there is damage to the structural integrity of the BBB.

The initial BBB model infection the three EV71 virus isolates used in the PBMC infection model. they were added to the BBB and the stability and integrity of the BBB was measured over time via TEER and viral load analysis. Isolate 1 showed limited TEER reduction across the time course, with a slight decrease in TEER starting at 120hpi, however it was not significant, there was also a slight increase in abluminal viral load across the time points. These results suggest that there was minimal damage

done to the BBB, as there was no significant reduction in its resistance. The minimal increase in abluminal viral load suggest there was possibly some para or transcellular viral transfer, however this low level could be attributed to the functionality of the immortalised cell line being used. The immortalisation procedure of hCMEC/D3 was found to have led to the lower expression of many surface molecules, such as claudin-5, occludin and JAM2, as well as Glut1, than primary cerebral endothelial cells (215, 216). Therefore, a certain degree of baseline paracellular leakiness would always be present.

Infection with isolate 3 showed a much bigger disruption of the BBB with TEER significantly decreasing at 96hpi, and there had been a large disruption of the barrier's integrity by144hpi, this evidence was backed up by a much larger increase in abluminal viral load. There are no cells on the abluminal side in this model, so there cannot be any replication coming from that side, so all the increase must be coming as para or transcellular viral transfer from the luminal side. This significant decrease in BBB resistance, disruption to the BBB and increase in abluminal viral suggest that this virus has the ability to cross the BBB. This could be a major factor in this isolates ability to cause a more severe disease than isolate 1.

During infection with EV71 isolate 5, there is a large drop in TEER and a sharp increase in viral load in the abluminal region, which indicates that paracellular flux of virions from the luminal to the abluminal side is very likely. Isolate 5's increase in viral load in both the luminal and abluminal

regions suggest that EV71 could be able to cross the BBB transcellularly, as well as via the paracellular route. This isolate shows a similar ability to disrupt the BBB to isolate 3. However, isolate 5 disruption seems to occur much faster and causes a higher level of BBB disruption. This speed and increase destruction could be the reason why this isolate causes the most severe onset of symptoms, which lead to systemic issues, and ultimately, a fatality.

During infection with CHIKV, no change in TEER was noted, indicating that there was no disruption of the BBB, meaning the paracellular flux of virions from the luminal side to the abluminal side is unlikely. This assessment was further supported by a consistent unchanged viral load in the abluminal region, meaning that there was no increase in virus particles entering the brain side of the barrier. This could be due to the inability of CHIKV in even establishing infection in the first place as shown by the absence of a detected infected population, much less replication as shown by the consistent viral load in the luminal region.

This inability of CHIKV to cause any BBB damage and pass into the abluminal side could be due to the polarised infection ability of CHIKV. More specifically, CHIKV has been shown to preferentially infect endothelial cells on the abluminal side of the BBB as oppose to the luminal side (217-219). The E1, E2 and E3 glycoproteins of the CHIKV envelope contain N-glycans, which have been suggested to act as apical sorting signals, leading to the preferential release of the virus into the luminal

domain. Therefore, CHIKV has a lower proclivity to cause neurological infections as it struggles to transcellularly traverse across the BBB. Furthermore, as there was no increase in viral load in either the luminal and abluminal region throughout the infection time course, this suggests there was a lack of viral replication and infection. So, these results from the *in vitro* BBB model suggest that CHIKV is highly unlikely to cross the BBB either paracellularly or transcellularly in an *in vivo* setting.

If I was to repeat this experiment I would add in another condition which would be a positive control such as the West Nile virus, which has been proven to infect the BBB and cause damage to the barrier (220). This would prove a good comparison to compare the level of infection, TEER readings and gene expression profile against as it would show the comparative level of EV71 BBB disruption.

Flow cytometry was attempted after the infection experiment to measure the infection level of the isolates in the BBB model. However, despite several attempts, the cells could not be removed from the insert membrane without damaging them and rendering them unusable for flow cytometry. If I were to repeat the experiment, instead of attempting flow cytometry I would use one of the three inserts (all experiments were done as technical triplicates) for confocal microscopy or IHC staining. This would not only allow visualisation of proof of infection, as well as a certain level of quantification it would also allow the viewing of the level of destruction of the tight junctions of the BBB. This would be achieved by the staining of

the TJ proteins. With the other two inserts, I would remove the cells and use them in a western blot experiment to test for the presence of viral particles to add further proof and quantification of infection.

5.3.2 Gene expression of the BBB during an EV71 infection vs a non-neurotropic CHIKV infection

Next, I looked at the gene expression levels within these infections to assess if there were any genes that could be playing a role in the regulation or disruption of the BBB. Due to certain restraints, only data for isolates 5 and CHIKV was able to be collected. A number of genes were screened, relating to different functions related to the BBB. these included 7 receptor genes, 6 genes encoding for tight junction proteins and adhesion factors, 6 IFN production genes and 5 IFN-associated genes.

There was an overall down-regulation in the mRNA expression of the tight junction and inter-endothelial adhesion proteins of the BBB, during the initial disruption in BBB integrity at 72hpi, detected by the first significant decrease in TEER. This down-regulation of TJ and adhesion protein genes was consistent throughout EV71 infection and seemed to be further downregulated at 144hpi, which could give an explanation to the continual large decrease in TEER. Downregulation of other tight and adherens junction proteins may also play a role in the disruption and permeability of the BBB for example, cadherin is known to associate with ZO-1, another TJ protein, to regulate TJ assembly (221). As well as function as an adhesive membrane protein that links the intracellular actin cytoskeleton to

intermediary proteins such as catenins to form inter-endothelial cell contacts (183).

Conversely CHIKV showed a continued up-regulation of these TJ and adherens protein genes throughout the infection time course, giving further evidence that CHIKV does not cause increased BBB permeability. Also, that there could be a direct link between EV71 infection and disruption of the BBB via the downregulation/destruction of the TJ and adherens junction proteins.

CHIKV showed an expected up-regulation of type I interferons and downstream effectors throughout the infection time course, which also coincided with an up-regulation in the expression level of BBB TJ and AJ proteins. It has been widely reported that CHIKV is a known trigger of high IFN responses as a potent anti-viral response. This has been shown in various immortalised and primary cell lines such as HEK293T, macrophages, fibroblasts, pDCs (222, 223)

EV71 infection showed a quite opposite effect, it led to the continuous suppression of type I IFN responses throughout the time course of the infection. This downregulation indicates that the suppression of the type I interferon response could play an interesting role in the increased permeability of the BBB. The suppression of type I IFNs has been previously reported during EV71 infection, where the virus downregulates IFNAR expression levels to evade immune responses by the host (111,

139). The method of action for this has been suggested that the EV71 2A protein is involved in the cleavage of IFNAR. The disruption of this receptor has further knock on effects down the line, such as blocking the IFN mediated phosphorylation of STAT, which would therefore inhibit downstream cytokines, chemokines and other interferon stimulated genes. Another pathway for the suppression of type I IFN by EV71 that has been reported is the cleavage of the IFN transcription factor IRF-7 by the EV71 viral protease 3C. The cleavage of IRF-7 directly prevents the activation of IFN promoter transcription (115). 3C has also been reported to inhibit the nuclear translocation of IRF-3, which like IRF-7 is an important promoter of transcription for type I IFNs (Lei *et al*, 2010).

There is evidence to suggest that the downregulation and suppression of type I IFNs could increase the permeability of the blood-brain barrier, by virtue of disrupting the balance of two small, regulatory, antagonistic GTPases, called Rac1 and RhoA. Rac1 which inhibits the molecule cofilin and recruits cortacin, to stabilise cortical actin fibres, has been shown to be activated and enhanced by type I IFNs. This adds stability to the TJs and AJs within the endothelial cell, this giving greater structural integrity to the BBB. The RhoA GTPase, through its Rho kinase, destabilises the barrier proteins of endothelial cells by up-regulating myosin light chain kinase-dependent contraction of stress fibres Which leads to the weakening of the BBB by decreasing the stability of the tight and adherens junctions. Type I IFNs have also been shown to inhibit the RhoA GTPase (224).

This adds further evidence to suggest that type I IFN responses could form a protective response against BBB permeability. EV71 shows the ability to suppress these responses. This could be viewed as a virulence factor which certain neurotropic viruses could utilise to further destabilise the TJ and AJs within the BBB, leading to the ability of the virus to transverse into the brain. This indicates that as well as their many antiviral and immune-active properties IFNs could also be a protective pathway against BBB breakdown and disruption.

5.4.0 Host Response Pathways and Their Link to EV71 Severity

5.4.1 The host response cascade

During any attack by a foreign body, the host normally mounts a response to eliminate the pathogen and stop any damage being done to the host, that may occur as a direct or side product of the foreign body's invasion. Most of the time, the body mounts an appropriate response. The pathogen is dealt with and the host can carry on as normal. However, sometimes the host mounts an underwhelming response, and the pathogen is not cleared, or the host unleashes too big of a response and causes itself damage in the process. There can be many reasons for these responses, for example pathogen immune evasion or over expression and production of cytokines. If these specific pathways can be deciphered; and the reasons why certain

viruses or isolates cause much more severe infections can be ascertained, then opportunities will arise for products that can limit or stop these effects.

To attempt to assess the pathways that could be linked to EV71 severity, I analysed the total RNA from a human primary PBMC EV71 infection, using isolates of differing severity. It is well established that leukocytes are the key players in host immune responses. As such, PBMCs are a great way to study the host immune pathways. Due to the technique for isolating PBMCs, all the plasma and serum is removed, Therefore, there can be no cross contamination from outside influences, such as cytokine levels present in serum.

To analyse the extracted total RNA, I decided to use RNASeq, as it would provide me with a high throughput, wide ranging analysis, that would not pigeon-hole in to certain genes but give me the full picture. This stops any genes being missed or overlooked and provides me with a in depth look at the total gene expression.

There are some downsides to using RNASeq on these sorts of samples, as well as the many benefits. For example, the samples are from PBMC infections, there are no single cell type populations, they are all of mixed lineages, so any increases in gene expression in a specific cell type may be masked or negated by a large baseline expression of the same gene in a different cell type with in the PBMC population. Another disadvantage is that it only shows mRNA expression levels, which do not always concur

with the active protein expression levels. This means further experiments may be necessary to add a proof of concept.

5.4.2 The role of IL-6 on EV71 severity

IL-6 is one of the major pro-inflammatory cytokines linked with stimulating the immune response during an infection. It is secreted by macrophages and T cells to initiate this response. Usually in response to PAMPs, which bind to PRRs and induce the intracellular signalling cascade, which results in the inflammatory cytokine production. IL-6 signals through its IL-6 receptor, which consists of the ligand binding part, CD126 and CD130, which is the signal transduction component. Once IL-6 has bound and activated its receptor, it then initiates a signalling cascade through the JAK/STAT pathway.

IL-6 has already been reported to play a major role in the severity of EV71 infection (81, 225, 226). There has been evidence shown that that high levels of IL-6 could possibly overwhelm the host immune defence leading to a chronic inflammatory disease (227). There have been numerous clinical studies that have suggested overproduction of IL-6 may be responsible for severe EV71 brainstem encephalitis (81, 84, 187, 228-230). One experiment showed that patient treated with IVIG resulted in a rapid decrease in both serum and CNS levels of IL-6, however, there was no significant change in anti-EV71 titres (228). These findings suggest that an EV71 induced systemic inflammatory reaction could be the result of the

overproduction of IL-6. Furthermore, this overproduction may be a contributing factor in the severe complications such as encephalitis and cardio-respiratory failure.

My findings give further evidence to this theory, showing largely increased expression of IL-6 in the more severe isolates, both of which were taken from patients who suffered neurological complications.

As a next step in proving this theory, I would run a simple IL-6 ELISA on the cell samples, this could add further evidence to the theory that high IL-6 levels play a role in EV71 severity, as well as adding to our knowledge that this mRNA expression increase was translated into protein expression levels. If the ELISA proves high levels of IL-6 are established, it would be interesting to see what effect, if any, could be seen on IL-6 levels during a BBB infection with EV71, and if there was an increase in IL-6 levels as severity increased, as there may be an interesting link between the immune response and the BBB.

5.1.3 IL-12β and its downstream effects during EV71 infection

IL-12β is a subunit of IL-12 which acts on NK and T cells. It is naturally produced by DCs, macrophages and neutrophils after antigenic stimulation. IL-12 is known to stimulate the production of IFN-γ and TNF-α from T cells and NK cells. These two cytokines are part of two of the main antiviral pathways in the immune system. IFN-γ is a type II interferon which

is an important activator of macrophages and induces MHCII molecule expression. It has the ability to directly inhibit viral replication, and has extremely important immunostimulatory effects. TNF-α is cytokine produced mainly by macrophages, that is involved in systemic inflammation. It is produced to regulate immune cells, but can also induce fever, inhibit viral replication and cause inflammation. Increased expression of IL-12 can lead to the overproduction of IFN-γ and TNF-α, which, along with IL-6 are the main players in systemic inflammation (231). Systemic inflammation can lead to a cytokine storm, which can lead to severe neurological complications, and organ failures, such as pulmonary oedema and cardiac arrest. My results suggest that the more severe isolates have an upregulated expression of IL-12β which could be driving this systemic inflammation, through the IFN-γ and TNF-α channels (232).

The next step I would take in regards to this experiment would be to run an ELISA for IL-12 to see if this increase in IL-12β expression was directly relatable into an increase in IL-12 protein expression. If there was an increase in IL-12 expression levels, I would next run a qPCR experiment on the levels of IFN-γ and TNF-α to get a more in depth look to see to what extent this pathway has been activated, and to see if this has led to an increase in product of IFN-γ and TNF-α.

5.1.4 IL-36γ as a novel cytokine linked to EV71 severity and HFMD

IL-36γ is a member of the IL-1 cytokine family, which has be reported to be stimulated by the cytokines IL-1β, IFN-γ and TNF-α. This cytokine has been linked to psoriasis lesions, as well as being induced during HSV infection. This link between three of the main, induced inflammatory cytokines reported during EV71; its expression being linked to skin lesions; its induction by HSV; and that EV71 infection causes similar style lesions on patients during HFMD, may be the initial findings to a novel pathway during EV71 infection. This theory is furthered when my results, which show that the more severe isolates cause a large upregulation in IL-36γ gene expression (233). As more IL-1β, IFN-γ and TNF-α are produced, there will be an increase in the expression of IL-36γ, this increase leads to a more severe form of HFMD, which in turn creates a greater production of inflammatory cytokines, which could eventually lead to systemic inflammation and complications.

As IL-36 requires proteolytic cleavage of its inactivate pro form before it becomes the active cytokine, the mRNA expression levels would have to be validated by a protein expression study, such as an ELISA or a Western blot for the active cytokine, before this theory can be confirmed. I believe this could open an interesting area of investigation into EV71 severity, and not only the severity, but also the lesions caused by EV71 infection.

As well as running an ELISA, I would also run a qPCR test on both IL-36 and IL-36γ to get a more focussed view on the expression level of these cytokines and tie this in with the ELISA data. If this data proved interesting, this could be furthered with a mouse model. I would like see a IL-36 knock-out mouse, to see if this would cause any change in the level of severity of infection compared to a wild type mouse. This model could provide very useful information on the pathways involved during EV71 infection and involved in the increase of pathogenesis.

5.1.5 The role and regulation of ISG15 and ISG20 during EV71 infection

Interferon is one of the innate immune responses first line of defence against viral pathogens. The pathogens are recognised via PRRs which leads to the production of IFNs, these IFNs then signal, through the JAK/STAT pathway to induce IFN stimulated genes (ISGs). During viral infection, you would expect to see a large increase in IFNs during the early stages of infection, which would translate into large increases in ISGs. However, due to EV71's immune evasion techniques mentioned in the previous chapter, EV71 has the ability to downregulate type I IFNs through its viral proteases. My results add further evidence to this to this theory. There is an initial large increase in ISG15 and ISG20 gene expression between 0 and 6hpi. This would normally be expected to continue to rise, however, there is no more significant increase in ISG15 and ISG20 expression (234). They plateau from 6hpi until the end of the time course suggesting there is no more increase in IFN stimulation.

This theory could be further tested with the addition of a positive infectious control. A virus that is known to infect PBMCs (Sendai virus for example). The infection profile of this virus could be compared to the EV71 profile, you would expect the positive control virus to cause a high level of ISG15 and ISG20 expression, which would constantly increase across the time points. This comparison could add further weight to the theory that EV71 severity is linked to the virus's ability to evade immune detection.

5.1.6 The downregulation of MADCAM1 linked to EV71 severity

MADCAM1is the gene which encodes for the protein addressin. Addressins act as ligands for the homing receptors of lymphocytes, and with the aid of their receptors, determine the tissue the lymphocyte will next enter. They are normally used to direct leukocytes into mucosal and inflamed tissue. As mucosal and inflamed tissues are normally the primary infection sites for EV71 e.g. Peyer's patches and tonsils, this protein is likely to home lymphocytes to these virally infected areas to remove and destroy the viruses. However during EV71 infection with isolate 5, the severe isolate, the expression of this protein is downregulated. This suggests a possible theory that this downregulation of MADCAM1 is a further technique of immune evasion by EV71 (235). This downregulation is not seen in the other two milder isolates, suggesting that early detection avoidance, whilst in the primary infection and replication sites, may lead to a more severe infection outcome.

This theory would need a few more experiments to strengthen its case. Firstly it would need to be determined if this decrease in mRNA expression would lead to a decrease in protein expression (via ELISA), as it is the protein that is the ligand for the homing receptor. If this was downregulated the next step would be to measure the gene and protein expression levels in mucosal endothelial cells as these would be the cells that actually release the ligand to attract lymphocytes to the site of infection. If there was a down regulation in the protein expression of MADCAM1 in these cells then this could be added to the well populated list of EV71 immune evasion techniques.

5.1.7 The effect of RBFOX3 on neural regulation

RBFOX3 is a gene which encodes for the RNA-binding FOX protein, which is involved regulation of alternative splicing of pre-mRNA. It plays a prominent role in the regulation of adult brain function and is expressed at its highest in the CNS (235). During the infection with the EV71 isolates, RBFOX3 was significantly downregulated when the PBMCs were infected with isolate 5. This downregulation could suggest that there may be a disruption in this pathway. This disruption could be lead to a dysregulation of brain function, this combined with a systemic inflammation could cause an increased level of neurological complication.

As mentioned with many of the other genes found to be up/downregulated during thisev71 PBMC infection, although the mRNA downregulation is a good starting point, this needs to be further qualified by a protein

expression study. As RBFOX3 plays its regulatory role as a protein, the protein level, as well as the mRNA level would have to be down regulated for this to have any effect. It is currently unclear as to what RBFOX3 function and role is in brain regulation, however it is thought to play a role in neurogenesis and synaptogenesis (236). If neurons have been damaged during EV71 infection, either due to direct viral lysis or through immune/cytokine damage, new neurons would be needed to help with the recovery of the brain. If a key part in this neurogenesis pathway has been downregulated, then this could be a reason why this isolate has much more severe effects.

5.1.8 Severe EV71 may cause the tight junction instability through RASIP1 downregulation

The RASIP1 gene codes for the protein Ras-interacting protein 1. This protein acts a critical regulator for adhesion and GTPase signalling. It also regulates RhoA GTPase activity by suppressing RhoA signalling. RhoA, mentioned in the previous chapter, acts through its Rho kinase to destabilise the barrier proteins of endothelial cells by up-regulating myosin light chain kinase-dependent contraction of stress fibres. This causes a weakening of the endothelial tight junctions in the BBB leading to decrease in the BBB integrity. During the PBMC infection with EV71, isolates 3 and 5 both downregulated the RASIP1 gene (237). This downregulation would cause a decrease in suppression of the RhoA GTPase, leading to decrease in BBB stability. As previously stated, type I IFNs have been shown to inhibit the RhoA GTPase. Whether this downregulation of RASIP1 is linked

to IFN suppression is unknown, however this could be an interesting pathway to examine to look at BBB integrity.

I believe an interesting area of further research to look at would be to link these results to the RhoA/Rac1 and IFN results seen with the BBB infection. A good starting point would be to look the RASIP1, RhoA and Rac1 mRNA expression levels via qPCR in both the PBMC and BBB infection models, before moving on to the protein expression levels.

5.1.9 The role of ANKRD1 EV71 infection outcome severity

ANKRD1 encodes for the protein cardiac ankyrin repeat protein (CARD), it is a transcription factor involved in conditions of stress to the heart. During times of stress ANKRD1 is upregulated to induce CARP production which has been shown to be a remodelling and repair protein after disease or injury. During EV71 PBMC infection, ANKRD1 was upregulated during the more severe isolates' infection (238). This would suggest that the gene is being produced as a defence mechanism in case there is cardiac compromise. Some studies have also suggested, that whilst CARP performs a repairing role, it can actually have a negative effect on contractile function. This could be a step in the pathway that leads to cardiac dysfunction and pulmonary oedema during sever EV71 infection.

One suggestion I would have if I was going to run further experiments in this area would be to try and look at the RNASeq data from just the infected PBMCs (i.e. remove the uninfected PBMCs). As these PBMC infections

yielded quite low levels of infectivity and replication, some of the effects that the virus is having on the immune system and gene expression levels may be masked or diluted by the non-infected cells, or by cells that have not come in to high levels of contact with the virus. This could be done by sorting the cells using FACS, however this would require fixing the cells first which would decrease the amount of RNA available for extraction. Nonetheless it would be very interesting to see if any new or different changes in gene expression could be seen in these concentrated infected cells. I hypothesise that there may be several more pathways of interest that could be uncovered with this experiment.

Novel Findings and Overall Conclusions From This Work

Viral infectivity and replication play a big role in outcome severity

- Viruses that cause a greater level of severity in patients have significantly increased levels of infection and replication *in vitro.*

Virus isolates from patients with severe outcomes have higher levels of infectivity

- Isolate 1 showed limited infectivity during the PBMC infection
- Isolates 3 and 5, which both came from patients suffering neurological complications, showed significantly higher levels of infection in PBMCs

Only the isolates from the most severe patients can replicate in an *ex vivo* PBMC system

- Only isolate 5 showed signs of positive replication during the infection

Certain subsets of PBMC show higher susceptibility for infection

- Monocytes, T cells and B cells showed significantly higher levels of infection than the other subsets.

CD4+ T Cells are the main instigators of EV71 replication in PBMCs

- Only CD4+ T cells showed an increase in replication during severe EV71 infection

Severe EV71 isolates show an increased ability to disrupt the BBB

- Both isolate 3 and 5 show greater levels BBB disruption, with isolate 5 being the most destructive

EV71 can downregulate BBB tight junction and adherens junction proteins

- TJ and AJ gene expression was down regulated during EV71 infection, compared to mock infected and a non-neurotropic virus infection

EV71 can downregulate immune response genes which may lead to a weakened BBB

- The downregulation of IFN and IFN related genes may lead to instability in the BBB junction proteins

Severe EV71 infection leads to the upregulation of IL-6

- Isolate 3 and 5 show higher levels of IL-6 gene expression

IL-36γ could be a involved in a novel pathway related to infection severity

Immune avoidance could play an early role in EV71 severity

- The downregulation of MADCAM1 may lead to immune avoidance and increased pathogenicity

References

1. Yan J-J, Su I-J, Chen P-F, Liu C-C, Yu C-K, Wang J-R. Complete genome analysis of enterovirus 71 isolated from an outbreak in Taiwan and rapid identification of enterovirus 71 and coxsackievirus A16 by RT-PCR. Journal of Medical Virology. 2001;65(2):331-9.
2. Lo SH, Huang YC, Huang CG, Tsao KC, Li WC, Hsieh YC, et al. Clinical and epidemiologic features of Coxsackievirus A6 infection in children in northern Taiwan between 2004 and 2009. Journal of microbiology, immunology, and infection = Wei mian yu gan ran za zhi. 2011;44(4):252-7.
3. Second J, Velter C, Calès S, Truchetet F, Lipsker D, Cribier B. Clinicopathologic analysis of atypical hand, foot, and mouth disease in adult patients. Journal of the American Academy of Dermatology. 2017;76(4):722-9.
4. Ooi MH, Wong SC, Lewthwaite P, Cardosa MJ, Solomon T. Clinical features, diagnosis, and management of enterovirus 71. The Lancet Neurology. 2010;9(11):1097-105.
5. Chang L-Y, Lin T-Y, Hsu K-H, Huang Y-C, Lin K-L, Hsueh C, et al. Clinical features and risk factors of pulmonary oedema after enterovirus-71-related hand, foot, and mouth disease. The Lancet. 1999;354(9191):1682-6.
6. Shah VA, Chong CY, Chan KP, Ng W, Ling AE. Clinical characteristics of an outbreak of hand, foot and mouth disease in Singapore. Ann Acad Med Singapore. 2003;32(3):381-7.
7. McMinn P, Stratov I, Nagarajan L, Davis S. Neurological Manifestations of Enterovirus 71 Infection in Children during an Outbreak of Hand, Foot, and Mouth Disease in Western Australia. Clinical Infectious Diseases. 2001;32(2):236-42.
8. Chan LG, Parashar UD, Lye MS, Ong FG, Zaki SR, Alexander JP, et al. Deaths of children during an outbreak of hand, foot, and mouth disease in sarawak, malaysia: clinical and pathological characteristics of the disease. For the Outbreak Study Group. Clinical infectious diseases : an official publication of the Infectious Diseases Society of America. 2000;31(3):678-83.
9. Chang LY, Lin TY, Huang YC, Tsao KC, Shih SR, Kuo ML, et al. Comparison of enterovirus 71 and coxsackie-virus A16 clinical illnesses during the Taiwan enterovirus epidemic, 1998. The Pediatric infectious disease journal. 1999;18(12):1092-6.
10. Sutton-Hayes S, Weisse ME, Wilson NW, Ogershok PR. A Recurrent Presentation of Hand, Foot, and Mouth Disease. Clinical Pediatrics. 2006;45(4):373-6.
11. Crabol Y, Pean P, Mey C, Duong V, Richner B, Laurent D, et al. A prospective, comparative study of severe neurological and uncomplicated hand, foot and mouth forms of paediatric enterovirus 71 infections. International Journal of Infectious Diseases. 2017;59:69-76.
12. Bracho MA, González-Candelas F, Valero A, Córdoba J, Salazar A. Enterovirus Co-infections and Onychomadesis after Hand, Foot, and Mouth Disease, Spain, 2008. Emerging infectious diseases. 2011;17(12):2223-31.

13. Rabenau HF, Richter M, Doerr HW. Hand, foot and mouth disease: seroprevalence of Coxsackie A16 and Enterovirus 71 in Germany. Medical microbiology and immunology. 2010;199(1):45-51.
14. Mirand A, Henquell C, Archimbaud C, Ughetto S, Antona D, Bailly JL, et al. Outbreak of hand, foot and mouth disease/herpangina associated with coxsackievirus A6 and A10 infections in 2010, France: a large citywide, prospective observational study. Clinical Microbiology and Infection. 2012;18(5):E110-E8.
15. Castro CM, Cruz AC, Silva EE, Gomes Mde L. Molecular and seroepidemiologic studies of Enterovirus 71 infection in the State of Para, Brazil. Revista do Instituto de Medicina Tropical de Sao Paulo. 2005;47(2):65-71.
16. Machain-Williams C, Dzul-Rosado AR, Yeh-Gorocica AB, Rodriguez-Ruz KG, Noh-Pech H, Talavera-Aguilar L, et al. Detection of hand, foot and mouth disease in the yucatan peninsula of Mexico. Infectious disease reports. 2014;6(4):5627.
17. Flett K, Youngster I, Huang J, McAdam A, Sandora TJ, Rennick M, et al. Hand, Foot, and Mouth Disease Caused by Coxsackievirus A6. Emerging infectious diseases. 2012;18(10):1702-4.
18. Bendig JW, Fleming DM. Epidemiological, virological, and clinical features of an epidemic of hand, foot, and mouth disease in England and Wales. Communicable disease report CDR review. 1996;6(6):R81-6.
19. Ferson MJ, Bell SM. Outbreak of Coxsackievirus A16 hand, foot, and mouth disease in a child day-care center. American journal of public health. 1991;81(12):1675-6.
20. Kar BR, Dwibedi B, Kar SK. An outbreak of hand, foot and mouth disease in Bhubaneswar, Odisha. Indian pediatrics. 2013;50(1):139-42.
21. Tu PV, Thao NT, Perera D, Huu TK, Tien NT, Thuong TC, et al. Epidemiologic and virologic investigation of hand, foot, and mouth disease, southern Vietnam, 2005. Emerging infectious diseases. 2007;13(11):1733-41.
22. Ho M, Chen ER, Hsu KH, Twu SJ, Chen KT, Tsai SF, et al. An epidemic of enterovirus 71 infection in Taiwan. Taiwan Enterovirus Epidemic Working Group. The New England journal of medicine. 1999;341(13):929-35.
23. Kim KH. Enterovirus 71 infection: An experience in Korea, 2009. Korean journal of pediatrics. 2010;53(5):616-22.
24. Komatsu H, Shimizu Y, Takeuchi Y, Ishiko H, Takada H. Outbreak of severe neurologic involvement associated with Enterovirus 71 infection. Pediatric neurology. 1999;20(1):17-23.
25. Lin TY, Twu SJ, Ho MS, Chang LY, Lee CY. Enterovirus 71 outbreaks, Taiwan: occurrence and recognition. Emerging infectious diseases. 2003;9(3):291-3.
26. McMinn P, Stratov I, Dowse G. Enterovirus 71 outbreak in Western Australia associated with acute flaccid paralysis. Preliminary report. Communicable diseases intelligence. 1999;23(7):199.
27. Tan X, Huang X, Zhu S, Chen H, Yu Q, Wang H, et al. The persistent circulation of enterovirus 71 in People's Republic of China: causing emerging nationwide epidemics since 2008. PloS one. 2011;6(9):e25662.

28. Wu Y, Yeo A, Phoon MC, Tan EL, Poh CL, Quak SH, et al. The largest outbreak of hand; foot and mouth disease in Singapore in 2008: The role of enterovirus 71 and coxsackievirus A strains. International Journal of Infectious Diseases. 2010;14(12):e1076-e81.
29. Sazaly A, Sam IC, Jaliha Y, Meng Keang L, Suzana M, Poh-Sim H. Enterovirus 71 Outbreak, Brunei. Emerging Infectious Disease journal. 2009;15(1):79.
30. Fujimoto T, Chikahira M, Yoshida S, Ebira H, Hasegawa A, Totsuka A, et al. Outbreak of Central Nervous System Disease Associated with Hand, Foot, and Mouth Disease in Japan during the Summer of 2000: Detection and Molecular Epidemiology of Enterovirus 71. Microbiology and Immunology. 2002;46(9):621-7.
31. Wang SM, Liu CC. Enterovirus 71: epidemiology, pathogenesis and management. Expert review of anti-infective therapy. 2009;7(6):735-42.
32. Ooi MH, Wong SC, Podin Y, Akin W, del Sel S, Mohan A, et al. Human Enterovirus 71 Disease in Sarawak, Malaysia: A Prospective Clinical, Virological, and Molecular Epidemiological Study. Clinical Infectious Diseases. 2007;44(5):646-56.
33. Wang S-M, Liu C-C, Tseng H-W, Wang J-R, Huang C-C, Chen Y-J, et al. Clinical Spectrum of Enterovirus 71 Infection in Children in Southern Taiwan, with an Emphasis on Neurological Complications. Clinical Infectious Diseases. 1999;29(1):184-90.
34. Gantt S, Yao L, Kollmann TR, Casper C, Zhang J, Self SG. Implications of Age-Dependent Immune Responses to Enterovirus 71 Infection for Disease Pathogenesis and Vaccine Design. Journal of the Pediatric Infectious Diseases Society. 2013;2(2):162-70.
35. Huang M-L, Chiang P-S, Chia M-Y, Luo S-T, Chang L-Y, Lin T-Y, et al. Cross-reactive Neutralizing Antibody Responses to Enterovirus 71 Infections in Young Children: Implications for Vaccine Development. PLOS Neglected Tropical Diseases. 2013;7(2):e2067.
36. Zhang H, An D, Liu W, Mao Q, Jin J, Xu L, et al. Analysis of Cross-Reactive Neutralizing Antibodies in Human HFMD Serum with an EV71 Pseudovirus-Based Assay. PloS one. 2014;9(6):e100545.
37. Mizuta K, Aoki Y, Suto A, Ootani K, Katsushima N, Itagaki T, et al. Cross-antigenicity among EV71 strains from different genogroups isolated in Yamagata, Japan, between 1990 and 2007. Vaccine. 2009;27(24):3153-8.
38. Zhuang Z-C, Kou Z-Q, Bai Y-J, Cong X, Wang L-H, Li C, et al. Epidemiological Research on Hand, Foot, and Mouth Disease in Mainland China. Viruses. 2015;7(12):6400-11.
39. AbuBakar S, Chee H-Y, Al-Kobaisi MF, Xiaoshan J, Bing Chua K, Kit Lam S. Identification of enterovirus 71 isolates from an outbreak of hand, foot and mouth disease (HFMD) with fatal cases of encephalomyelitis in Malaysia. Virus Research. 1999;61(1):1-9.
40. Tee KK, Lam TT, Chan YF, Bible JM, Kamarulzaman A, Tong CY, et al. Evolutionary genetics of human enterovirus 71: origin, population dynamics, natural selection, and seasonal periodicity of the VP1 gene. Journal of virology. 2010;84(7):3339-50.

41. Flewett TH, Warin RP, Clarke SKR. `Hand, foot, and mouth disease' associated with Coxsackie A5 virus. Journal of Clinical Pathology. 1963;16(1):53-5.
42. Hu YF, Yang F, Du J, Dong J, Zhang T, Wu ZQ, et al. Complete Genome Analysis of Coxsackievirus A2, A4, A5, and A10 Strains Isolated from Hand, Foot, and Mouth Disease Patients in China Revealing Frequent Recombination of Human Enterovirus A. Journal of Clinical Microbiology. 2011;49(7):2426-34.
43. Ang LW, Koh BK, Chan KP, Chua LT, James L, Goh KT. Epidemiology and control of hand, foot and mouth disease in Singapore, 2001-2007. Ann Acad Med Singapore. 2009;38(2):106-12.
44. Hughes RO, Roberts C. Hand, foot, and mouth disease associated with Coxsackie A9 virus. Lancet. 1972;2(7780):751-2.
45. Andreoni AR, Colton AS. Coxsackievirus B5 associated with hand-foot-mouth disease in a healthy adult. JAAD Case Reports. 2017;3(2):165-8.
46. Lindenbaum JE, Van Dyck PC, Allen RG. Hand, foot and mouth disease associated with coxsackievirus group B. Scandinavian journal of infectious diseases. 1975;7(3):161-3.
47. Huang H-I, Shih S-R. Neurotropic Enterovirus Infections in the Central Nervous System. Viruses. 2015;7(11):6051-66.
48. Lin T-Y, Chang L-Y, Hsia S-H, Huang Y-C, Chiu C-H, Hsueh C, et al. The 1998 Enterovirus 71 Outbreak in Taiwan: Pathogenesis and Management. Clinical Infectious Diseases. 2002;34(Supplement_2):S52-S7.
49. Schmidt NJ, Lennette EH, Ho HH. An apparently new enterovirus isolated from patients with disease of the central nervous system. The Journal of infectious diseases. 1974;129(3):304-9.
50. Chumakov M, Voroshilova M, Shindarov L, Lavrova I, Gracheva L, Koroleva G, et al. Enterovirus 71 isolated from cases of epidemic poliomyelitis-like disease in Bulgaria. Archives of virology. 1979;60(3-4):329-40.
51. Nagy G, Takatsy S, Kukan E, Mihaly I, Domok I. Virological diagnosis of enterovirus type 71 infections: experiences gained during an epidemic of acute CNS diseases in Hungary in 1978. Archives of virology. 1982;71(3):217-27.
52. Ishimaru Y, Nakano S, Yamaoka K, Takami S. Outbreaks of hand, foot, and mouth disease by enterovirus 71. High incidence of complication disorders of central nervous system. Archives of disease in childhood. 1980;55(8):583-8.
53. Hagiwara A, Tagaya I, Yoneyama T. Epidemic of hand, foot and mouth disease associated with enterovirus 71 infection. Intervirology. 1978;9(1):60-3.
54. Lum LC, Wong KT, Lam SK, Chua KB, Goh AY, Lim WL, et al. Fatal enterovirus 71 encephalomyelitis. The Journal of pediatrics. 1998;133(6):795-8.
55. Brown BA, Pallansch MA. Complete nucleotide sequence of enterovirus 71 is distinct from poliovirus. Virus Research. 1995;39(2):195-205.

56. Plevka P, Perera R, Cardosa J, Kuhn RJ, Rossmann MG. Crystal Structure of Human Enterovirus 71. Science (New York, NY). 2012;336(6086):1274-.
57. Xie S, Wang K, Yu W, Lu W, Xu K, Wang J, et al. DIDS blocks a chloride-dependent current that is mediated by the 2B protein of enterovirus 71. Cell Research. 2011;21(8):1271-5.
58. Wang C, Jiang P, Sand C, Paul AV, Wimmer E. Alanine Scanning of Poliovirus 2CATPase Reveals New Genetic Evidence that Capsid Protein/2CATPase Interactions Are Essential for Morphogenesis. Journal of virology. 2012;86(18):9964-75.
59. Cho MW, Teterina N, Egger D, Bienz K, Ehrenfeld E. Membrane rearrangement and vesicle induction by recombinant poliovirus 2C and 2BC in human cells. Virology. 1994;202(1):129-45.
60. Zheng Z, Li H, Zhang Z, Meng J, Mao D, Bai B, et al. Enterovirus 71 2C protein inhibits TNF-alpha-mediated activation of NF-kappaB by suppressing IkappaB kinase beta phosphorylation. Journal of immunology. 2011;187(5):2202-12.
61. Li JP, Baltimore D. An intragenic revertant of a poliovirus 2C mutant has an uncoating defect. Journal of virology. 1990;64(3):1102-7.
62. McMinn PC. An overview of the evolution of enterovirus 71 and its clinical and public health significance. FEMS Microbiology Reviews. 2002;26(1):91-107.
63. Lei X, Xiao X, Zhang Z, Ma Y, Qi J, Wu C, et al. The Golgi protein ACBD3 facilitates Enterovirus 71 replication by interacting with 3A. Scientific reports. 2017;7:44592.
64. Sun Y, Wang Y, Shan C, Chen C, Xu P, Song M, et al. Enterovirus 71 VPg Uridylation Uses a Two-Molecular Mechanism of 3D Polymerase. Journal of virology. 2012;86(24):13662-71.
65. Lu G, Qi J, Chen Z, Xu X, Gao F, Lin D, et al. Enterovirus 71 and Coxsackievirus A16 3C Proteases: Binding to Rupintrivir and Their Substrates and Anti-Hand, Foot, and Mouth Disease Virus Drug Design. Journal of virology. 2011;85(19):10319-31.
66. Shih SR, Chiang C, Chen TC, Wu CN, Hsu JT, Lee JC, et al. Mutations at KFRDI and VGK domains of enterovirus 71 3C protease affect its RNA binding and proteolytic activities. J Biomed Sci. 2004;11(2):239-48.
67. Lei X, Sun Z, Liu X, Jin Q, He B, Wang J. Cleavage of the Adaptor Protein TRIF by Enterovirus 71 3C Inhibits Antiviral Responses Mediated by Toll-Like Receptor 3. Journal of virology. 2011;85(17):8811-8.
68. Lei X, Liu X, Ma Y, Sun Z, Yang Y, Jin Q, et al. The 3C protein of enterovirus 71 inhibits retinoid acid-inducible gene I-mediated interferon regulatory factor 3 activation and type I interferon responses. J Virol. 2010;84(16):8051-61.
69. Wu Y, Lou Z, Miao Y, Yu Y, Dong H, Peng W, et al. Structures of EV71 RNA-dependent RNA polymerase in complex with substrate and analogue provide a drug target against the hand-foot-and-mouth disease pandemic in China. Protein Cell. 2010;1(5):491-500.
70. Bessaud M, Razafindratsimandresy R, Nougairede A, Joffret ML, Deshpande JM, Dubot-Peres A, et al. Molecular comparison and evolutionary analyses of VP1 nucleotide sequences of new African human

enterovirus 71 isolates reveal a wide genetic diversity. PloS one. 2014;9(3):e90624.
71. MA Pallansch RR. Enteroviruses: polioviruses, coxsackieviruses, echoviruses, and newer enteroviruses
. in: DM Knipe, PM Howley, DE Griffin (Eds), et al, Fields Virology, vol 1, Lippincott, Williams & Wilkins, Hagerstown, MD, USA2001. p. pp. 723–75 1:.
72. Solomon T, Lewthwaite P, Perera D, Cardosa MJ, McMinn P, Ooi MH. Virology, epidemiology, pathogenesis, and control of enterovirus 71. The Lancet Infectious diseases. 2010;10(11):778-90.
73. Chung PW, Huang YC, Chang LY, Lin TY, Ning HC. Duration of enterovirus shedding in stool. Journal of Microbiology, Immunology and Infection. 2001;34(3):167-70.
74. He Y, Ong KC, Gao Z, Zhao X, Anderson VM, McNutt MA, et al. Tonsillar crypt epithelium is an important extra-central nervous system site for viral replication in EV71 encephalomyelitis. The American journal of pathology. 2014;184(3):714-20.
75. Cheng HY, Huang YC, Yen TY, Hsia SH, Hsieh YC, Li CC, et al. The correlation between the presence of viremia and clinical severity in patients with enterovirus 71 infection: a multi-center cohort study. BMC infectious diseases. 2014;14:417.
76. Lee M-S, Chiang P-S, Luo S-T, Huang M-L, Liou G-Y, Tsao K-C, et al. Incidence Rates of Enterovirus 71 Infections in Young Children during a Nationwide Epidemic in Taiwan, 2008–09. PLOS Neglected Tropical Diseases. 2012;6(2):e1476.
77. Chen C-S, Yao Y-C, Lin S-C, Lee Y-P, Wang Y-F, Wang J-R, et al. Retrograde Axonal Transport: a Major Transmission Route of Enterovirus 71 in Mice. Journal of virology. 2007;81(17):8996-9003.
78. Nishimura Y, Shimojima M, Tano Y, Miyamura T, Wakita T, Shimizu H. Human P-selectin glycoprotein ligand-1 is a functional receptor for enterovirus 71. Nat Med. 2009;15(7):794-7.
79. Chang CY, Li JR, Ou YC, Chen WY, Liao SL, Raung SL, et al. Enterovirus 71 infection caused neuronal cell death and cytokine expression in cultured rat neural cells. IUBMB life. 2015;67(10):789-800.
80. Chang SC, Lin JY, Lo LY, Li ML, Shih SR. Diverse apoptotic pathways in enterovirus 71-infected cells. Journal of neurovirology. 2004;10(6):338-49.
81. Lin T-Y, Hsia S-H, Huang Y-C, Wu C-T, Chang L-Y. Proinflammatory Cytokine Reactions in Enterovirus 71 Infections of the Central Nervous System. Clinical Infectious Diseases. 2003;36(3):269-74.
82. Griffiths MJ, Ooi MH, Wong SC, Mohan A, Podin Y, Perera D, et al. In enterovirus 71 encephalitis with cardio-respiratory compromise, elevated interleukin 1beta, interleukin 1 receptor antagonist, and granulocyte colony-stimulating factor levels are markers of poor prognosis. The Journal of infectious diseases. 2012;206(6):881-92.
83. Ye N, Gong X, Pang LL, Gao WJ, Zhang YT, Li XL, et al. Cytokine responses and correlations thereof with clinical profiles in children with enterovirus 71 infections. BMC infectious diseases. 2015;15:225.
84. Lin TY, Chang LY, Huang YC, Hsu KH, Chiu CH, Yang KD. Different proinflammatory reactions in fatal and non‐fatal enterovirus 71 infections:

implications for early recognition and therapy. Acta Paediatrica. 2002;91(6):632-5.
85. Wang SM, Lei HY, Huang KJ, Wu JM, Wang JR, Yu CK, et al. Pathogenesis of enterovirus 71 brainstem encephalitis in pediatric patients: roles of cytokines and cellular immune activation in patients with pulmonary edema. The Journal of infectious diseases. 2003;188(4):564-70.
86. Kao SJ, Yang FL, Hsu YH, Chen HI. Mechanism of Fulminant Pulmonary Edema Caused by Enterovirus 71. Clinical Infectious Diseases. 2004;38(12):1784-8.
87. Yamayoshi S, Yamashita Y, Li J, Hanagata N, Minowa T, Takemura T, et al. Scavenger receptor B2 is a cellular receptor for enterovirus 71. Nat Med. 2009;15(7):798-801.
88. Yang B, Chuang H, Yang KD. Sialylated glycans as receptor and inhibitor of enterovirus 71 infection to DLD-1 intestinal cells. Virology journal. 2009;6(1):141.
89. Tan CW, Poh CL, Sam IC, Chan YF. Enterovirus 71 uses cell surface heparan sulfate glycosaminoglycan as an attachment receptor. Journal of virology. 2013;87(1):611-20.
90. Yang SL, Chou YT, Wu CN, Ho MS. Annexin II binds to capsid protein VP1 of enterovirus 71 and enhances viral infectivity. Journal of virology. 2011;85(22):11809-20.
91. Yamayoshi S, Fujii K, Koike S. Receptors for enterovirus 71. Emerg Microbes Infect. 2014;3:e53.
92. Yamayoshi S, Koike S. Identification of a Human SCARB2 Region That Is Important for Enterovirus 71 Binding and Infection. Journal of virology. 2011;85(10):4937-46.
93. Hirata T, Merrill-Skoloff G, Aab M, Yang J, Furie BC, Furie B. P-Selectin Glycoprotein Ligand 1 (Psgl-1) Is a Physiological Ligand for E-Selectin in Mediating T Helper 1 Lymphocyte Migration. The Journal of Experimental Medicine. 2000;192(11):1669-76.
94. Nishimura Y, Wakita T, Shimizu H. Tyrosine Sulfation of the Amino Terminus of PSGL-1 Is Critical for Enterovirus 71 Infection. PLOS Pathogens. 2010;6(11):e1001174.
95. Kataoka C, Suzuki T, Kotani O, Iwata-Yoshikawa N, Nagata N, Ami Y, et al. The Role of VP1 Amino Acid Residue 145 of Enterovirus 71 in Viral Fitness and Pathogenesis in a Cynomolgus Monkey Model. PLOS Pathogens. 2015;11(7):e1005033.
96. Takeuchi O, Akira S. Innate immunity to virus infection. Immunological reviews. 2009;227(1):75-86.
97. Mogensen TH. Pathogen Recognition and Inflammatory Signaling in Innate Immune Defenses. Clinical Microbiology Reviews. 2009;22(2):240-73.
98. Tang D, Kang R, Coyne CB, Zeh HJ, Lotze MT. PAMPs and DAMPs: Signal 0s that Spur Autophagy and Immunity. Immunological reviews. 2012;249(1):158-75.
99. Fukata M, Vamadevan AS, Abreu MT. Toll-like receptors (TLRs) and Nod-like receptors (NLRs) in inflammatory disorders. Seminars in immunology. 2009;21(4):242-53.
100. Pathinayake PS, Hsu ACY, Wark PAB. Innate Immunity and Immune Evasion by Enterovirus 71. Viruses. 2015;7(12):6613-30.

101. Fitzgerald KA, McWhirter SM, Faia KL, Rowe DC, Latz E, Golenbock DT, et al. IKKepsilon and TBK1 are essential components of the IRF3 signaling pathway. Nature immunology. 2003;4(5):491-6.
102. Wang B, Xi X, Lei X, Zhang X, Cui S, Wang J, et al. Enterovirus 71 protease 2Apro targets MAVS to inhibit anti-viral type I interferon responses. PLoS Pathog. 2013;9(3):e1003231.
103. Lei X, Sun Z, Liu X, Jin Q, He B, Wang J. Cleavage of the adaptor protein TRIF by enterovirus 71 3C inhibits antiviral responses mediated by Toll-like receptor 3. Journal of virology. 2011;85(17):8811-8.
104. Kontsek P. Human type I interferons: structure and function. Acta virologica. 1994;38(6):345-60.
105. Reid E, Charleston B. Type I and III interferon production in response to RNA viruses. Journal of interferon & cytokine research : the official journal of the International Society for Interferon and Cytokine Research. 2014;34(9):649-58.
106. Yi L, He Y, Chen Y, Kung HF, He ML. Potent inhibition of human enterovirus 71 replication by type I interferon subtypes. Antiviral therapy. 2011;16(1):51-8.
107. Liu ML, Lee YP, Wang YF, Lei HY, Liu CC, Wang SM, et al. Type I interferons protect mice against enterovirus 71 infection. The Journal of general virology. 2005;86(Pt 12):3263-9.
108. Lin J-Y, Chen T-C, Weng K-F, Chang S-C, Chen L-L, Shih S-R. Viral and host proteins involved in picornavirus life cycle. Journal of Biomedical Science. 2009;16(1):103.
109. Shih SR, Stollar V, Li ML. Host factors in enterovirus 71 replication. Journal of virology. 2011;85(19):9658-66.
110. Feng Q, Langereis MA, Lork M, Nguyen M, Hato SV, Lanke K, et al. Enterovirus 2Apro targets MDA5 and MAVS in infected cells. Journal of virology. 2014;88(6):3369-78.
111. Lu J, Yi L, Zhao J, Yu J, Chen Y, Lin MC, et al. Enterovirus 71 disrupts interferon signaling by reducing the level of interferon receptor 1. Journal of virology. 2012;86(7):3767-76.
112. Morrison JM, Racaniello VR. Proteinase 2Apro is essential for enterovirus replication in type I interferon-treated cells. Journal of virology. 2009;83(9):4412-22.
113. Liu Y, Zhang Z, Zhao X, Yu R, Zhang X, Wu S, et al. Enterovirus 71 inhibits cellular type I interferon signaling by downregulating JAK1 protein expression. Viral immunology. 2014;27(6):267-76.
114. Hung HC, Wang HC, Shih SR, Teng IF, Tseng CP, Hsu JT. Synergistic inhibition of enterovirus 71 replication by interferon and rupintrivir. The Journal of infectious diseases. 2011;203(12):1784-90.
115. Lei X, Xiao X, Xue Q, Jin Q, He B, Wang J. Cleavage of interferon regulatory factor 7 by enterovirus 71 3C suppresses cellular responses. Journal of virology. 2013;87(3):1690-8.
116. Lin JY, Shih SR, Pan M, Li C, Lue CF, Stollar V, et al. hnRNP A1 interacts with the 5' untranslated regions of enterovirus 71 and Sindbis virus RNA and is required for viral replication. Journal of virology. 2009;83(12):6106-14.

117. Pilipenko EV, Viktorova EG, Guest ST, Agol VI, Roos RP. Cell‐specific proteins regulate viral RNA translation and virus‐induced disease. The EMBO Journal. 2001;20(23):6899-908.
118. Thompson SR, Sarnow P. Enterovirus 71 contains a type I IRES element that functions when eukaryotic initiation factor eIF4G is cleaved. Virology. 2003;315(1):259-66.
119. Huang P-N, Lin J-Y, Locker N, Kung Y-A, Hung C-T, Lin J-Y, et al. Far upstream element binding protein 1 binds the internal ribosomal entry site of enterovirus 71 and enhances viral translation and viral growth. Nucleic Acids Research. 2011;39(22):9633-48.
120. Chen L-L, Kung Y-A, Weng K-F, Lin J-Y, Horng J-T, Shih S-R. Enterovirus 71 Infection Cleaves a Negative Regulator for Viral Internal Ribosomal Entry Site-Driven Translation. Journal of virology. 2013;87(7):3828-38.
121. Wong KT, Munisamy B, Ong KC, Kojima H, Noriyo N, Chua KB, et al. The Distribution of Inflammation and Virus in Human Enterovirus 71 Encephalomyelitis Suggests Possible Viral Spread by Neural Pathways. Journal of Neuropathology & Experimental Neurology. 2008;67(2):162-9.
122. Nagata N, Shimizu H, Ami Y, Tano Y, Harashima A, Suzaki Y, et al. Pyramidal and extrapyramidal involvement in experimental infection of cynomolgus monkeys with enterovirus 71. J Med Virol. 2002;67(2):207-16.
123. Lin YW, Wang SW, Tung YY, Chen SH. Enterovirus 71 infection of human dendritic cells. Exp Biol Med (Maywood). 2009;234(10):1166-73.
124. Yamayoshi S, Yamashita Y, Li J, Hanagata N, Minowa T, Takemura T, et al. Scavenger receptor B2 is a cellular receptor for enterovirus 71. Nat Med. 2009;15.
125. Abadier M, Ley K. P-selectin glycoprotein ligand-1 in T cells. Current opinion in hematology. 2017;24(3):265-73.
126. Laszik Z, Jansen PJ, Cummings RD, Tedder TF, McEver RP, Moore KL. P-selectin glycoprotein ligand-1 is broadly expressed in cells of myeloid, lymphoid, and dendritic lineage and in some nonhematopoietic cells. Blood. 1996;88(8):3010-21.
127. Liu L, Zhao H, Zhang Y, Wang J, Che Y, Dong C, et al. Neonatal rhesus monkey is a potential animal model for studying pathogenesis of EV71 infection. Virology. 2011;412(1):91-100.
128. Pérez-Ruiz M, Navarro-Marí JM, Palacios del Valle E, Rosa-Fraile M. Human rhabdomyosarcoma cells for rapid detection of enteroviruses by shell-vial assay. Journal of Medical Microbiology. 2003;52(9):789-91.
129. Wang W, Xiao F, Wan P, Pan P, Zhang Y, Liu F, et al. EV71 3D Protein Binds with NLRP3 and Enhances the Assembly of Inflammasome Complex. PLOS Pathogens. 2017;13(1):e1006123.
130. Chen L-C, Yeh T-M. Enterovirus 71 infection of human immune cells induces the production of proinflammatory cytokines. J Biomed Lab Sci. 2009;21(1):82-90.
131. Peng H, Shi M, Zhang L, Li Y, Sun J, Zhang L, et al. Activation of JNK1/2 and p38 MAPK signaling pathways promotes enterovirus 71 infection in immature dendritic cells. BMC Microbiology. 2014;14(1):147.
132. Fujii K, Nagata N, Sato Y, Ong KC, Wong KT, Yamayoshi S, et al. Transgenic mouse model for the study of enterovirus 71

neuropathogenesis. Proceedings of the National Academy of Sciences of the United States of America. 2013;110(36):14753-8.
133. Arita M, Ami Y, Wakita T, Shimizu H. Cooperative Effect of the Attenuation Determinants Derived from Poliovirus Sabin 1 Strain Is Essential for Attenuation of Enterovirus 71 in the NOD/SCID Mouse Infection Model. Journal of virology. 2008;82(4):1787-97.
134. Chua BH, Phuektes P, Sanders SA, Nicholls PK, McMinn PC. The molecular basis of mouse adaptation by human enterovirus 71. The Journal of general virology. 2008;89(Pt 7):1622-32.
135. Khong WX, Yan B, Yeo H, Tan EL, Lee JJ, Ng JKW, et al. A Non-Mouse-Adapted Enterovirus 71 (EV71) Strain Exhibits Neurotropism, Causing Neurological Manifestations in a Novel Mouse Model of EV71 Infection. Journal of virology. 2012;86(4):2121-31.
136. Ong KC, Badmanathan M, Devi S, Leong KL, Cardosa MJ, Wong KT. Pathologic characterization of a murine model of human enterovirus 71 encephalomyelitis. Journal of neuropathology and experimental neurology. 2008;67(6):532-42.
137. Chen YC, Yu CK, Wang YF, Liu CC, Su IJ, Lei HY. A murine oral enterovirus 71 infection model with central nervous system involvement. The Journal of general virology. 2004;85(Pt 1):69-77.
138. Wang Y-F, Chou C-T, Lei H-Y, Liu C-C, Wang S-M, Yan J-J, et al. A Mouse-Adapted Enterovirus 71 Strain Causes Neurological Disease in Mice after Oral Infection. Journal of virology. 2004;78(15):7916-24.
139. Lee YP, Wang YF, Wang JR, Huang SW, Yu CK. Enterovirus 71 blocks selectively type I interferon production through the 3C viral protein in mice. J Med Virol. 2012;84(11):1779-89.
140. Shultz LD, Brehm MA, Garcia JV, Greiner DL. Humanized mice for immune system investigation: progress, promise and challenges. Nature reviews Immunology. 2012;12(11):786-98.
141. Liu J, Dong W, Quan X, Ma C, Qin C, Zhang L. Transgenic expression of human P-selectin glycoprotein ligand-1 is not sufficient for enterovirus 71 infection in mice. Archives of virology. 2012;157(3):539-43.
142. Nagata N, Iwasaki T, Ami Y, Tano Y, Harashima A, Suzaki Y, et al. Differential localization of neurons susceptible to enterovirus 71 and poliovirus type 1 in the central nervous system of cynomolgus monkeys after intravenous inoculation. The Journal of general virology. 2004;85(Pt 10):2981-9.
143. Zhang Y, Cui W, Liu L, Wang J, Zhao H, Liao Y, et al. Pathogenesis study of enterovirus 71 infection in rhesus monkeys. Laboratory investigation; a journal of technical methods and pathology. 2011;91(9):1337-50.
144. Zhang G, Zhou F, Gu B, Ding C, Feng D, Xie F, et al. In vitro and in vivo evaluation of ribavirin and pleconaril antiviral activity against enterovirus 71 infection. Archives of virology. 2012;157(4):669-79.
145. Li ZH, Li CM, Ling P, Shen FH, Chen SH, Liu CC, et al. Ribavirin reduces mortality in enterovirus 71-infected mice by decreasing viral replication. The Journal of infectious diseases. 2008;197(6):854-7.
146. Rotbart HA, Webster AD. Treatment of potentially life-threatening enterovirus infections with pleconaril. Clinical infectious diseases : an

official publication of the Infectious Diseases Society of America. 2001;32(2):228-35.
147. Zhang X, Song Z, Qin B, Zhang X, Chen L, Hu Y, et al. Rupintrivir is a promising candidate for treating severe cases of enterovirus-71 infection: evaluation of antiviral efficacy in a murine infection model. Antiviral Res. 2013;97(3):264-9.
148. Liu Y-C, Kuo R-L, Lin J-Y, Huang P-N, Huang Y, Liu H, et al. Cytoplasmic Viral RNA-Dependent RNA Polymerase Disrupts the Intracellular Splicing Machinery by Entering the Nucleus and Interfering with Prp8. PLOS Pathogens. 2014;10(6):e1004199.
149. Chen T-C, Chang H-Y, Lin P-F, Chern J-H, Hsu JT-A, Chang C-Y, et al. Novel Antiviral Agent DTriP-22 Targets RNA-Dependent RNA Polymerase of Enterovirus 71. Antimicrobial Agents and Chemotherapy. 2009;53(7):2740-7.
150. Shia KS, Li WT, Chang CM, Hsu MC, Chern JH, Leong MK, et al. Design, synthesis, and structure-activity relationship of pyridyl imidazolidinones: a novel class of potent and selective human enterovirus 71 inhibitors. Journal of medicinal chemistry. 2002;45(8):1644-55.
151. Shih SR, Chen SJ, Hakimelahi GH, Liu HJ, Tseng CT, Shia KS. Selective human enterovirus and rhinovirus inhibitors: An overview of capsid-binding and protease-inhibiting molecules. Medicinal research reviews. 2004;24(4):449-74.
152. Chern JH, Shia KS, Hsu TA, Tai CL, Lee CC, Lee YC, et al. Design, synthesis, and structure-activity relationships of pyrazolo[3,4-d]pyrimidines: a novel class of potent enterovirus inhibitors. Bioorganic & medicinal chemistry letters. 2004;14(10):2519-25.
153. Chang CS, Lin YT, Shih SR, Lee CC, Lee YC, Tai CL, et al. Design, synthesis, and antipicornavirus activity of 1-[5-(4-arylphenoxy)alkyl]-3-pyridin-4-ylimidazolidin-2-one derivatives. Journal of medicinal chemistry. 2005;48(10):3522-35.
154. Chen TC, Liu SC, Huang PN, Chang HY, Chern JH, Shih SR. Antiviral activity of pyridyl imidazolidinones against enterovirus 71 variants. J Biomed Sci. 2008;15(3):291-300.
155. Plevka P, Perera R, Yap ML, Cardosa J, Kuhn RJ, Rossmann MG. Structure of human enterovirus 71 in complex with a capsid-binding inhibitor. Proceedings of the National Academy of Sciences. 2013;110(14):5463-7.
156. Shih SR, Tsai MC, Tseng SN, Won KF, Shia KS, Li WT, et al. Mutation in enterovirus 71 capsid protein VP1 confers resistance to the inhibitory effects of pyridyl imidazolidinone. Antimicrob Agents Chemother. 2004;48(9):3523-9.
157. Rong L, Perelson AS. Treatment of hepatitis C virus infection with interferon and small molecule direct antivirals: viral kinetics and modeling. Critical reviews in immunology. 2010;30(2):131-48.
158. Chea S CY, Chokephaibulkit K, Chotpitayasunondh T, van Doorn HR, Hafy Z, et al. . Workshop on use of intravenous immunoglobulin in hand, foot and mouth disease in Southeast Asia [online report]. Emerg Infect Dis [Internet]. 2015.
159. Palivizumab, a humanized respiratory syncytial virus monoclonal antibody, reduces hospitalization from respiratory syncytial virus infection

in high-risk infants. The IMpact-RSV Study Group. Pediatrics. 1998;102(3 Pt 1):531-7.
160. Fenton C, Scott LJ, Plosker GL. Palivizumab: a review of its use as prophylaxis for serious respiratory syncytial virus infection. Paediatric drugs. 2004;6(3):177-97.
161. Plevka P, Lim P-Y, Perera R, Cardosa J, Suksatu A, Kuhn RJ, et al. Neutralizing antibodies can initiate genome release from human enterovirus 71. Proceedings of the National Academy of Sciences. 2014;111(6):2134-9.
162. Ku Z, Shi J, Liu Q, Huang Z. Development of murine monoclonal antibodies with potent neutralization effects on enterovirus 71. Journal of Virological Methods. 2012;186(1–2):193-7.
163. Ye X, Fan C, Ku Z, Zuo T, Kong L, Zhang C, et al. Structural Basis for Recognition of Human Enterovirus 71 by a Bivalent Broadly Neutralizing Monoclonal Antibody. PLOS Pathogens. 2016;12(3):e1005454.
164. Kiener TK, Jia Q, Meng T, Chow VTK, Kwang J. A Novel Universal Neutralizing Monoclonal Antibody against Enterovirus 71 That Targets the Highly Conserved "Knob" Region of VP3 Protein. PLOS Neglected Tropical Diseases. 2014;8(5):e2895.
165. Pliaka V, Kyriakopoulou Z, Markoulatos P. Risks associated with the use of live-attenuated vaccine poliovirus strains and the strategies for control and eradication of paralytic poliomyelitis. Expert Rev Vaccines. 2012;11(5):609-28.
166. Yu CK, Chen CC, Chen CL, Wang JR, Liu CC, Yan JJ, et al. Neutralizing antibody provided protection against enterovirus type 71 lethal challenge in neonatal mice. J Biomed Sci. 2000;7(6):523-8.
167. Arita M, Nagata N, Iwata N, Ami Y, Suzaki Y, Mizuta K, et al. An attenuated strain of enterovirus 71 belonging to genotype a showed a broad spectrum of antigenicity with attenuated neurovirulence in cynomolgus monkeys. Journal of virology. 2007;81(17):9386-95.
168. Zhu FC, Meng FY, Li JX, Li XL, Mao QY, Tao H, et al. Efficacy, safety, and immunology of an inactivated alum-adjuvant enterovirus 71 vaccine in children in China: a multicentre, randomised, double-blind, placebo-controlled, phase 3 trial. Lancet. 2013;381(9882):2024-32.
169. Chung YC, Ho MS, Wu JC, Chen WJ, Huang JH, Chou ST, et al. Immunization with virus-like particles of enterovirus 71 elicits potent immune responses and protects mice against lethal challenge. Vaccine. 2008;26(15):1855-62.
170. Wang M, Jiang S, Wang Y. Recombinant VP1 protein expressed in Pichia pastoris induces protective immune responses against EV71 in mice. Biochem Biophys Res Commun. 2013;430(1):387-93.
171. Foo DG, Alonso S, Phoon MC, Ramachandran NP, Chow VT, Poh CL. Identification of neutralizing linear epitopes from the VP1 capsid protein of Enterovirus 71 using synthetic peptides. Virus Res. 2007;125(1):61-8.
172. Meng T, Kwang J. Attenuation of human enterovirus 71 high-replication-fidelity variants in AG129 mice. Journal of virology. 2014;88(10):5803-15.

173. Tung WS, Bakar SA, Sekawi Z, Rosli R. DNA vaccine constructs against enterovirus 71 elicit immune response in mice. Genetic vaccines and therapy. 2007;5:6.
174. Ong KC, Devi S, Cardosa MJ, Wong KT. Formaldehyde-inactivated whole-virus vaccine protects a murine model of enterovirus 71 encephalomyelitis against disease. Journal of virology. 2010;84(1):661-5.
175. Wu CN, Lin YC, Fann C, Liao NS, Shih SR, Ho MS. Protection against lethal enterovirus 71 infection in newborn mice by passive immunization with subunit VP1 vaccines and inactivated virus. Vaccine. 2001;20(5-6):895-904.
176. Li Y-P, Liang Z-L, Gao Q, Huang L-R, Mao Q-Y, Wen S-Q, et al. Safety and immunogenicity of a novel human Enterovirus 71 (EV71) vaccine: A randomized, placebo-controlled, double-blind, Phase I clinical trial. Vaccine. 2012;30(22):3295-303.
177. Zhu F-C, Liang Z-L, Li X-L, Ge H-M, Meng F-Y, Mao Q-Y, et al. Immunogenicity and safety of an enterovirus 71 vaccine in healthy Chinese children and infants: a randomised, double-blind, placebo-controlled phase 2 clinical trial. The Lancet.381(9871):1037-45.
178. Li R, Liu L, Mo Z, Wang X, Xia J, Liang Z, et al. An inactivated enterovirus 71 vaccine in healthy children. The New England journal of medicine. 2014;370(9):829-37.
179. Zhu F, Xu W, Xia J, Liang Z, Liu Y, Zhang X, et al. Efficacy, safety, and immunogenicity of an enterovirus 71 vaccine in China. The New England journal of medicine. 2014;370(9):818-28.
180. Begley DJ, Brightman MW. Structural and functional aspects of the blood-brain barrier. Progress in drug research Fortschritte der Arzneimittelforschung Progres des recherches pharmaceutiques. 2003;61:39-78.
181. Abbott NJ, Ronnback L, Hansson E. Astrocyte-endothelial interactions at the blood-brain barrier. Nature reviews Neuroscience. 2006;7(1):41-53.
182. Wolburg H, Lippoldt A. Tight junctions of the blood–brain barrier. Vascular Pharmacology. 2002;38(6):323-37.
183. Ballabh P, Braun A, Nedergaard M. The blood-brain barrier: an overview: structure, regulation, and clinical implications. Neurobiology of disease. 2004;16(1):1-13.
184. Hawkins BT, Davis TP. The blood-brain barrier/neurovascular unit in health and disease. Pharmacological reviews. 2005;57(2):173-85.
185. Obermeier B, Daneman R, Ransohoff RM. Development, maintenance and disruption of the blood-brain barrier. Nat Med. 2013;19(12):1584-96.
186. Chi C, Sun Q, Wang S, Zhang Z, Li X, Cardona CJ, et al. Robust antiviral responses to enterovirus 71 infection in human intestinal epithelial cells. Virus Research. 2013;176(1):53-60.
187. Hornung V, Ellegast J, Kim S, Brzozka K, Jung A, Kato H, et al. 5'-Triphosphate RNA is the ligand for RIG-I. Science. 2006;314(5801):994-7.
188. Feng Q, Hato Stanleyson V, Langereis Martijn A, Zoll J, Virgen-Slane R, Peisley A, et al. MDA5 Detects the Double-Stranded RNA Replicative Form in Picornavirus-Infected Cells. Cell Reports. 2012;2(5):1187-96.

189. Wang C, Ji L, Yuan X, Jin Y, Cardona CJ, Xing Z. Differential Regulation of TLR Signaling on the Induction of Antiviral Interferons in Human Intestinal Epithelial Cells Infected with Enterovirus 71. PloS one. 2016;11(3):e0152177.
190. Kato H, Takeuchi O, Sato S, Yoneyama M, Yamamoto M, Matsui K, et al. Differential roles of MDA5 and RIG-I helicases in the recognition of RNA viruses. Nature. 2006;441(7089):101-5.
191. Iwasaki A, Medzhitov R. Toll-like receptor control of the adaptive immune responses. Nature immunology. 2004;5(10):987-95.
192. Perry AK, Chen G, Zheng D, Tang H, Cheng G. The host type I interferon response to viral and bacterial infections. Cell Res. 2005;15(6):407-22.
193. Samuel CE. Antiviral actions of interferon. Interferon-regulated cellular proteins and their surprisingly selective antiviral activities. Virology. 1991;183(1):1-11.
194. Pestka S, Langer JA, Zoon KC, Samuel CE. Interferons and their actions. Annual review of biochemistry. 1987;56:727-77.
195. Randall RE, Goodbourn S. Interferons and viruses: an interplay between induction, signalling, antiviral responses and virus countermeasures. The Journal of general virology. 2008;89(Pt 1):1-47.
196. Daniels BP, Holman DW, Cruz-Orengo L, Jujjavarapu H, Durrant DM, Klein RS. Viral pathogen-associated molecular patterns regulate blood-brain barrier integrity via competing innate cytokine signals. mBio. 2014;5(5):e01476-14.
197. Jou T-S, Schneeberger EE, James Nelson W. Structural and Functional Regulation of Tight Junctions by RhoA and Rac1 Small GTPases. The Journal of Cell Biology. 1998;142(1):101-15.
198. Etienne-Manneville S, Hall A. Rho GTPases in cell biology. Nature. 2002;420(6916):629-35.
199. Pinto AK, Ramos HJ, Wu X, Aggarwal S, Shrestha B, Gorman M, et al. Deficient IFN Signaling by Myeloid Cells Leads to MAVS-Dependent Virus-Induced Sepsis. PLoS Pathogens. 2014;10(4):e1004086.
200. Tan EL, Yong LL, Quak SH, Yeo WC, Chow VT, Poh CL. Rapid detection of enterovirus 71 by real-time TaqMan RT-PCR. Journal of clinical virology : the official publication of the Pan American Society for Clinical Virology. 2008;42(2):203-6.
201. Reed LJ MH. A simple method of estimating fifty per cent endpoints. . Am J Hyg. 1938;27:493–7.
202. Her Z, Malleret B, Chan M, Ong EK, Wong SC, Kwek DJ, et al. Active infection of human blood monocytes by Chikungunya virus triggers an innate immune response. Journal of immunology. 2010;184(10):5903-13.
203. Lum FM, Low DK, Fan Y, Tan JJ, Lee B, Chan JK, et al. Zika Virus Infects Human Fetal Brain Microglia and Induces Inflammation. Clinical infectious diseases : an official publication of the Infectious Diseases Society of America. 2017;64(7):914-20.
204. Martin M. Cutadapt removes adapter sequences from high-throughput sequencing reads. 2011. 2011;17(1).

205. Kim D, Pertea G, Trapnell C, Pimentel H, Kelley R, Salzberg SL. TopHat2: accurate alignment of transcriptomes in the presence of insertions, deletions and gene fusions. Genome Biology. 2013;14(4):R36.
206. Langmead B, Salzberg SL. Fast gapped-read alignment with Bowtie 2. Nature methods. 2012;9(4):357-9.
207. Lu J, He YQ, Yi LN, Zan H, Kung HF, He ML. Viral kinetics of Enterovirus 71 in human abdomyosarcoma cells. World Journal of Gastroenterology : WJG. 2011;17(36):4135-42.
208. Barbas CF, Hu D, Dunlop N, Sawyer L, Cababa D, Hendry RM, et al. In vitro evolution of a neutralizing human antibody to human immunodeficiency virus type 1 to enhance affinity and broaden strain cross-reactivity. Proceedings of the National Academy of Sciences. 1994;91(9):3809-13.
209. Chatterjee A, Smith PF, Perelson AS. Hepatitis C Viral Kinetics The Past, Present, and Future. Clinics in liver disease. 2013;17(1):13-26.
210. Hatta Y, Hershberger K, Shinya K, Proll SC, Dubielzig RR, Hatta M, et al. Viral Replication Rate Regulates Clinical Outcome and CD8 T Cell Responses during Highly Pathogenic H5N1 Influenza Virus Infection in Mice. PLoS Pathogens. 2010;6(10):e1001139.
211. Fukuhara M, Iwami S, Sato K, Nishimura Y, Shimizu H, Aihara K, et al. Quantification of the Dynamics of Enterovirus 71 Infection by Experimental-Mathematical Investigation. Journal of virology. 2013;87(1):701-5.
212. Shih S-R, Stollar V, Li M-L. Host Factors in Enterovirus 71 Replication. Journal of Virology. 2011;85(19):9658-66.
213. Lee YR, Wang PS, Wang JR, Liu HS. Enterovirus 71-induced autophagy increases viral replication and pathogenesis in a suckling mouse model. J Biomed Sci. 2014;21:80.
214. Srinivasan B, Kolli AR, Esch MB, Abaci HE, Shuler ML, Hickman JJ. TEER measurement techniques for in vitro barrier model systems. Journal of laboratory automation. 2015;20(2):107-26.
215. Vu K, Weksler B, Romero I, Couraud P-O, Gelli A. Immortalized Human Brain Endothelial Cell Line HCMEC/D3 as a Model of the Blood-Brain Barrier Facilitates In Vitro Studies of Central Nervous System Infection by Cryptococcus neoformans. Eukaryotic Cell. 2009;8(11):1803-7.
216. Urich E, Lazic SE, Molnos J, Wells I, Freskgård P-O. Transcriptional Profiling of Human Brain Endothelial Cells Reveals Key Properties Crucial for Predictive In Vitro Blood-Brain Barrier Models. PloS one. 2012;7(5):e38149.
217. Delacour D, Jacob R. Apical protein transport. Cell Mol Life Sci. 2006;63(21):2491-505.
218. Weisz OA, Rodriguez-Boulan E. Apical trafficking in epithelial cells: signals, clusters and motors. J Cell Sci. 2009;122(Pt 23):4253-66.
219. Lim PJ, Chu JJH. A Polarized Cell Model for Chikungunya Virus Infection: Entry and Egress of Virus Occurs at the Apical Domain of Polarized Cells. PLOS Neglected Tropical Diseases. 2014;8(2):e2661.
220. Daniels BP, Holman DW, Cruz-Orengo L, Jujjavarapu H, Durrant DM, Klein RS. Viral Pathogen-Associated Molecular Patterns Regulate

Blood-Brain Barrier Integrity via Competing Innate Cytokine Signals. mBio. 2014;5(5).
221. Matter K, Balda MS. Signalling to and from tight junctions. Nature reviews Molecular cell biology. 2003;4(3):225-36.
222. Couderc T, Chrétien F, Schilte C, Disson O, Brigitte M, Guivel-Benhassine F, et al. A Mouse Model for Chikungunya: Young Age and Inefficient Type-I Interferon Signaling Are Risk Factors for Severe Disease. PLOS Pathogens. 2008;4(2):e29.
223. Schilte C, Couderc T, Chretien F, Sourisseau M, Gangneux N, Guivel-Benhassine F, et al. Type I IFN controls chikungunya virus via its action on nonhematopoietic cells. The Journal of Experimental Medicine. 2010;207(2):429-42.
224. Spindler V, Schlegel N, Waschke J. Role of GTPases in control of microvascular permeability. Cardiovascular research. 2010;87(2):243-53.
225. Huang SW, Lee YP, Hung YT, Lin CH, Chuang JI, Lei HY, et al. Exogenous interleukin-6, interleukin-13, and interferon-gamma provoke pulmonary abnormality with mild edema in enterovirus 71-infected mice. Respiratory research. 2011;12:147.
226. Khong WX, Foo DGW, Trasti SL, Tan EL, Alonso S. Sustained High Levels of Interleukin-6 Contribute to the Pathogenesis of Enterovirus 71 in a Neonate Mouse Model. Journal of virology. 2011;85(7):3067-76.
227. Huang C-C, Liu C-C, Chang Y-C, Chen C-Y, Wang S-T, Yeh T-F. Neurologic Complications in Children with Enterovirus 71 Infection. New England Journal of Medicine. 1999;341(13):936-42.
228. Wang S-M, Lei H-Y, Huang M-C, Su L-Y, Lin H-C, Yu C-K, et al. Modulation of cytokine production by intravenous immunoglobulin in patients with enterovirus 71-associated brainstem encephalitis. Journal of Clinical Virology.37(1):47-52.
229. Wang SM, Lei HY, Su LY, Wu JM, Yu CK, Wang JR, et al. Cerebrospinal fluid cytokines in enterovirus 71 brain stem encephalitis and echovirus meningitis infections of varying severity. Clinical Microbiology and Infection.13(7):677-82.
230. Weng KF, Chen LL, Huang PN, Shih SR. Neural pathogenesis of enterovirus 71 infection. Microbes and infection. 2010;12(7):505-10.
231. Aste-Amezaga M, Ma X, Sartori A, Trinchieri G. Molecular mechanisms of the induction of IL-12 and its inhibition by IL-10. Journal of immunology. 1998;160(12):5936-44.
232. Balk RA. Systemic inflammatory response syndrome (SIRS): Where did it come from and is it still relevant today? Virulence. 2014;5(1):20-6.
233. McCarthy DJ, Chen Y, Smyth GK. Differential expression analysis of multifactor RNA-Seq experiments with respect to biological variation. Nucleic Acids Res. 2012;40.
234. Schoggins JW, Rice CM. Interferon-stimulated genes and their antiviral effector functions. Current opinion in virology. 2011;1(6):519-25.
235. Leung E, Berg RW, Langley R, Greene J, Raymond LA, Augustus M, et al. Genomic organization, chromosomal mapping, and analysis of the 5' promoter region of the human MAdCAM-1 gene. Immunogenetics. 1997;46(2):111-9.
236. Lin Y-S, Wang H-Y, Huang D-F, Hsieh P-F, Lin M-Y, Chou C-H, et al. Neuronal Splicing Regulator RBFOX3 (NeuN) Regulates Adult

Hippocampal Neurogenesis and Synaptogenesis. PLoS One. 2016;11(10):e0164164.
237. Barry DM, Koo Ys, Norden PR, Wylie LA, Xu K, Wichaidit C, et al. Rasip1-Mediated Rho GTPase Signaling Regulates Blood Vessel Tubulogenesis via Non-Muscle Myosin II. Circulation Research. 2016.
238. Zolk O, Marx M, Jackel E, El-Armouche A, Eschenhagen T. Beta-adrenergic stimulation induces cardiac ankyrin repeat protein expression: involvement of protein kinase A and calmodulin-dependent kinase. Cardiovascular research. 2003;59(3):563-72.